Mathematical Models of Locomotion: Legged Crawling, Snake-like Motility, and Flagellar Swimming

---

PhD Thesis

Canditate
Giancarlo Cicconofri

Advisor
Antonio DeSimone

Sector of Mathematical Analysis,
Modelling, and Applications

SISSA, International School for Advanced Studies
Via Bonomea 265, 34136 Trieste - Italy

August 2015

To Paolo,
Donatella,
& Rita.

Abstract

Three different models of motile systems are studied: a vibrating legged robot, a snake-like locomotor, and two kinds of flagellar microswimmers.

The vibrating robot crawls by modulating the friction with the substrate. This also leads to the ability to switch direction of motion by varying the vibration frequency. A detailed account of this phenomenon is given through a fully analytical treatment of the model. The analysis delivers formulas for the average velocity of the robot and for the frequency at which the direction switch takes place. A quantitative description of the mechanism for the friction modulation underlying the motility of the robot is also provided.

Snake-like locomotion is studied through a system consisting of a planar, internally actuated, elastic rod. The rod is constrained to slide longitudinally without slipping laterally. This setting is inspired by undulatory locomotion of snakes, where frictional resistance is typically larger in the lateral direction than in the longitudinal one. The presence of constraints leads to non-standard boundary conditions, that lead to the possibility to close and solve uniquely the equations of motion. Explicit formulas are derived, which highlight the connection between observed trajectories, internal actuation, and forces exchanged with the environment.

The two swimmer models (one actuated externally and the other internally) provide an example of propulsion at low Reynolds number resulting from the periodical beating of a passive elastic filament. Motions produced by generic periodic actuations are studied within the regime of small compliance of the filament. The analysis shows that variations in the velocity of beating can generate different swimming trajectories. Motion control through modulations of the actuation velocity is discussed.

Contents

Introduction

The study of the mechanics of walking, crawling, swimming, and flying has been an active field of research for decades, and it is still developing. Pioneering works include those by zoologists like J. Gray [1, 2] or R. M. Alexander [3] and applied mathematicians like G.I. Taylor [4] or J. Lighthill [5]. Since their times biological locomotion investigations have explored a wide range of phenomena, from the swarms of bacteria to the migration of tumour cells [6]. Lessons learnt from nature have been also used to design of bio-inspired robotic locomotors, to the point that, now, boundaries between biologic and robotic motility studies have become permeable and cross-fertilization between the two field is occurring. Practical applications of bio-inspired engineering range from legged and snake-like robots for search and rescue operations [7] to swimming microrobots targeted to biomedical purposes, such as diagnostics or drug delivery [8, 9].

The field of locomotion mechanics is highly cross-disciplinary. It involves engineering, physics, mathematics and biology, both experimental and theoretical. From the theoretical viewpoint a modelling effort is often needed. In particular, a reductionist approach in the description of (otherwise too complex) real systems can deepen the understanding of the key physical mechanism underlying motility. This is the spirit guiding this thesis. Three different models of motile systems are formalized and analysed: a vibrating legged robot [10], an active elastic snake-like locomotor [11], and two kinds of flagellar swimmers [12].

The three systems exploit different locomotion strategies and they are analysed with different mathematical tools. They are unified by the fundamental question: what makes locomotion possible? When we refer to locomotion we are implicitly considering two things: the locomotor and the environment it is interacting with. In particular, we need to formulate the physical laws describing the mechanical interactions between the two. In the case studies presented here the interaction is given by friction. In general, an object interacting with a frictional environment can be subject to forces that either oppose or support its motion in a given direction. We can define as a "frictional locomotor" a propelling object undergoing periodic shape changes alongside with periodic frictional interactions with the environment. Every frictional locomotor relies on a general propulsion "principle" that can be stated in the following way. In order to propel, a locomotor must mobilize at each period of interaction a larger amount of frictional force supporting its motion in a given direction, and a smaller amount of force opposing it. This "principle", despite its apparent simplicity, applies in many non-trivial ways due to a) locomotor kinematics, leading to a restriction of possible movements enabling propulsion and b) different frictional laws of interaction with the environment. The three models reported here illustrate this non-triviality.

Consider the case of the body-and-legs crawler in Chapter 1. The model describes a vibrating 'bristle-bot' consisting of body with an internal rotary engine, driving vertical oscillations, and rigid legs attached to it by rotational springs. Legs exert contact friction on the substrate, and friction is proportional to the normal force on the ground. So, in this case, friction is modulated: it is stronger when vertical inertia pushes down and it is weaker when inertial force tends to lift the robot up. Legs slide on the substrate with the same frequency of the rotary engine, and we have net propulsion in the direction opposite to the sliding occurring during downward pushes. The question of which direction of motion the system chooses is non-trivial. Indeed, the legged robot moves backward for small frequencies, inverts the direction of motion, and forward for larger frequencies of excitation. This happens because the phase of oscillation between the forcing term and leg sliding changes, just like in the case of a driven spring-mass-dumper system. The analysis in Chapter 1 puts in a quantitative framework this physical picture. The governing equations are solved through a rigorously proven asymptotic scheme, and a formula for the inversion frequency is derived. A formula for the average robot velocity in terms of normal force and legs relative velocity is also obtained.

For the snake-like locomotion and flagellar swimming, we consider no active modulation of friction. Both cases consist in elongated bodies subjected to a field of friction forces that depends on the direction of motion. Because of the structural conformation of their bellies, real snakes are subject to a frictional force opposing lateral slip that is larger compared to the force opposing longitudinal sliding. Fluid forces on a small and slender object like a flagellum act, at first approximation, in the same way: friction is larger in the lateral direction and smaller in the longitudinal one. The anisotropy of friction is crucial for both system to apply the general "principle" stated earlier to generate propulsion. Frictional forces are dry in the first case case and viscous in the second, however. Moreover, the two model locomotors analysed differ in their ability to move: the "snake" is modelled as an elastic inextensible rod which is actuated by a distributed internal torque, while the flagellar swimmers consist in a rigid head attached to a passive elastic tail. In spite of these similarities, the two model systems are substantially different in the details, as explained further below.

The analysis of snake-like locomotion in Chapter 2 is carried out in the formal limit of infinite ratio between lateral and longitudinal friction, so that no lateral slip is allowed. The model snake then moves along a curve on a plane, which is created during motion. Once this curve is known the kinematics of the system simplifies: since the active-rod-snake is inextensible, the system has only one degree of freedom, namely the curvilinear coordinate of one end of the rod. The force balance equations for material and external friction reactions are, on the other hand, non-trivial. Previous studies did not contain a derivation of such forces as a result of internal activity. We are able to close the equations of motion thanks to a careful choice of boundary conditions, proving the well-posedness of the problem and reducing the dynamics of the system to the equation for the end-point coordinate only. The interplay between internal activation, kinematics, and forces is captured and discussed.

Also flagellar swimming consists in an elastic structure interacting with the environment in an anisotropic way. This is an approximation of the interaction between a slender object and the surrounding fluid in the low Reynolds num-

bers regime. In Chapter 3 two kinds of swimmers are analysed consisting of a spherical rigid head and an elastic tail. In the first one, the tail is clamped to the head and oscillations of the system are caused by external actuation. In the second one, head and tail are connected by a joint allowing the angle between them to vary periodically, as a result of internal actuation. Previous studies on these models were restricted to sinusoidal oscillations of either the external or the internal actuation, showing that the swimmers can in fact propel while moving on average along a straight line, whose direction is given by the symmetry axis around which beating takes place. The study reported in Chapter 3 extends these results to motions produced by generic (non-sinusoidal) periodic actuations within the regime of small compliance of the flagella. We find that modulation in the velocity of actuation can provide a mechanism to select different directions of motion. With velocity modulated inputs the externally actuated swimmer can translate laterally with respect to the symmetry axis of beating, while the internally actuated one is able to move along curved trajectories. The results are presented in the spirit of geometric robotic locomotion, and illustrated through the use of motility maps.

Chapter 1

Legged Crawling

Together with swimming, flying [3, 16, 17], walking, running and hopping [23], research has focused on crawling gaits. Both soft and hard devices have been designed in order to crawl over a surface in the presence of a directional (asymmetric) dynamic friction coefficient, creating a mechanical ratchet [21, 28, 29]. A different example of crawling locomotion is given by gastropods, which glide over a mucus layer by generating travelling waves of localized contraction: by sliding over the rapidly contracting part and sticking in the remaining part they produce the tractions necessary for propulsion [18, 26, 27]. Caterpillars [15] and soft robots [31] can detach partially from the substrate: they move by exerting a grip on the ground with their leading limbs, pulling forward the trailing (detached) part of their bodies. In all these systems, a periodic internal activation can lead to sustained propulsion through a variable interaction between the body of the locomotor and the environment, alternating high friction in some parts and low friction in others during one period [32].

Vibrating legged robots provide a different, but related example of such system. They have been proposed as model locomotors to study the emergence of collectively organized motion [22]. Moreover, they have recently been the subject of thorough theoretical and experimental investigations in the robotics literature [13, 14, 25]. Nevertheless the study of their individual propulsion mechanism still offers many interesting and challenging questions. It has been suggested [22] that net displacements come from the modulation of friction in time due to the oscillations of the normal forces, leading to a stick-slip motion of their feet. A bristle-bot would move forward during the stick phase, which occurs because of the larger frictional forces caused by the robot pushing more forcefully downwards during one phase of its vertical oscillations. When such oscillations causes a decrease of the vertical pushing, then the frictional force is reduced and the robot feet slip on the ground. This results in a much smaller horizontal force in the backward direction; the periodic vertical oscillations are then accompanied by a net forward displacement. DeSimone and Tatone [19] have proposed a simplified model to study this mechanism, in which the tangential frictional force is given by

$$T = -\mu N \dot{X}$$

where N is the normal reaction force exerted by the (rigid) substrate, $\dot{X}$ is the foot velocity and μ is a phenomenological proportionality constant. A striking observation in [19] is that the robot may be able to switch direction of motion by tuning the frequency of the engine powering the vertical oscillations. The goal of this Chapter is to investigate this issue and the whole propulsive mechanism of bristle-bots in detail.

Through a full analytical treatment of the bristle-bot model, we are able to provide an approximate expression for the average velocity and an explicit formula for the inversion frequency, namely,

$$\Omega_{\text{inv}} = \sqrt{\frac{k}{M}}\,\frac{1}{L\cos\alpha} \tag{1.1}$$

where M is the total mass of the robot, L is the length of the legs, α is their angle in the unloaded state and k is the rotational stiffness of the spring joining the legs to the robot's body (see Fig.**??**). As for the average velocity $\bar{v}$, we prove that the foot velocity $\dot{X}$ stabilizes after an initial transient, getting close to a periodic function given by the sum $\dot{X} \simeq \bar{v} + \dot{X}_{\text{osc}}$ where

$$\bar{v} \simeq -\frac{1}{\bar{N}} \fint N\dot{X}_{\text{osc}}\,, \tag{1.2}$$

with $\fint$ denoting time average, and $\bar{N}$ being the average value of the normal force N (which is also close to a periodic function). Formula (1.2) puts in a quantitative framework the stick-slip picture. Indeed, the average velocity $\bar{v}$ proves to be the negative of a weighted average of $\dot{X}_{\text{osc}}$, the feet velocity relative to $\bar{v}$, the weight being the reactive normal force N transmitted by the ground during the oscillations. Therefore, in order to move, say, forward, the robot legs exploit a stronger grip due to a larger normal force when sliding backwards, and then recover when N is smaller.

The argument above explains why the average velocity of the robot may be non-zero. The question of determining the actual direction of motion, i.e., the sign of $\bar{v}$, is more subtle and depends, as (1.2) indicates, on the relative phase between the oscillations $\dot{X}_{\text{osc}}$ of the feet and of the normal force N. This is discussed in detail in Section 1.3.

The rest of the Chapter is organized as follows. We set up the equations of motion in Section 1.1 and solve them formally through an asymptotic expansion in Section 1.2. Therein we calculate the first three orders of such expansion, obtaining (1.1) and the expression for the approximate average velocity. The convergence of our asymptotic solution, together with its regularity, periodicity and stability are analysed in the Appendix. In Section 1.3 we derive (1.2) and provide a quantitative description of the locomotion process.

1.1 The model

We consider the robot legs as massless and rigid, joined to the body with a rotational spring of stiffness k, while we assume that their feet are in frictional contact with the substrate. The system is driven by a force F_Ω internal to the body coming from a mass oscillating vertically at frequency Ω. For simplicity, we assume that rotations of the body are not allowed and that the legs are

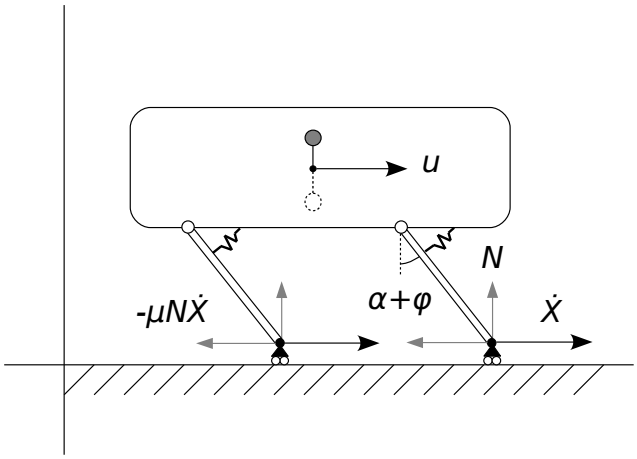

Figure 1.1: Schematic description of the model bristle-robot.

always in contact with the substrate. So the only degrees of freedom in our model are the horizontal coordinate of the body u, and the deviation φ from the angle in the unloaded state α, namely the angle the legs form with the vertical direction when no torque is exerted on the rotational springs. We remark that real bristle-bots are known to display typically more complex dynamics. Nevertheless, there exist settings (e.g., robots moving inside a closely fitting channel or robots resting on rubber feet of large transversal width as in [28]) where our one-linear-degree-of-freedom assumption would not be too far from reality.

Balancing all forces we end up with the following equations of motion

$$M\ddot{h} = N(t) - Mg + F_\Omega(t) \tag{1.3}$$

$$k\varphi = N(t)L\sin(\alpha+\varphi) - \mu N(t)\dot{X}L\cos(\alpha+\varphi) \tag{1.4}$$

$$M\ddot{u} = -\mu N(t)\dot{X} \tag{1.5}$$

where N is the normal reaction force exerted by the (rigid) substrate, M is the body mass, L is the length of the legs while

$$h = L\cos(\alpha+\varphi) \quad \text{and} \quad X = u + L\sin(\alpha+\varphi)\,.$$

We will first discuss a heuristic approach to solve the problem using an asymptotic expansion in terms of a small parameter. Instead of solving the problem directly, we will pursue the following strategy: we first give an ansatz on N by choosing it in a suitable family of oscillatory functions depending on parameters. Then we find an asymptotic solution to equations (1.4) and (1.5) for the variables φ and $v = \dot{u}$, that will depend on our choice of N. We then

obtain the expression for F_Ω from (1.3), and we find the appropriate N, after tuning the parameters, in order to have an approximate solution to the system in the case when the robot is driven by an oscillating internal force.

1.2 Formal asymptotics

Let us use the following ansatz for the normal force

$$N(t) = N^* + \widetilde{N}\sin\Omega t + (N_2^c\cos 2\Omega t + N_2^s \sin 2\Omega t) + \text{o.h.}$$

Here N^* stands for the approximate average of the normal force, for which we take

$$N^* = Mg\,.$$

This choice will be justified by the results in Section 1.3. The term o.h. stands for "other harmonics" of any order, which can be neglected at first approximation. Specifically, we are considering the normalized normal force n, where

$$N(t) = N^* n(\Omega t)\,,$$

to be a power series expansion in the parameter η in which the first three orders are given

$$n(\tau) = 1 + \eta\sin\tau + \eta^2(n_2^c\cos 2\tau + n_2^s\sin 2\tau) + \mathcal{O}(\eta^3)\,. \tag{1.6}$$

The coefficients (n_2^c, n_2^s) are the tuning parameters that will be chosen appropriately later, while we assume that η, namely the ratio between the amplitude of the first "relevant" harmonic and the average normal force, is a small parameter

$$\frac{\widetilde{N}}{N^*} = \eta \ll 1\,.$$

1.2.1 Non-dimensionalization and orders of magnitude of the parameters

We now normalize the dynamical variables, which can also be expanded into power series of η, as show below. By defining the constants

$$\sigma = \sin(\alpha) \quad \text{and} \quad \chi = \cos(\alpha)$$

together with the angle ϵ given by

$$\epsilon = \frac{N^* L\,\sigma}{k} \tag{1.7}$$

we determine the new dynamical variables (θ, w) through the equalities

$$\varphi(t) = \epsilon\,\theta(\Omega t) \quad \text{and} \quad v(t) = \epsilon L\chi\Omega\, w(\Omega t)\,. \tag{1.8}$$

Applying all the definitions above we can rewrite equations (1.4) and (1.5) as the equivalent system

$$\begin{cases} \theta = n(\tau)\dfrac{\sin(\alpha+\epsilon\theta)}{\sigma} - \xi\, n(\tau)\left(w + \dot\theta\,\dfrac{\cos(\alpha+\epsilon\theta)}{\chi}\right)\dfrac{\cos(\alpha+\epsilon\theta)}{\chi} \\[2ex] \dot w = -\lambda\, n(\tau)\left(w + \dot\theta\,\dfrac{\cos(\alpha+\epsilon\theta)}{\chi}\right) \end{cases} \tag{1.9}$$

where $\tau = \Omega t$ is the non-dimensionalized time, while

$$\xi = \frac{\mu N^* L^2 \chi^2 \Omega}{k} \quad \text{and} \quad \lambda = \frac{\mu N^*}{M\Omega}. \tag{1.10}$$

Finally we normalize equation (1.3), obtaining

$$-\left(\frac{\sigma\omega}{\chi}\right)^2 \ddot{\theta}\,\frac{\sin(\alpha+\epsilon\theta)}{\sigma} - \epsilon\frac{\sigma\omega^2}{\chi}\,\dot{\theta}^2\,\frac{\cos(\alpha+\epsilon\theta)}{\chi} \quad = \quad n(\tau) - 1 + f(\tau) \tag{1.11}$$

where f and ω are, respectively, the normalized force and frequency defined by the equations

$$F_\Omega(t) = N^* f(\Omega t) \quad \text{and} \quad \Omega = \sqrt{\frac{k}{M}}\,\frac{\omega}{L\chi}. \tag{1.12}$$

In the next section we will formally solve (1.9), by calculating the asymptotic expansions up to the second order

$$\theta = \theta_0 + \eta\theta_1 + \eta^2\theta_2 + \mathcal{O}(\eta^3) \quad \text{and} \quad w = w_0 + \eta w_1 + \eta^2 w_2 + \mathcal{O}(\eta^3) \tag{1.13}$$

by first making the following assumptions on the parameters, needed in order to enforce the separation between $\mathcal{O}(1)$ quantities and smaller ones. We take

$$\omega\,,\,\xi\,,\,\lambda\,,\,\frac{\sigma}{\chi} = \mathcal{O}(1) \quad \text{and} \quad \epsilon = \mathcal{O}(\eta^2)\,. \tag{1.14}$$

Such a choice of orders is always possible. Indeed we can take $\sigma, \chi = \mathcal{O}(1)$, provided that we exclude the cases in which the legs are either close to perpendicular or close to parallel to the body of the robot. Then we assume $\omega = \mathcal{O}(1)$, that is coherent with the fact that, as we will see, these are the order of values of ω around which the inversion of the direction of motion occurs, and that this is precisely the regime we are interested in. Finally, we can first set ϵ to be of order $\mathcal{O}(\eta^2)$, and then, exploiting the fact that ξ and λ are the only parameters depending on μ, we can assume that the latter is in a range of values consistent with (1.14).

We only stress here the fact that hypothesis (1.14), and specifically the one on ϵ, are not strictly necessary to apply the solving technique developed here, but they simplify consistently the formal developments. In particular, in the case $\epsilon = \mathcal{O}(\eta^K)$ with either $K = 0$ or $K = 1$ a similar analysis is still possible. However, a more complicated function for n instead of (1.6) should be used, making the solution of the formal asymptotics, as well as the calculations needed for proving the rigorous results, more involved.

1.2.2 Asymptotic expansion

We remark again that up to now we have just rewritten equations (1.4) and (1.5) in the completely equivalent system (1.9). From now on, we proceed formally to find approximating solutions to our problem. In the Appendix we will provide a rigorous proof that those solutions are indeed good approximations of the solutions of the original system, by using theorems from perturbation theory of periodic ODEs.

Taking $\epsilon = c\eta^2$, with c being a fixed constant, we replace the series expansions (1.13) of θ and w in (1.9) and develop both sides of the equations into power series with respect to η. By matching coefficients of equal powers, we end up with a sequence of systems to be solved successively. At zero-order we have

$$\begin{cases} \theta_0 = 1 \; - \; \xi \left(w_0 + \dot{\theta}_0 \right) \\ \\ \dot{w}_0 = - \, \lambda \left(w_0 + \dot{\theta}_0 \right) \end{cases}$$

We will prove in the Appendix that this equation, and the others to come, have only one periodic solution and every other solution converge asymptotically to such periodic one. We take as (θ_j, w_j) with $j = 0, 1, 2, \ldots$ the only periodic solution to the problem at each order. The zero-order periodic solution is

$$\theta_0 = 1 \quad , \quad w_0 = 0 \, . \tag{1.15}$$

A constant solution is coherent with the fact that, at this stage, only the non-oscillating part of n is affecting the dynamics.

Proceeding with the calculation of our expansion, the first order system is

$$\begin{cases} \theta_1 = \sin\tau - \xi \left(w_1 + \dot{\theta}_1 + \sin\tau (w_0 + \dot{\theta}_0) \right) \\ \\ \dot{w}_1 = -\lambda \left(w_1 + \dot{\theta}_1 + \sin\tau (w_0 + \dot{\theta}_0) \right) \end{cases}$$

Notice that $\sin\tau$ is the first order term in the expansion (1.6), and that this is the first time that the oscillating part of n enters in the problem. Solving these equations, imposing that the zero-order terms be the one we just found, this time we have the non-trivial periodic solution

$$\theta_1(\tau) = \theta_1^c \cos\tau + \theta_1^s \sin\tau \quad , \quad w_1(\tau) = w_1^c \cos\tau + w_1^s \sin\tau \tag{1.16}$$

where

$$\begin{aligned} \theta_1^c &= \tfrac{-\xi}{1+(\xi-\lambda)^2} \, , \quad \theta_1^s = \tfrac{1-\lambda(\xi-\lambda)}{1+(\xi-\lambda)^2} \, , \\ w_1^c &= \tfrac{\lambda(\xi-\lambda)}{1+(\xi-\lambda)^2} \, , \quad w_1^s = \tfrac{-\lambda}{1+(\xi-\lambda)^2} \, . \end{aligned} \tag{1.17}$$

Notice that the average velocity is still zero up to the first order, and that in order to recover a non-zero average velocity we need to calculate the next order expansion in η. We have

$$\begin{cases} \theta_2 = \theta_0 c \dfrac{\chi}{\sigma} \; + \; n_2^s \sin 2\tau \; + \; n_2^c \cos 2\tau \; + \; 2\xi (w_0 + \dot{\theta}_0) \, \theta_0 c \dfrac{\sigma}{\chi} \\ \qquad - \; \xi \big((w_2 + \dot{\theta}_2) + \sin\tau (w_1 + \dot{\theta}_1) + (n_2^s \sin 2\tau + n_2^c \cos 2\tau)(w_0 + \dot{\theta}_0) \big) \\ \\ \dot{w}_2 = \lambda (w_0 + \dot{\theta}_0) \, \theta_0 \, c \dfrac{\sigma}{\chi} \\ \qquad - \; \lambda \left((w_2 + \dot{\theta}_2) + \sin\tau (w_1 + \dot{\theta}_1) + (n_2^s \sin 2\tau + n_2^c \cos 2\tau)(w_0 + \dot{\theta}_0) \right) \end{cases}$$

The only periodic solution is, in this case

$$\theta_2(\tau) = c \frac{\chi}{\sigma} + \theta_2^c \cos 2\tau + \theta_2^s \sin 2\tau \quad , \quad w_2(\tau) = w^* + w_2^c \cos 2\tau + w_2^s \sin 2\tau \tag{1.18}$$

where

$$\begin{aligned}
\theta_2^c &= \frac{1}{2}\left(\frac{(1-\theta_1^s)-\theta_1^c(2\xi-\frac{\lambda}{2})}{1+(2\xi-\frac{\lambda}{2})^2}\right) + \frac{(1-\frac{\lambda}{2}(2\xi-\frac{\lambda}{2}))n_2^c-2\xi n_2^s}{1+(2\xi-\frac{\lambda}{2})^2}\,,\\
\theta_2^s &= \frac{1}{2}\left(\frac{\theta_1^c+(1-\theta_1^s)(2\xi-\frac{\lambda}{2})}{1+(2\xi-\frac{\lambda}{2})^2}\right) + \frac{2\xi n_2^c+(1-\frac{\lambda}{2}(2\xi-\frac{\lambda}{2}))n_2^s}{1+(2\xi-\frac{\lambda}{2})^2}\,,\\
w_2^c &= -\frac{1}{4}\left(\frac{w_1^s+w_1^c(2\xi-\frac{\lambda}{2})}{1+(2\xi-\frac{\lambda}{2})^2}\right) + \lambda\left(\frac{(2\xi-\frac{\lambda}{2})n_2^s-n_2^c}{1+(2\xi-\frac{\lambda}{2})^2}\right),\\
w_2^s &= \frac{1}{4}\left(\frac{w_1^c-w_1^s(2\xi-\frac{\lambda}{2})}{1+(2\xi-\frac{\lambda}{2})^2}\right) - \lambda\left(\frac{(2\xi-\frac{\lambda}{2})n_2^c+n_2^s}{1+(2\xi-\frac{\lambda}{2})^2}\right)
\end{aligned} \tag{1.19}$$

and

$$w^\star = -\frac{1}{2}\left(\frac{\xi-\lambda}{1+(\xi-\lambda)^2}\right). \tag{1.20}$$

This last equation provides us with an explicit formula for the approximate (normalized) average velocity, and shows how its sign depends on that of the difference between the two parameters (ξ,λ), and ultimately on the frequency. It also allow us to calculate the frequency at which the inversion of motion occurs, namely, $\omega_{\text{inv}} = 1$ for the normalized quantity, and

$$\Omega_{\text{inv}} = \sqrt{\frac{k}{M}}\,\frac{1}{L\chi}$$

for the dimensional one. Notice that, unlike the rest of the coefficients of the second order expansion, the average velocity does not depend on the two parameters n_2^s and n_2^c, that can be now chosen in order to solve asymptotically equation (1.11), in the case when f is a sinusoidal function.

1.2.3 Tuning the parameters

Just by rewriting (1.11) we have the following expression for the normalized force

$$f(\tau) = 1 - n(\tau) - \left(\frac{\sigma\omega}{\chi}\right)^2 \ddot{\theta}\,\frac{\sin(\alpha+\epsilon\theta)}{\sigma} - \epsilon\frac{\sigma\omega^2}{\chi}\,\dot{\theta}^2\,\frac{\cos(\alpha+\epsilon\theta)}{\chi}\,.$$

Substituting the expression (1.6) we assumed for n and the one we calculated for θ, and then formally expanding into a power series, the second member of the previous equation becomes

$$\eta\left\{\begin{array}{c}\text{sinusoidal}\\ \text{terms}\end{array}\right\} + \eta^2\left\{\left(\frac{\sigma^2\omega^2}{\chi^2}\,\theta_2^c - n_2^c\right)\cos 2\tau + \left(\frac{\sigma^2\omega^2}{\chi^2}\,\theta_2^s - n_2^s\right)\sin 2\tau\right\} + \mathcal{O}(\eta^3)\,.$$

Now, in order to have a sinusoidal force to within $\mathcal{O}(\eta^3)$, we must require that

$$\frac{\sigma^2\omega^2}{\chi^2}\,\theta_2^c - n_2^c = 0 \quad\text{and}\quad \frac{\sigma^2\omega^2}{\chi^2}\,\theta_2^s - n_2^s = 0\,.$$

Since we found that

$$\begin{pmatrix}\theta_2^c\\ \theta_2^s\end{pmatrix} = \begin{pmatrix}\tilde{\theta}_2^c\\ \tilde{\theta}_2^s\end{pmatrix} + \Theta_2\begin{pmatrix}n_2^c\\ n_2^s\end{pmatrix} \quad\text{with}\quad \Theta_2 = \begin{pmatrix} \frac{1-\frac{\lambda}{2}(2\xi-\frac{\lambda}{2})}{1+(2\xi-\frac{\lambda}{2})^2} & \frac{-2\xi}{1+(2\xi-\frac{\lambda}{2})^2} \\ \\ \frac{2\xi}{1+(2\xi-\frac{\lambda}{2})^2} & \frac{1-\frac{\lambda}{2}(2\xi-\frac{\lambda}{2})}{1+(2\xi-\frac{\lambda}{2})^2} \end{pmatrix}$$

and $(\tilde{\theta}_2^c, \tilde{\theta}_2^s)$ are constants, this requirement is fulfilled if the matrix

$$\frac{\sigma^2\omega^2}{\chi^2}\Theta_2 - \mathrm{Id}$$

is invertible. As it can be easily checked, this is true under the only assumption that $\xi > 0$, which is guaranteed by its definition (1.10).

Finally let us analyze the oscillating force that we found. We have the following asymptotic equality

$$f(\tau) = \eta f_1(\tau) + \mathcal{O}(\eta^3)$$

where f_1 can be calculated to be

$$f_1(\tau) = \frac{\sigma^2\omega^2}{\chi^2}\theta_1^c \cos\tau + \frac{\sigma^2\omega^2}{\chi^2}\theta_1^s \sin\tau - \sin\tau = \omega^2\rho_\omega \sin(\tau - \phi_\omega) \tag{1.21}$$

with

$$\rho_\omega = \frac{\sigma^2}{\chi^2}\sqrt{\left(\theta_1^c\right)^2 + \left(\theta_1^s - \frac{\chi^2}{\sigma^2\omega^2}\right)^2} \quad \text{and} \quad \phi_\omega = \arctan\left(\frac{\frac{\chi^2}{\sigma^2\omega^2} - \theta_1^s}{\theta_1^c}\right).$$

Now, since we consider our robot as driven by a vertically oscillating mass, we have $F_\Omega(t) = mA\Omega^2\sin(\Omega t)$, where A and m are the amplitude and weight, respectively, of the ocillating mass. From (1.12) follows that

$$f(\tau) = \omega^2\,\frac{mA\Omega_{\mathrm{inv}}^2}{N^*}\sin(\tau)\,.$$

In order to recover such expression for f (at least up to a $\mathcal{O}(\eta^3)$ error), we must require η to be ω-dependent by imposing

$$\eta_\omega = \frac{mA\Omega_{\mathrm{inv}}^2}{\rho_\omega N^*}\,, \tag{1.22}$$

and considering the new time variable $\tau' = \tau - \phi_\omega$, where τ' can be viewed as the proper (normalized) time of the internal oscillating force (1.21), while τ is the time relative to the first order harmonic of the normal force (1.6). Notice that both these operations do not affect the analysis we proposed. Indeed, the only requirement we imposed on η is that of being a small parameter. We can then consider it as ω-dependent and satisfying (1.22) if $mA\Omega_{\mathrm{inv}}^2/N^*$ is small enough, and by eventually restricting the range of values of ω in order for $mA\Omega_{\mathrm{inv}}^2/N^*\rho_\omega$ to be small enough as well for all such values. Moreover, the transformation $\tau \to \tau'$ leaves the form of the equation of motion (as well as the form of each system of equations in the asymptotic expansion) invariant, therefore all the presented results still apply.

Having found the expression for η in terms of the given dynamical parameters of the problem, it is worth to check whether our hypothesis (1.14) is compatible with the order of magnitude of variables relative to real physical systems. Taking $M = 42\mathrm{gr}$, $L = 10\mathrm{mm}$, $k = 20\mathrm{Nmm}$, $\alpha = 45°$, $A = 5\mathrm{mm}$, $m = 2\mathrm{gr}$ as in [14] and $\mu = 3\mathrm{sm}^{-1}$, instead of the value for the dry friction coefficient $\mu_{\mathrm{dry}} = 0.9$ used in [14], the choice of order (1.14) in the paper is fulfilled for frequencies varying

from 10Hz to 70Hz. This range contains our predicted inversion frequency $f_{\text{inv}} = \Omega_{\text{inv}}/2\pi \approx 15.5\text{Hz}$. With the value $\mu = 0.9\text{sm}^{-1}$ (1.14) is not fulfilled, hence our estimate for f_{inv} is not directly relevant for the system studied in [14].

In the following, we will continue to denote the small parameter as η, without explicitly considering its dependence on ω, in order to avoid complications. Also, we will keep τ as the normalized time variable of the system.

The expressions that we found for θ and w provide approximate solutions to the equations (1.9)-(1.11) which are justified, at this stage, only through a formal argument. In the Appendix we will prove that the system (1.9)-(1.11) has a unique, asymptotically stable, periodic solution (θ, w) that can be expressed by a power series in η whose first three orders of expansion are indeed given by (1.15), (1.16) and (1.18).

1.3 Discussion of the physical implications

Let us turn back to the original, dimensional, equations. From the results in the Appendix it follows that the dynamical variables (φ, v) converge asymptotically to periodic functions, provided that their initial conditions at, say, $t = 0$ are close enough to the equilibrium configuration of the non-actuated system. So, for large enough values of t, after the initial transient, both variables can be written in a unique way as a sum of a constant (the mean value) and an "oscillating" periodic function with zero average

$$\varphi \simeq \bar{\varphi} + \varphi_{\text{osc}} \qquad v \simeq \bar{v} + v_{\text{osc}} \,.$$

The same thing then must hold for any other function depending on them, in particular

$$N \simeq \bar{N} + N_{\text{osc}} \quad \text{and} \quad \dot{X} \simeq \bar{\dot{X}} + \dot{X}_{\text{osc}} \,.$$

By looking at equation (1.5) we can see that N can be written as the sum of the constant weight force Mg, the sinusoidal function F_Ω and the derivative of another periodic function, which therefore has zero average. So we have that

$$\bar{N} = N^* = Mg \,.$$

The same kind of argument shows that the second term of the last member of the equation

$$\dot{X} = v + \dot{\varphi} L \cos(\alpha + \varphi) \simeq \bar{v} + \left(v_{\text{osc}} + \dot{\varphi} L \cos(\alpha + \varphi)\right)$$

has also zero average. Since the representation of a periodic function as a sum of its average and of an oscillating part is unique, we have that

$$\bar{\dot{X}} = \bar{v} \quad \text{and} \quad \dot{X}_{\text{osc}} = v_{\text{osc}} + \dot{\varphi} L \cos(\alpha + \varphi) \,.$$

Now we can use the asymptotic representations of the various relevant quantities in equation (1.5), namely

$$M\dot{v} = -\mu N \dot{X} \,.$$

Then, by integrating both members of the last equality and taking the time-averages on an interval $[T, T + 2\pi/\omega]$, for T big enough, we obtain the formula for the average velocity of the robot

$$\bar{v} \simeq -\frac{1}{\bar{N}} \fint N\dot{X}_{\text{osc}} \,. \tag{1.23}$$

This formula shows that net forward motion is due to the oscillation of N, which biases the product $N\dot{X}_{\text{osc}}$ and leads to non-zero average speed even though $\dot{X}_{\text{osc}}$ has zero average. In physical terms, the robot moves, say, more forward than backward thanks to the stronger grip available while its feet slip backward because, at these times, the robot is pushing more forcefully downwards. What 'selects' the direction of motion is therefore the relative oscillation phase between normal force N and the foot velocity $\dot{X}_{\text{osc}}$, the latter being the combination of the velocity of the robot's center of mass and the one of the feet with respect to the body frame. From the first order system in Section 1.2 we have

$$w_1(\tau) = \rho_{w_1}\sin(\tau - \delta_{w_1}) \quad \text{and} \quad \dot{\theta}_1(\tau) = \rho_{\dot{\theta}_1}\sin(\tau - \delta_{\dot{\theta}_1})$$

where all the involved quantities ρ_{w_1}, $\rho_{\dot{\theta}_1}$, δ_{w_1} and $\delta_{\dot{\theta}_1}$ can be deduced from (1.16) and (1.17). All of these quantities are frequency-dependent. The functions w_1 and $\dot{\theta}_1$ can be viewed, respectively, as the approximate (and normalized) center of mass velocity, and the feet velocity with respect to the body frame. Their sum enters in the first approximation of the oscillating part of $\dot{X}$ according to the following equation

$$\dot{X}_{\text{osc}} = \epsilon L\chi\Omega\eta\big(w_1 + \dot{\theta}_1 + \mathcal{O}(\eta)\big)\,.$$

The center of mass velocity and the feet velocity with respect to the body frame have, at first order approximation, the typical behavior of a driven damped oscillator: they both vary at the same frequency of the driving force with a frequency-dependent delay and amplitude. In order to show how these delays affect the direction of motion we must recover from (1.23) the approximate average velocity (1.20). Let us notice first that

$$\bar{v} \simeq -\epsilon L\chi\Omega\Big(\fint n(w_{\text{osc}} + \dot{\theta}\,) \;+\; \mathcal{O}(\,\eta^3)\Big)\,,$$

where w_{osc} is the oscillating part of w. Now, since sines and cosines average to zero, we have

$$\begin{aligned}
\fint n(\tau)(w_{\text{osc}}(\tau) + \dot{\theta}(\tau)) \;&=\; \fint \eta^2 \sin\tau\,\big(\,\rho_{w_1}\sin(\tau - \delta_{w_1}) + \rho_{\dot{\theta}_1}\sin(\tau - \delta_{\dot{\theta}_1})\,\big) \\
&\quad + \fint \{\text{sines and cosines}\} + \mathcal{O}(\eta^3) \\
&=\; \tfrac{\eta^2}{2}\big(\,\rho_{w_1}\cos(\delta_{w_1}) + \rho_{\dot{\theta}_1}\cos(\delta_{\dot{\theta}_1})\,\big) + \mathcal{O}(\eta^3)
\end{aligned}$$

Using (1.17) and (1.24) we can express w^* as

$$w^* := -\frac{1}{2}(w_1^s - \theta_1^c) = -\frac{1}{2}\big(\,\rho_{w_1}\cos(\delta_{w_1}) + \rho_{\dot{\theta}_1}\cos(\delta_{\dot{\theta}_1})\,\big)\,, \tag{1.24}$$

therefore (1.23) becomes

$$\bar{v} \simeq \epsilon L\chi\Omega\eta^2\big(w^* + \mathcal{O}(\eta)\big)\,. \tag{1.25}$$

Formulas (1.24) and (1.25) above show that the sign of w^*, and hence of $\bar{v}$, is selected by the relative magnitude of two constants that are affected by the interplay of the two frequency-dependent delays δ_{w_1} and $\delta_{\dot{\theta}_1}$. Both signs are possible, with positive sign prevailing in the frequency range $[0, \Omega_{\rm inv})$ and negative sign emerging in the range $(\Omega_{\rm inv}, \infty)$.

1.4 Appendix. Existence, stability and uniqueness of a periodic solution: rigorous convergence results

Let us start by writing down the normalized equations of our system

$$\begin{cases} -\left(\frac{\sigma\omega}{\chi}\right)^2 \ddot{\theta}\, \frac{\sin(\alpha+\epsilon\theta)}{\sigma} - \epsilon \frac{\sigma\omega^2}{\chi}\, \dot{\theta}^2 \frac{\cos(\alpha+\epsilon\theta)}{\chi} = n(\tau) - 1 + f(\tau) \\ \theta = n(\tau)\frac{\sin(\alpha+\epsilon\theta)}{\sigma} - \xi\, n(\tau)\Big(w + \dot{\theta}\, \frac{\cos(\alpha+\epsilon\theta)}{\chi}\Big)\frac{\cos(\alpha+\epsilon\theta)}{\chi} \\ \dot{w} = -\lambda\, n(\tau)\Big(w + \dot{\theta}\, \frac{\cos(\alpha+\epsilon\theta)}{\chi}\Big) \end{cases} \tag{1.26}$$

The function $n(\tau)$ is now a *derivative* quantity, that can be written in terms of f, θ and its derivatives from the first equation. On the other hand the active force f is now *given* and we set it to be

$$f = \eta f_1$$

where f_1 is given by (1.21).

We are going to prove that, for every η sufficiently small, this system has one and only one 2π-periodic solution, which is asymptotically stable and analytic in η. This result will put the expansion of Section 1.2 on firm grounds. In fact, the uniqueness of the periodic solution together with the uniqueness of the power series representation for the functions involved, guarantees that we have constructed the actual solution of our problem.

By introducing the auxiliary variable $y = \dot{\theta}$ one can rewrite (1.26) obtaining the standard system of ODEs

$$\begin{pmatrix} \dot{\theta} \\ \dot{y} \\ \dot{w} \end{pmatrix} = G_\eta(\theta, y, w; \tau)\,,$$

where G_η is an analytic function with respect to all the variables, and it is 2π-periodic in τ. We first study the unperturbed case

$$\begin{pmatrix} \dot{\theta}_0 \\ \dot{y}_0 \\ \dot{w}_0 \end{pmatrix} = G_0(\theta_0, y_0, w_0; \tau)\,, \tag{1.27}$$

or, more explicitly,

$$\begin{cases} \dot{\theta}_0 = y_0 \\ \\ \dot{y}_0 = \dfrac{\chi^2}{\sigma^2\omega^2}\left(1 - \dfrac{\theta_0}{1-\xi(w_0+y_0)}\right) \\ \\ \dot{w}_0 = -\lambda\left(\dfrac{\theta_0}{1-\xi(w_0+y_0)}\right)(w_0+y_0) \end{cases}$$

As we expected G_0 is independent of τ because we ruled out the oscillating force. It can be immediately checked that

$$q_0 := \begin{pmatrix} 1 \\ 0 \\ 0 \end{pmatrix}$$

is a solution, which is coherent with the results in Section 1.2.2. We calculate now the Jacobian matrix DG_0 at the point q_0. This will give us information about the stability of the autonomous system and will be crucial in the proof related to existence. We have

$$DG_0(q_0) = \begin{pmatrix} 0 & 1 & 0 \\ \frac{-\chi^2}{\sigma^2\omega^2} & \frac{-\chi^2\xi}{\sigma^2\omega^2} & \frac{-\chi^2\xi}{\sigma^2\omega^2} \\ 0 & -\lambda & -\lambda \end{pmatrix}.$$

The characteristic polynomial p associated with the matrix $DG_0(q_0)$ then reads

$$p(x) = -\det(DG_0(q_0) - x\mathrm{Id}) = x^3 + \frac{\chi^2(\lambda+\xi)}{\sigma^2\omega^2}\,x^2 + x + \frac{\chi^2\lambda}{\sigma^2\omega^2}\,.$$

We can see that p has the form $p(x) = p_3x^3 + p_2x^2 + p_1x + p_0$ where all the coefficients p_j are strictly positive and, moreover, $p_1p_2 - p_0p_3 > 0$. As a straightforward consequence of the Routh-Hurwitz criterion (see e.g. [30]) all the three roots of p have strictly positive real parts. This proves that q_0 is a (locally) asymptotically stable solution of the unperturbed system. Nonetheless this is also a sufficient condition (see [20], theorems 6.1.1, 6.1.2 and 6.1.3) to guarantee the existence, uniqueness, periodicity and asymptotic stability of the solution of the general (η-dependent) system (1.26). We give here a sketch of the proof for the reader's convenience.

We have to consider the solution

$$\begin{pmatrix} \theta(\tau) \\ y(\tau) \\ w(\tau) \end{pmatrix} = s(q,\eta,\tau)$$

to the η-dependent problem with initial data

$$\begin{pmatrix} \theta(0) \\ y(0) \\ w(0) \end{pmatrix} = q\,.$$

The general theory of ODEs guarantees that such a solution exists locally for small enough values of η and initial data q close enough to q_0 and that, for such values, it is analytic. In addition, we also know that $s(q,\eta,\cdot)$ converges to the solution of the unperturbed system as its maximal interval of definition approaches the whole real line (since the solution to (1.27) with initial value close to the equilibrium ones is defined on $\mathbb{R}$). There are no restriction then to suppose that $s(q,\eta,\cdot)$ is defined on, say, the interval $[0,2\pi]$, for every small enough values of η. One can easily check that $s(q,\eta,\cdot)$ is 2π-periodic (and therefore defined on $\mathbb{R}$) if and only if

$$s(q,\eta,2\pi) - q = \begin{pmatrix} 0 \\ 0 \\ 0 \end{pmatrix}. \tag{1.28}$$

Indeed, if $s(q,\eta,\cdot)$ is a 2π-periodic solution, then (1.28) holds. Vice versa, if we have a solution $s(q,\eta,\cdot)$ of (1.26) defined on $[0,2\pi]$ such that (1.28) is verified, then we can extend (with regularity) the function on the whole line by periodicity. The function so obtained is a solution of (1.26) for every τ.

Now, we already know that

$$s(q_0,0,2\pi) = q_0$$

since the solution of the unperturbed system is constant for the initial data q_0. To prove that there exists one and only one function

$$\eta \mapsto q_\eta$$

defined around $\eta = 0$ and such that

$$s(q_\eta,\eta,2\pi) - q_\eta = \begin{pmatrix} 0 \\ 0 \\ 0 \end{pmatrix}$$

one needs to apply the implicit function theorem. We have to verify that

$$\det\left(D_q s(q_0,0,2\pi) - \mathrm{Id}\right) \neq 0\,. \tag{1.29}$$

From its definition we know that $s(q,0,\cdot)$ is the solution to the problem

$$\begin{cases} \dot{s}(q,0,\tau) = G_0(s(q,0,\tau)) \\ s(q,0,0) = q \end{cases}$$

We can therefore differentiate both members of the previous equations and obtain that

$$\begin{cases} \dfrac{d}{d\tau} D_q s(q_0,0,\tau) = DG_0(q_0) D_q s(q_0,0,\tau) \\ D_q s(q_0,0,0) = \mathrm{Id} \end{cases}$$

From this we have

$$D_q s(q_0,0,2\pi) = e^{2\pi DG_0(q_0)}\,.$$

But then relation (1.29) is verified since all of the eigenvalues of $DG_0(q_0)$ have negative real part. Thanks again to the implicit function theorem we can conclude that the only periodic solution

$$(\eta,\tau) \mapsto s(q_\eta,\eta,\tau)$$

to problem (1.26) is analytic in η being the composition of analytic functions.

The asymptotic stability of the general solution for small enough values of η, which is inherited by the asymptotic stability of the unperturbed one, follows now by applying classical theorems, see [20] (theorem 6.1.3).

Chapter 2

Snake-like Locomotion

Snake locomotion has fascinated natural scientists for a long time. More recently, it has become a topic of great interest as one of the key examples of soft bio-inspired robotics. This is a new and recent paradigm in robotic science [33, 34], whereby inspiration is sought from nature to endow robots with new capabilities in terms of dexterity (e.g., the manipulation abilities of an elephant trunk or of an octopus arm) and adaptability (e.g., the ability of snakes to handle unexpected interactions with unstructured environments and move successfully on uneven terrains by adapting their gait to ground properties that change from place to place in an unpredictable way).

The way snakes move has been the subject of seminal works by Gray [1, 2], see also [35, 3]. In these early studies Gray described the mechanics underlying snake locomotion inside closely fitting channels and on a surface in the presence of external push-points. Subsequently, muscular activity as well as forces transmitted by snakes to arrays of pegs among which they move have been measured [36, 37]. More recently, focus has turned to the importance of anisotropy in the frictional forces between snake ventral skin and flat surfaces on which they move, stimulating both experimental and theoretical research [38, 39, 40, 41, 42].

The idea that frictional anisotropy plays a role in snake locomotion was put forward long ago in the engineering literature [35] and, most notably, by Hirose in his seminal work on robotic snake-like locomotion [44]. Hirose was among the first to call attention on the potential of biological inspiration in designing robots by studying snake-like locomotors and manipulators [44]. Technological advances in this field have led to the development of models for snake robots crafted with more and more jointed active segments, eventually leading to the use of continuum theories [45]. In some more recent contributions [46, 47, 48, 49], Cosserat models are used for the mechanics of slender flexible robots, described as deformable rods.

Inspired by the literature on snake-like locomotion recalled above, in this Chapter we study a model system similar to the one used in [50] in the context of undulatory swimming, and consisting of a planar inextensible elastic rod that is able to control its spontaneous curvature. This is the curvature the rod would exhibit in the absence of external forces, which can be non-zero in the presence of internal actuation (see the sketch in Fig.2.1B). Local control of this quantity provides an internal actuation mechanism that can be used to mimic muscular activity in undulatory locomotion. Travelling waves of spontaneous curvature

can put the system in motion when the environment exerts constraints or forces that the prevent the rod to be deformed everywhere according to its spontaneous curvature.

To show how control of spontaneous curvature in the presence of external constraints leads to locomotion, we use a Cosserat model, and derive the equations of motion for two special cases: one in which the rod can only move along a prescribed curve (prescribed-path case), and one in which the rod is constrained to slide longitudinally without slipping laterally, but the path is not fixed a-priori (free-path case). The first case corresponds to a rod confined in a channel with frictionless walls. The second case is inspired by the slithering motion of snakes, that interact through anisotropic frictional forces with a flat surface on which they are free to move. Frictional resistance is typically larger in the lateral direction than in the longitudinal one. Our setting corresponds to the limiting case of infinite ratio between lateral and longitudinal friction coefficients, in which longitudinal sliding is allowed while lateral slipping is forbidden, as in [42].

Our model is related to the ones studied in [40, 41, 42], with some important differences. We do not allow for lateral slipping and for lifting of portions of the body (hence neglecting the corresponding modulation of frictional forces) as in [40] where, however, the curvature of the visible trajectory is assumed to be known. By contrast, in our model, only the spontaneous curvature (the proxy for muscular activity) is prescribed, and the curvature of the resulting trajectory, which is a-priori unknown, emerges from the solution of the equations of motion. We also do not consider internal viscous dissipations and non-linearities of the longitudinal frictional force, as done in [42] where, however, only periodic solutions are studied (effectively considering a system of infinite length) and the equations are closed by imposing an ansatz on the lateral forces exchanged with the ground surface. By contrast, our model deals with a system of finite length, and the equations are closed by carefully considering edge-effects, which lead to non-standard boundary conditions. Moreover, no a-priori assumptions are made on the reactive forces imposing no lateral slipping, which emerge instead from the solution of the equations of motion.

Our main new results are the following. We formulate direct and inverse locomotion problems (direct: find the motion produced by a given actuation history; inverse: find the actuation history required to produce a given motion), and show existence and uniqueness of the solution of direct problems, non-uniqueness for the inverse ones. Our goal is to study the connection between observed motion, internal actuation, and lateral forces exchanged with the environment, with the aid of a model system (active elastic rod). Our approach delivers explicit analytic formulas that enable us also to explore how this connection is affected by the passive elastic properties of the system (the rod bending stiffness).

In the prescribed-path case, we reduce the dynamics of the system to a single ordinary differential equation for the tail end coordinate (the only degree of freedom for an inextensible rod forced to slide along a given curve). This equation reveals clearly the mechanism by which a flexible rod can actively propel itself inside a channel, whenever the channel exhibits a variation of curvature along its track, and provides a quantitative framework to revisit some of the classical findings on snake motility by Gray. In addition, we provide explicit formulas to calculate the forces exchanged with the environment.

In the free-path case, we are again able to close the equation of motion and reduce the dynamics of the system to a single equation, this time an integro-differential equation for the tail end coordinate. A particularly interesting outcome of our analysis is the emergence of an asymmetry in the mechanical boundary conditions at the (leading) head and the (trailing) tail. This is not only a mathematical subtlety, but it is also deeply grounded in the physics of the problem. While the tail follows the path traced by the preceding interior points, the head is free to veer laterally, 'creating' the path as the motion progresses. We show that the curvature of this newly created path is set by the time history of spontaneous curvatures at the leading head. Recognising this steering role of the spontaneous curvature leads to a procedure to generate solutions for the free-path case from those of the prescribed-path case, based on modifying them near the leading head, in order to account for steering. Again, we provide explicit formulas to calculate the lateral forces transmitted to the ground surface.

The rest of the Chapter is organized as follows. In Section 2.1 we present our mathematical model of flexible robot as an active rod, and formulate direct and inverse locomotion problems. In Section 2.2 we derive the governing equations and the appropriate boundary conditions for motion inside a channel with frictionless walls (prescribed-path), solve them in some simple geometries, and discuss the physical implications of our results. In Section 2.3 we derive the governing equations and corresponding boundary conditions for the motion of an active rod sliding longitudinally without slipping laterally on a flat surface (free-path) and propose a class of analytical serpentine solutions. Possible connections of our results with observations made in the context of biological snake locomotion are briefly summarised in the Discussion section, while the existence and uniqueness of the solution of the equations of motion for the free-path case is proved in the Appendix.

2.1 The flexible robot model

We consider a model consisting of a (long) chain of cross shaped elements (Fig.2.1B) linked together by ideal joints connected by deformable springs. We assume that each spring is able to actively change its rest length (the length at which the tension in the spring is zero). Following [47, 46, 48, 49] we model this system through a continuous description based on the planar Cosserat rod theory.

A configuration of a Cosserat rod of reference length L on the plane is defined by a pair of vector-valued functions

$$[0, L] \times [0, \infty) \ni (s, t) \mapsto \mathbf{r}(s, t)\,,\, \mathbf{b}(s, t) \tag{2.1}$$

where $\mathbf{b}$ is a unit vector (Fig.2.1A). As in [51], we introduce also the unit vector $\mathbf{a} := -\mathbf{e}_3 \times \mathbf{b}$, where $\mathbf{e}_3$ is the unit vector normal to the plane. We then define the *strain* variables ν and η through the following decomposition along the moving orthonormal frame $\{\mathbf{a}, \mathbf{b}\}$

$$\mathbf{r}_s = \nu\mathbf{a} + \eta\mathbf{b}$$

where the subscript s is used to denote the partial derivative with respect to the space variable. The function $\nu = \nu(s, t)$ describes the *stretch*, while $\eta = \eta(s, t)$

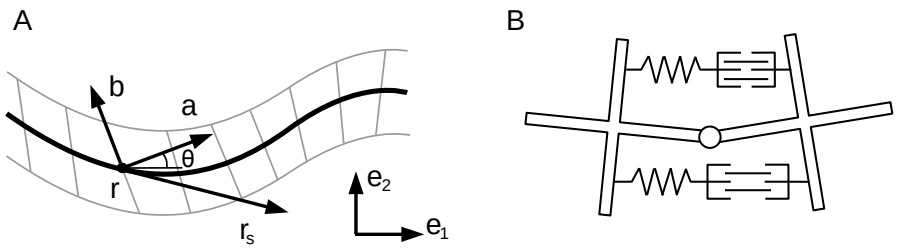

Figure 2.1: A) Variables describing a Cosserat rod configuration. B) Schematic model for the constitutive elements of the robot structure, illustrating a mechanism to produce non-zero curvature in the absence of external forces.

defines the *shear* strain. Finally the *bending* strain $\mu := \theta_s$ is obtained through the scalar valued function $\theta(s,t)$ defined by

$$\mathbf{a}(s,t) = \cos\theta(s,t)\mathbf{e}_1 + \sin\theta(s,t)\mathbf{e}_2$$

where $\{\mathbf{e}_1, \mathbf{e}_2\}$ is a fixed basis in the plane containing the rod. We consider our system as being made of an infinite number of elements like the ones in Fig.2.1B, each of them being of infinitesimal length, and assembled along the central curve $\mathbf{r}$ of the rod. Since we assume them to be rigid, we impose the constraints that the rod is inextensible and unshearable:

$$\nu(s,t) = 1 \quad \text{and} \quad \eta(s,t) = 0\,. \tag{2.2}$$

The ability of the robot to modify the equilibrium length of each of the connecting springs can be naturally modelled macroscopically by considering an elastic rod which can actively vary its spontaneous curvature, namely, the curvature the rod would exhibit in the absence of external loads. This is similar to what is done [50] in the context of swimming motility. We model this by introducing the elastic potential density

$$\mathcal{U}(\mu,s,t) = \frac{EJ}{2}\big(\mu - \alpha(s,t)\big)^2 \tag{2.3}$$

where EJ is the bending stiffness of the robot. Notice that if (2.2) hold, then $\mathbf{r}_s$ always coincides with the unit vector $\mathbf{a}$, and the bending strain $\mu(s,t)$ is equal to the curvature of the rod at the point $\mathbf{r}(s,t)$. The function α in (2.3) therefore can be viewed as the varying spontaneous curvature, which we assume to be freely controllable in order to set the robot in motion. The bending moment resulting from (2.3) is

$$M = EJ\big(\mu - \alpha\big) = EJ\theta_s + M^a \tag{2.4}$$

and can be seen as the sum of a passive elastic term $EJ\theta_s$ and of an active one $M^a := -EJ\alpha$ which can be varied at will by suitably tuning α. An active moment originating from muscular contraction is used also in the model of snake locomotion in [42].

Along with the elastic potential we define also the kinetic energy density

$$\mathcal{T}(\mathbf{r}_t, \theta_t) = \frac{\rho A}{2}\,\mathbf{r}_t \cdot \mathbf{r}_t + \frac{\rho J}{2}\,\theta_t^2$$

where the subscript t denotes the partial derivative with respect to time, ρA is the linear mass density and ρJ the linear moment of inertia. Finally, the Lagrangian density $\mathcal{L}$ of the system reads

$$\mathcal{L} = \mathcal{T} - \mathcal{U} - N(\nu - 1) - H\eta \tag{2.5}$$

where $N = N(s,t)$ and $H = H(s,t)$ are the reactive internal tractions (axial tension and shear force, respectively) enforcing constraints (2.2).

In the following sections, we will consider two types of locomotion problems arising form the interaction of prescribed spontaneous curvature and external constraints. The direct one can be formulated as follows: given a time history of spontaneous curvatures $\alpha(s,t)$, together with initial and boundary conditions, find the motion $\mathbf{r}(s,t)$ of the rod and the forces it exchanges with the environment. In the inverse one, the motion is prescribed, and we want to find a history $\alpha(s,t)$ that produces it, together with the corresponding forces. We will consider two types of external constraints and see that, in both cases, the direct problem has unique solution while, for the inverse one, the solution is not unique.

2.2 The case of prescribed path: sliding inside a channel

The first problem we consider is motion along a prescribed path. We place our robot model inside a curved channel fitting exactly its body, assuming that there is no friction between the walls of the channel and the active rod itself. We model such a setting by imposing the external (holonomic) constraint

$$\mathbf{r} \in \mathrm{Graph}\,\{\mathbf{\Gamma}\} \quad \text{or} \quad \phi_\Gamma(\mathbf{r}) = 0 \tag{2.6}$$

where the equation $\phi_\Gamma = 0$ defines (we assume, globally) the curve $\mathbf{\Gamma}$ which we interpret as the central line of the channel. There is no loss of generality in assuming $|\nabla\phi_\Gamma| = 1$.

2.2.1 Derivation of the equations of motion

We derive the equations of motion through Hamilton's Principle, adding to (2.5) an external reactive potential $-f\phi_\Gamma(\mathbf{r})$, where $f = f(s,t)$ is the Lagrange multiplier enforcing (2.6). A solution $(\mathbf{r},\theta)$ must satisfy

$$\delta \int_{t_1}^{t_2} \int_0^L \mathcal{L} - f\phi_\Gamma(\mathbf{r})\; ds dt = 0 \tag{2.7}$$

for every variations $\delta\mathbf{r}$ and $\delta\theta$ defined on $[0,L]\times[t_1,t_2]$ and vanishing at its boundary. If we define $\mathbf{n} := N\mathbf{a} + H\mathbf{b}$, the Euler-Lagrange equations we obtain from (2.7) are

$$\mathbf{n}_s - f\,\nabla\phi_\Gamma(\mathbf{r}) = \rho A\,\mathbf{r}_{tt} \quad , \quad M_s\,\mathbf{e}_3 + \mathbf{r}_s \times \mathbf{n} = \rho J\theta_{tt}\mathbf{e}_3$$

where the bending moment M is defined in (2.4). These are the classical dynamical equations for a planar Cosserat rod (see e.g. [51]) with an external force

given, in our case, by the transversal reaction imposing the constraint (2.6). The presence of a longitudinal frictional force per unit length

$$\mathbf{F}^{//} = -\gamma^{//}\frac{\mathbf{r}_s}{|\mathbf{r}_s|}\mathrm{Sgn}(\mathbf{r}_t \cdot \mathbf{r}_s)\,, \tag{2.8}$$

is handled by simply adding $\mathbf{F}^{//}$, where Sgn denotes the sign function, to the left hand side of the first equation.

To close the equations of motion we use the Principle of Mechanical Boundary Conditions (from now on: PoMBC) [52]. We define *generalized* edge loads acting on the system by considering the rate at which work is expended at the edges in virtual motions compatible with the constraints, and assume that all *generalized* edge loads acting on the system are explicitly prescribed.

In view of (2.6), we have that

$$\mathbf{r}(0,t) = \mathbf{\Gamma}(s_0(t))\ ,\ \mathbf{r}(L,t) = \mathbf{\Gamma}(s_L(t))\ ,\ \theta(0,t) = \Theta(s_0(t))\ ,\ \theta(L,t) = \Theta(s_L(t)) \tag{2.9}$$

where s_0 and s_L are the curvilinear coordinates relative to $\mathbf{\Gamma}$ of the two ends of the rod, which we call *generalized edge coordinates*, and Θ is the angle between the tangent vector to $\mathbf{\Gamma}$ and $\mathbf{e}_1$, so that

$$\mathbf{\Gamma}(\xi) = \mathbf{\Gamma}(\xi_0) + \int_{\xi_0}^{\xi} \cos\Theta(\lambda)\mathbf{e}_1 + \sin\Theta(\lambda)\mathbf{e}_2\ d\lambda\,. \tag{2.10}$$

Now, following the PoMBC, we write the work rate P_{edge} of the edge loads as

$$P_{\mathrm{edge}} = \mathbf{n}(s,t)\cdot\mathbf{r}_t(s,t)\Big|_{s=0}^{s=L} + M(s,t)\theta_t(s,t)\Big|_{s=0}^{s=L}\,. \tag{2.11}$$

Using (2.9) to derive the expressions for $\mathbf{r}_t$ and θ_t at $s = 0, L$ we obtain

$$\begin{aligned} P_{\mathrm{edge}} = {} & \dot{s}_L(t)\Big(\mathbf{n}(L,t)\cdot\mathbf{\Gamma}_s(s_L(t)) + M(L,t)k(s_L(t))\Big) \\ & - \dot{s}_0(t)\Big(\mathbf{n}(0,t)\cdot\mathbf{\Gamma}_s(s_0(t)) + M(0,t)k(s_0(t))\Big) \end{aligned}$$

where we used a "dot" to denote the time derivative of the generalized coordinates, and k is the curvature of $\mathbf{\Gamma}$. The coefficients multiplying the *generalized velocities* $\dot{s}_0(t)$ and $\dot{s}_L(t)$ are the *generalized edge loads* which, by the PoMBC, have to be prescribed. Since we suppose that no external edge forces are doing work on the system at either of the two ends, we enforce the condition $P_{\mathrm{edge}} = 0$ by setting such loads equal to zero.

Finally, conditions (2.2) and (2.6) must be added to the equations of the system. Since the active rod is assumed to be inextensible and unshearable, and its backbone curve $\mathbf{r}$ is forced inside the graph of $\mathbf{\Gamma}$, the constrained system can be described with only one degree of freedom, namely, the curvilinear coordinate relative to $\mathbf{\Gamma}$ of the first end of the robot model. Thus,

$$\mathbf{r}(s,t) = \mathbf{\Gamma}(s_0(t)+s) \quad , \quad \theta(s,t) = \Theta(s_0(t)+s) \tag{2.12}$$

and substituting these expressions in the equations of motion we obtain, accounting also for longitudinal friction,

$$N_s - kH - \gamma^{//}\mathrm{Sgn}(\dot{s}_0(t)) = \rho A\,\ddot{s}_0(t) \tag{2.13}$$

$$kN + H_s - f = \rho A\,k\dot{s}_0(t)^2 \tag{2.14}$$

$$EJ(k_s - \alpha_s) + H = \rho J(k\ddot{s}_0(t) + k_s\dot{s}_0(t)^2) \tag{2.15}$$

where $k = k(s_0(t) + s)$. As for the boundary conditions, they now read

$$\begin{aligned} &N(0,t) + EJ\big(k(s_0(t)) - \alpha(0,t)\big)k(s_0(t)) = 0\,, \\ &N(L,t) + EJ\big(k(s_0(t)+L) - \alpha(L,t)\big)k(s_0(t)+L) = 0\,. \end{aligned} \tag{2.16}$$

Summarizing, in order to solve the (direct) locomotion problem stated at the end of Section 2.1, we need to find the unknown functions $N(s,t)$, $H(s,t)$, $f(s,t)$ and $s_0(t)$. The equations we have for this purpose are the three equations of motion (2.13)-(2.14)-(2.15), and the two boundary conditions (2.16). We'll see that, by integrating (2.13), a first order ordinary differential equation (ODE), and using the two boundary conditions (2.16), we can derive an additional ODE containing the only unknown $s_0(t)$, which completely determines the motion of the system. This ODE is given below as equation (2.18), or (2.19) in a simplified version. Once s_0 is known, we can use (2.15), (2.13) and (2.14), together with the boundary condition (2.16) holding at $s = 0$, to determine H, N, and f respectively.

We show now how to obtain the ODE for $s_0(t)$. If we substitute in (2.13) the expression of H given by (2.15) then, integrating on the space variable, we have

$$\begin{aligned} m\ddot{s}_0 &= N\Big|_0^L + EJ\int_0^L (k_s - \alpha_s)k\,ds - \gamma'' \mathrm{Sgn}(\dot{s}_0)L - \rho J\,R - \rho J\,Q\ddot{s}_0 \\ &= N\Big|_0^L + EJ(k-\alpha)k\Big|_0^L - EJ\int_0^L (k-\alpha)k_s\,ds - \gamma'' \mathrm{Sgn}(\dot{s}_0)L - \rho J\,R - \rho J\,Q\ddot{s}_0 \end{aligned}$$

where $m = \int_0^L \rho A ds$ is the total mass of the rod,

$$\begin{aligned} R(\dot{s}_0(t), s_0(t)) &= \frac{\dot{s}_0(t)^2}{2}\left(k^2(s_0(t)+L) - k^2(s_0(t))\right) \\ \text{and} \quad Q(s_0(t)) &= \int_0^L k^2(s_0(t)+s)ds\,. \end{aligned} \tag{2.17}$$

If we now apply (2.16) we obtain the equation

$$\begin{aligned} \big(m + \rho J\,Q(s_0(t))\big)\,\ddot{s}_0(t) \;=\; & \frac{EJ}{2}\left(k^2(s_0(t)) - k^2(s_0(t)+L)\right) - \gamma'' \mathrm{Sgn}(\dot{s}_0(t))L \\ & -\gamma'' \mathrm{Sgn}(\dot{s}_0(t))L - \rho J\,R(\dot{s}_0(t), s_0(t)) \\ & +EJ\int_0^L \alpha(s,t)\,k_s(s_0(t)+s)\,ds \end{aligned} \tag{2.18}$$

which, complemented with initial position and velocity, defines s_0 uniquely. The shear force H is now uniquely defined by (2.15), while

$$\begin{aligned} N(s,t) = \int_0^s \{\rho A\,\ddot{s}_0(t) + \gamma'' \mathrm{Sgn}(\dot{s}_0(t)) + k(s_0(t)+\lambda)H(\lambda,t)\}\,d\lambda \\ - EJ\big(k(s_0(t)) - \alpha(0,t)\big)k(s_0(t))\,. \end{aligned}$$

Using all the expressions above we can recover f from (2.14).

Let us now suppose that our active rod is stiff and slender enough, so that $EJ, \rho A \gg \rho J$. We can then neglect the terms containing ρJ in (2.18), obtaining

the simplified equation

$$m\ddot{s}_0(t) = \frac{EJ}{2}\left(k^2(s_0(t)) - k^2(s_0(t)+L)\right) - \gamma'' \mathrm{Sgn}(\dot{s}_0(t))L + EJ\int_0^L \alpha(s,t)\, k_s(s_0(t)+s)\, ds\,. \tag{2.19}$$

Equation (2.19) shows that the dynamics of the robot model is reduced to that of a point particle of mass m subjected to a force given by the sum of three terms. The first one is a "potential" force depending exclusively on the geometry of $\mathbf{\Gamma}$, the second one is a friction term, while the third is an "active" force which depends on the spontaneous curvature α. The following examples illustrate the role played by these terms in the dynamics of the system.

2.2.2 Spiral channel

Let us consider only the first term in the right hand side of (2.19) by setting $\alpha, \gamma'' = 0$. The system described in this case is a passive elastic rod with straight rest configuration placed inside a curved channel with frictionless walls. Because of inextensibility, the driving force on the rod depends only on the curvature of the channel at the two ends of the body. Moreover, the sign of this force is such that the rod is always pushed towards the region of smaller curvature. As an example, consider the case of a spiral-shaped channel where $k(s) = K/s$, with $K > 0$ (see Fig.2.2). Then (2.19) with $\alpha = 0$ reads

$$m\ddot{s}_0(t) = -U'(s_0(t)) \quad \text{where} \quad U(s_0) = \frac{EJLK^2}{2(s_0+L)s_0}\,.$$

In order to thread the rod inside the spiral by varying the coordinate of the end point from ξ_2 to ξ_1 we need to perform a positive work

$$W = U(\xi_1) - U(\xi_2) = \frac{EJ}{2}\left(\frac{LK^2}{(\xi_1+L)\xi_1} - \frac{LK^2}{(\xi_2+L)\xi_2}\right) > 0 \tag{2.20}$$

since we have to increase the curvature at every point of the body. If we then release the rod it will accelerate towards the exit and return back to ξ_2 with a positive velocity

$$V = \sqrt{\frac{EJ}{m}\left(\frac{LK^2}{(\xi_1+L)\xi_1} - \frac{LK^2}{(\xi_2+L)\xi_2}\right)} > 0\,. \tag{2.21}$$

In other words, the system moves towards a "straighter" configuration, decreasing its elastic energy and therefore increasing its kinetic energy. Similar problems of passive elastic rods sliding inside frictionless sleeves have been studied, both analytically and experimentally, in [53].

Let us suppose now that $\alpha, \gamma'' \neq 0$. The active force term in (2.19) can assume any value if we suppose that we have no restrictions in the choice of α. This means, in particular, that an active elastic rod can slide *inside* the spiral without need of external pushing. More generally, the system can achieve motion in a predetermined direction when placed inside any channel which does not present circular or straight sections of length greater than L. This last

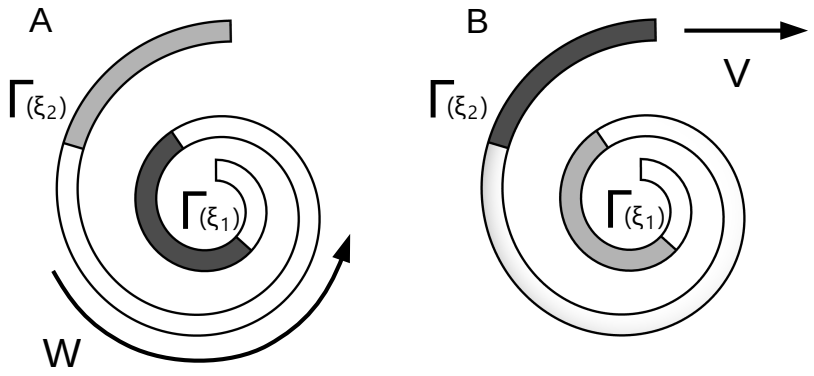

Figure 2.2: A) Two configurations of the elastic rod inside a spiral channel: initial (light grey) and final (dark grey). A positive work W is necessary to vary the position of the end point from $\mathbf{\Gamma}(\xi_2)$ to $\mathbf{\Gamma}(\xi_1)$ and force the rod inside the channel. B) Upon release, the first end point slides back from $\mathbf{\Gamma}(\xi_1)$ to $\mathbf{\Gamma}(\xi_2)$ and the rod exits the channel with velocity V.

result is reminiscent of theoretical and experimental findings of J. Gray in his study [1] of snake undulatory locomotion. Using an energy balance argument, he concludes that it is possible for a snake to slide inside a channel closely fitting its body only provided such a channel exhibits a variation of curvature along its track. He then shows experimentally that snakes are able to move in sinusoidal closely fitting channels, but motion in straight ones only occurs through a different gait (concertina), which is impossible if the width of the channel and of the snake body are comparable.

2.2.3 Sinusoidal channel

We address in this section an inverse locomotion problem. Let us consider a sinusoidal channel meandering around the horizontal axis

$$\mathbf{\Gamma}(\xi) = \int_0^{\xi} \cos\Theta\mathbf{e}_1 + \sin\Theta\mathbf{e}_2 \quad \text{where} \quad \Theta(\xi) = -\zeta\lambda\cos\left(\frac{\xi}{\lambda}\right) \tag{2.22}$$

and therefore

$$k(\xi) = \zeta\sin\left(\frac{\xi}{\lambda}\right). \tag{2.23}$$

For small values of the geometric parameter ζ, the channel is close to a straight tube while, as ζ grows, it becomes wavier and wavier. The wavelength λ dictates how many turns the channel has per unit length.

We want to find a history of spontaneous curvatures $\alpha(s,t)$ that produces motion along the sinusoidal channel (2.22) with constant longitudinal velocity

$$\dot{s}_0(t) = V > 0\,.$$

Assuming that the trailing edge of the active rod lies at the origin at $t = 0$, we must have $s_0(t) = Vt$. If we also assume that $L = 2\pi n\lambda$, where n is a positive

integer, then the potential term in equation (2.19) vanishes, and constant forward motion is realized only if the active force exactly matches the frictional one:

$$\gamma'' L = EJ \int_0^L \alpha(s,t) k_s(s+Vt) ds = \frac{EJ\zeta}{\lambda} \int_0^L \alpha(s,t) \cos\left(\frac{s+Vt}{\lambda}\right) ds\,. \quad (2.24)$$

Once we find a function α that solves (2.24) then $s_0(t) = Vt$ becomes automatically a solution for the equations of motion, and N, H and f can be explicitly written following the procedure illustrated in the previous section.

To show non-uniqueness of solution of this inverse locomotion, we generate two different solutions α by solving two constrained minimization problems. Among all α's satisfying (2.24), find the ones that minimizes either I_{bend} (the bending energy) or I_{act} (the activity), where

$$I_{\text{act}}[\alpha] = \frac{1}{2} \int_0^L \alpha^2(s,t)\, ds \ , \ I_{\text{bend}}[\alpha] = \frac{EJ}{2} \int_0^L \left(k(s+Vt) - \alpha(s,t)\right)^2 ds\,.$$

To solve, e.g., the second problem we consider the extended functional

$$\hat{I}_{\text{bend}}[\alpha; q] := I_{\text{bend}}[\alpha] + q \int_0^L \alpha(s,t) k_s(s+Vt)\, ds$$

where q is the Lagrange multiplier enforcing (2.24). The spontaneous curvature α_{bend} minimizing $\hat{I}_{\text{bend}}$ must then solve $\delta \hat{I}_{\text{bend}}[\alpha_{\text{bend}}; q] = 0$, where the variation of the extended functional is taken with respect to α. A straightforward calculation gives

$$\alpha_{\text{bend}}(s,t) = \frac{q}{EJ} k_s(s+Vt) + k(s+Vt)\,, \quad q = \frac{\gamma'' L}{\int_0^L k_s^2(s+Vt) ds} \quad (2.25)$$

where the second equality is obtained by plugging the expression for α_{bend} in (2.24). More explicitly, using (2.23), we get

$$\alpha_{\text{bend}}(s,t) = \zeta \sin\left(\frac{s+Vt}{\lambda}\right) + \frac{q}{EJ} \cos\left(\frac{s+Vt}{\lambda}\right) \quad \text{with} \quad q = \frac{\gamma'' L}{n\pi\zeta}\,.$$

From the equations of motion and the boundary conditions, taking again $\rho J = 0$, we then obtain

$$H_{\text{bend}} = -\frac{2\gamma''}{\zeta} \sin\left(\frac{s+Vt}{\lambda}\right), \quad N_{\text{bend}} = \frac{\gamma'' L}{4\pi n}\left(\sin 2\left(\frac{s+Vt}{\lambda}\right) + \sin 2\,\frac{Vt}{\lambda}\right)$$

and

$$\begin{aligned} f_{\text{bend}}(s,t) \ &= \ \gamma'' \frac{\zeta L}{4\pi n}\left(\sin 2\left(\frac{s+Vt}{\lambda}\right) + \sin 2\,\frac{Vt}{\lambda}\right) \sin\left(\frac{s+Vt}{\lambda}\right) \\ &\quad - \gamma'' \frac{4\pi n}{\zeta L} \cos\left(\frac{s+Vt}{\lambda}\right) - \rho A V^2 \zeta \sin\left(\frac{s+Vt}{\lambda}\right). \end{aligned}$$

Notice that none of the external and internal forces depend on the bending stiffness EJ. This allows us to consider the rigid limit $EJ \to \infty$, for which the observable motion and forces do not vary, while on the other hand $\alpha_{\text{bend}}(s,t) \to k(s+Vt)$. This limit case could be relevant for the steering of wheeled robots in which curvature control is achieved through internal motors.

Let us find $\alpha_{\rm act}$ that minimizes $I_{\rm act}$ by repeating the procedure above. We obtain in this case that the optimal α is proportional to k_s, whereby internal actuation is concentrated around inflexion points of the trajectory. This is reminiscent of patterns of muscular activity patterns observed in snake undulatory locomotion [36, 37]. More in detail,

$$\alpha_{\rm act}(s,t) = \frac{q}{EJ} k_s(s+Vt) = \frac{q}{EJ}\cos\left(\frac{s+Vt}{\lambda}\right), \tag{2.26}$$

with q given again by (2.25). In order to compare the two solutions we write

$$H_{\rm act}(s,t) = H_{\rm bend}(s,t) - EJ\,\frac{2\pi n}{L}\cos\left(\frac{s+Vt}{\lambda}\right),$$
$$N_{\rm act}(s,t) = N_{\rm bend}(s,t) + EJ\,\frac{\zeta^2}{4}\Big(\cos 2\left(\frac{s+Vt}{\lambda}\right) + \cos 2\,\frac{Vt}{\lambda}\Big)$$

and

$$\begin{aligned} f_{\rm act}(s,t) \;&=\; f_{\rm bend}(s,t) + EJ\left(\frac{2\pi n}{L}\right)^2 \zeta \sin\left(\frac{s+Vt}{\lambda}\right) \\ &\quad + EJ\,\frac{\zeta^3}{4}\Big(\cos 2\left(\frac{s+Vt}{\lambda}\right) + \cos 2\,\frac{Vt}{\lambda}\Big)\sin\left(\frac{s+Vt}{\lambda}\right) \end{aligned}$$

for internal and external forces generated by $\alpha_{\rm act}$, in terms of the corresponding quantities we found for $\alpha_{\rm bend}$. We observe that the two force fields differ by terms proportional to EJ, while they become indistinguishable when $EJ \to 0$.

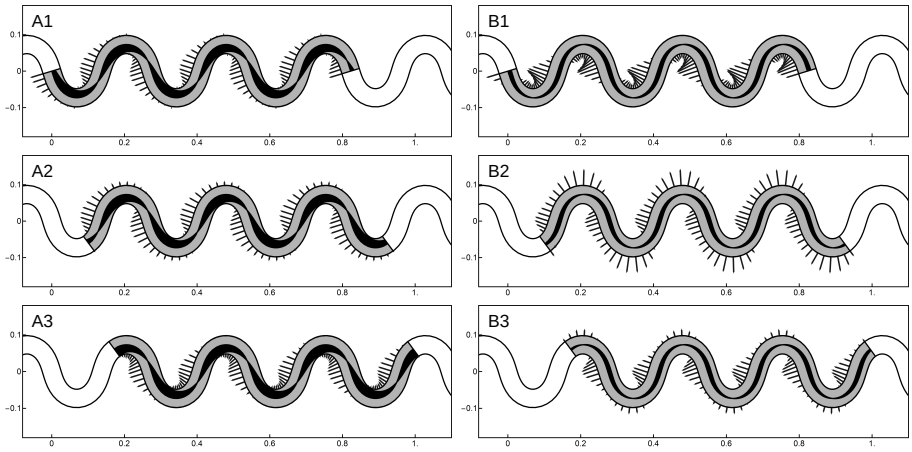

Figure 2.3: Snapshots for solution generated by A) $\alpha_{\rm bend}$ and B) $\alpha_{\rm act}$ at three times: 1) $Vt/\lambda = 0$, 2) $Vt/\lambda = 2\pi/3$ and 3) $Vt/\lambda = 4\pi/3$. Grey segments indicate the magnitude of the transversal force exerted by the active rod on the channel. Spontaneous curvatures are represented through the shaded areas along the rod's body.

We give here a graphical representation of the two solutions, using material parameters taken from the zoological literature. Based on [37] we set $L = 1.3$m and $\gamma^{//} = \mu^{//} mg/L$, where $\mu^{//} = 0.2$ is the longitudinal friction coefficient, $m = 0.8$kg and g is the gravitational acceleration constant. Following [40],

we neglect the inertial terms in all the expressions setting $\rho A V^2 = 0$. As for the bending stiffness, we can explore a range going from $EJ = 10^{-4}\mathrm{Nm}^2$ [54] to $EJ = 10^{-3}\mathrm{Nm}^2$ [42].

Results are shown in Fig.2.3. We set (arbitrarily) $n = 3$ and $\zeta = 18.5\mathrm{m}^{-1}$, while we choose the largest value of EJ in order to emphasises the difference between the two solutions. Segments indicate the direction and magnitude of the force exerted by the robot on the walls of the channel. The pattern and amplitude of spontaneous curvatures are indicated by the dark shaded area along the midline of the robot's body. The two solutions give very different results in terms of forces exerted on the channel walls. The force field f_{bend} consistently displays maxima in magnitude near the inflection points of curvature. On the other hand, f_{act} varies substantially during motion: at some times it displays local maxima at the points of maximal concavity and convexity, while at some other times maxima are located at the inflection points. Notice that at points of maximal concavity and convexity f is perpendicular to the direction of motion and does not contribute to the propulsive forces. We will comment further on these features in the next sections.

2.3 The free-path case

We now turn to the case in which the path is not a-priori known and study an active rod free to move on a flat surface through longitudinal sliding without lateral slipping. Accordingly, we impose the (non-holonomic) constraint

$$\mathbf{r}_s^{\perp} \cdot \mathbf{r}_t = 0 \tag{2.27}$$

where $\mathbf{r}_s^{\perp} = \mathbf{e}_3 \times \mathbf{r}_s$. We denote by $-f\,\mathbf{r}_s^{\perp}$ the transversal reactive force per unit length (exerted by the ground on the rod) enforcing the no-slip condition, where f is the Lagrange multiplier associated with constraint (2.27). At the same time, we suppose that a frictional force $\mathbf{F}^{//}$ given by (2.8) acts in the longitudinal direction.

Real snakes [38, 39, 40], as well as real snake-like robots [44], cannot rely on transversal frictional reactions of arbitrary magnitude to prevent lateral slipping. Solutions of interest for the realistic description of these systems can be considered, for instance, those for which the reactive force f imposing constraint (2.27) does not exceed a maximum value, which can be determined experimentally.

2.3.1 Derivation of the equations of motion

We deduce the equations of motion through the Lagrange-d'Alembert principle, similarly to what is done in [55] and [56]. The principle states that, in the presence of the dissipative force $\mathbf{F}^{//}$, a solution $(\mathbf{r}, \theta)$ that satisfies constraint (2.27) must solve

$$\delta \int_{t_1}^{t_2} \int_0^L \mathcal{L}\, ds dt + \int_{t_1}^{t_2} \int_0^L \mathbf{F}^{//} \cdot \delta\mathbf{r}\, ds dt = 0 \tag{2.28}$$

for every variations $\delta\mathbf{r}$ and $\delta\theta$ that vanish at the boundary of $[0, L] \times [t_1, t_2]$, while $\delta\mathbf{r}$ also satisfy

$$\mathbf{r}_s^{\perp} \cdot \delta\mathbf{r} = 0\,. \tag{2.29}$$

Calculating the variation on the left hand side of (2.28), after integration by parts and reordering, we have

$$\delta \int_{t_1}^{t_2} \int_0^L \mathcal{L}\, ds dt + \int_{t_1}^{t_2} \int_0^L \mathbf{F}^{//} \cdot \delta\mathbf{r}(s,t)\, ds dt =$$
$$\int_{t_1}^{t_2} \int_0^L \left\{-\rho A\, \mathbf{r}_{tt} + (\widetilde{N}\mathbf{a})_s + (\widetilde{H}\mathbf{b})_s + \mathbf{F}^{//}\right\} \cdot \delta\mathbf{r}\, ds dt$$
$$+ \int_{t_1}^{t_2} \int_0^L \left\{-\rho J \theta_{tt} + EJ(\theta_{ss} - \alpha_s) + (\nu\widetilde{H} - \eta\widetilde{N})\right\} \delta\theta\, ds dt$$

Since (2.28) holds for all the variations satisfying (2.29), it forces the coefficient multiplying $\delta\theta$ to vanish, while the coefficient relative to $\delta\mathbf{r}$ must take the form $f\mathbf{r}_s^{\perp}$, where $f = f(s,t)$ is the unknown Lagrange multiplier enforcing constraint (2.27). The equations of motion then read

$$\mathbf{n}_s + \mathbf{F}^{//} - f\mathbf{r}_s^{\perp} = \rho A\, \mathbf{r}_{tt} \quad , \quad M_s\, \mathbf{e}_3 + \mathbf{r}_s \times \mathbf{n} = \rho J \theta_{tt} \mathbf{e}_3$$

We complement these equations with boundary conditions by relying again on the PoMBC.

Let us consider a typical configuration of the robot model in motion while subjected to the external constraint (2.27). We suppose that such a movement is directed head-first, where we denote the head as $\mathbf{r}(L,t)$ and the tail as $\mathbf{r}(0,t)$. As shown in Fig.2.4A, an asymmetry between head and tail emerges. Because of (2.27), the tail position and director can change only by assuming the values previously taken at an adjacent internal point. We can therefore impose on $s = 0$ the same conditions we had in the channel case, namely,

$$\mathbf{r}_t(0,t) = v_0(t)\, \mathbf{r}_s(0,t) \quad \text{and} \quad \theta_t(0,t) = v_0(t) k(0,t)$$

where v_0 is the (only) generalized velocity at $s = 0$ and $k(0,t)$ is the curvature of $\mathbf{r}$ evaluated in $s = 0$ at time t. As for the head configuration, since the path is no longer predetermined, we have an extra degree of freedom. Condition (2.27) requires $\mathbf{r}_t$ and $\mathbf{r}_s$ to be collinear, therefore this extra degree of freedom must come from the rotation of the director. We then impose

$$\mathbf{r}_t(L,t) = v_L(t)\, \mathbf{r}_s(L,t) \quad \text{and} \quad \theta_t(L,t) = \omega_L(t)$$

where v_L and ω_L are the generalized velocities for the system at $s = L$. The work rate of the external edge forces is

$$P_{\text{edge}} = \mathbf{n}(L,t) \cdot \mathbf{r}_s(L,t) v_L(t) + M(L,t)\omega_L(t)$$
$$- \Big(\mathbf{n}(0,t) \cdot \mathbf{r}_s(L,t) + M(0,t)k(0,t)\Big) v_0(t)\,.$$

Thus, there are two generalized edge loads at $s = L$, namely, the axial tension $\mathbf{n} \cdot \mathbf{r}_s$ and the bending moment M, and one at $s = 0$, with the same expression it had in the channel case. We prescribe that they vanish because, just like in the previous section, we suppose that no external edge force is doing work on the system.

Alongside with the boundary conditions coming from the vanishing of the generalized edge loads, the system must be complemented with equations (2.2) and (2.27).

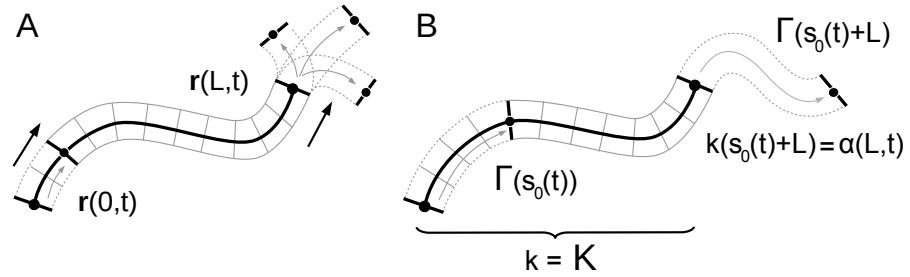

Figure 2.4: A) Sketch of the system moving while subjected to the constraint (2.27). Arrows indicate the direction of motion. Tail position and director change by assuming the values taken previously at an internal point. The head configuration has an extra degree of freedom, since it is allowed to turn freely. B) Motion generated by a given spontaneous curvature history $\alpha(s,t)$. The curvature of the path at the leading edge is determined by the spontaneous curvature at $s = L$.

The non-holonomic constraint (2.27) compels the active rod to move within a curve in the plane, much like it was for the channel case in the previous section. This time, however, the path is not a-priori determined but is created during the motion, and it is an unknown of the problem. In fact, constraints (2.2) and (2.27) lead to the existence of some function s_0 and *some* curve $\mathbf{\Gamma}$, which have *both* to be determined, such that (2.12) holds. Since the boundary conditions we derived hold only for head-first motions, we only consider solutions satisfying

$$\dot{s}_0(t) > 0\,. \tag{2.30}$$

The equations of motion written in components are formally identical to the ones derived for the channel case

$$N_s - kH - \gamma'' = \rho A\,\ddot{s}_0(t) \tag{2.31}$$

$$kN + H_s - f = \rho A\,k\,\dot{s}_0(t)^2 \tag{2.32}$$

$$EJ(k_s - \alpha_s) + H = \rho J(k\,\ddot{s}_0(t) + k_s\,\dot{s}_0(t)^2) \tag{2.33}$$

but $k = k(s_0(t) + s)$ is no longer predetermined. On the other hand, the equations are closed through the boundary conditions obtained by setting the three generalized edge loads to zero

$$\begin{aligned} &N(0,t) + EJ\big(k(s_0(t)) - \alpha(0,t)\big)k(s_0(t) = 0\,,\\ &N(L,t) = 0\,,\ \ EJ\big(k(s_0(t) + L) - \alpha(L,t)\big) = 0 \end{aligned} \tag{2.34}$$

together with the initial curvature $k(s_0(t_0) + s) = K(s)$, with $s \in [0, L]$, and the initial values for s_0 and $\dot{s}_0$ at $t = t_0$. Such values must satisfy the compatibility relations

$$\dot{s}_0(t_0) > 0 \quad , \quad K(L) = \alpha(L, t_0) \quad \text{and} \quad K_s(L)\dot{s}_0(t_0) = \dot{\alpha}(L, t_0)\,. \tag{2.35}$$

In order to solve the locomotion problem, we need to find the unknown functions $N(s,t)$, $H(s,t)$, $f(s,t)$, together with $s_0(t)$ and $k(s_0(t) + s)$. The

three equations of motion and the three boundary conditions (2.34) are sufficient to solve this problem uniquely. This leads to a unique solution also for $\mathbf{r}$ and θ, once the initial position $\mathbf{r}(0,t_0)$ and orientation $\theta(0,t_0)$ of the first end are prescribed, by integrating the equations $\theta_s = k$ and $\mathbf{r}_s = \mathbf{\Gamma}$ as done, e.g., in [40, 41]. The detailed proof is provided in the Appendix, and we only sketch here the heuristic argument behind it.

A key role is played by the third boundary condition in (2.34), coming from the vanishing of the bending moment at the leading edge. This latter condition, namely,

$$k(s_0(t)+L) = \alpha(L,t) \tag{2.36}$$

assigns a crucial role to the spontaneous curvature at the leading edge in determining the path followed by the system. Thus, the value of α at $s = L$ operates as a "steering wheel" while the internal values of the spontaneous curvature supply the active force for propulsion, as it was for the channel case.

Let us see how s_0 and k can be determined. There is no loss of generality if we take $t_0 = 0$ and $s_0(0) = 0$. On the other hand, let us assume $\dot{s}_0(t) > 0$ for $t \in [0, t^*)$ so that s_0 is invertible in the whole interval, and let's also assume that t^* is small enough so that $s_0(t) < L$ for every t. Clearly, $k(s) = K(s)$ is known for $s \in [0, L]$ from the initial condition. For $s > L$ we can recover k from the history of spontaneous curvatures at the leading edge because each point of the path $\mathbf{\Gamma}(\xi)$ with $\xi > L$ generated between t_0 and t^* is the location of the leading edge at some time $s_0^{-1}(\xi - L)$, see Fig.2.3B. Thus, setting

$$k(\xi) := \begin{cases} K(\xi) & \text{if } 0 \le \xi \le L \\ \alpha(L, s_0^{-1}(\xi - L)) & \text{if } \xi \ge L \end{cases} \tag{2.37}$$

we can recover $k(s_0(t)+s)$ from the initial conditions, the given α and the knowledge of s_0. In turn, s_0 can be determined by substituting the expression for H given by (2.33) into (2.31) and integrating with respect to s. Using (2.34), we deduce

$$\begin{aligned} \big(m + \rho J\, Q(s_0(t))\big)\, \ddot{s}_0(t) \;=\; & \frac{EJ}{2}\big(k^2(s_0(t)) - k^2(s_0(t)+L)\big) \\ & -\gamma'' L - \rho J\, R(\dot{s}_0(t), s_0(t)) \\ & +EJ \int_0^L \alpha(s,t)\, k_s(s_0(t)+s)\, ds \end{aligned} \tag{2.38}$$

where R and Q are given by (2.17). Moreover, using (2.37) and the change of variable $s = \xi - s_0(t)$, the last integral in (2.38) can be written as the sum

$$\int_{s_0(t)}^{L} \alpha(\xi - s_0(t), t)\, K_s(\xi)\, d\xi + \int_{L}^{L+s_0(t)} \alpha(\xi - s_0(t), t)\, k_s(\xi)\, d\xi$$

The second summand in the last expression can be rewritten further, using the change of variable $\xi = s_0(\tau) + L$, as

$$\begin{aligned} \int_{L}^{L+s_0(t)} \alpha(\xi - s_0(t), t)\, k_s(\xi)\, d\xi \;&=\; \int_0^t \alpha(s_0(\tau) - s_0(t) + L, t)\, k_s(s_0(\tau)+L)\dot{s}_0(\tau)\, d\tau \\ &=\; \int_0^t \alpha(s_0(\tau) - s_0(t) + L, t)\, \dot{\alpha}(L,\tau)\, d\tau \end{aligned}$$

where we have used the identity $k_s(s_0(t)+L)\dot{s}_0(t) = \dot{\alpha}(L,t)$ following from (2.36). Finally, observing that in view of our assumption $s_0(t) < L$ we have $k(s_0(t)) = K(s_0(t))$ and $k(s_0(t)+L) = \alpha(L,t)$, also

$$R = \frac{\dot{s}_0(t)^2}{2}\left(\alpha^2(L,t) - K^2(s_0(t))\right) \quad \text{and}$$
$$Q = \int_{s_0(t)}^{L} K^2(\xi)d\xi + \int_0^t \alpha^2(L,\tau)\dot{s}_0(\tau)\,d\tau\,.$$

Equation (2.38) is in fact

$$\begin{aligned}\left(m+\rho J\,Q\right)\ddot{s}_0(t) = \frac{EJ}{2}\left(K^2(s_0(t)) - \alpha^2(L,t)\right) - \gamma'' L \\ - \rho J\,R + EJ\int_{s_0(t)}^{L}\alpha(\xi - s_0(t),t)\,K_s(\xi)\,d\xi \\ + EJ\int_0^t \alpha(s_0(\tau) - s_0(t) + L,t)\,\dot{\alpha}(L,\tau)\,d\tau\end{aligned}$$

an integro-differential equation on s_0 alone which can be uniquely solved in terms of the data of the problem, as proven in the Appendix.

Just like in the channel case, once s_0 and k are known, the unknown functions H, N and f can be readily deduced from (2.33), (2.31) and (2.32) respectively.

2.3.2 Serpentine solutions

In this section we provide a class of explicit serpentine solutions for the free-path locomotion problem, by exploiting solutions constructed for the channel case. We obtain these solutions by solving an inverse locomotion problem, prescribing the motion first and then looking for a history of spontaneous curvatures $\alpha(s,t)$ that produces it.

Let us consider the sinusoidal path Γ given by (2.22) and assume $s_0(t) = Vt$. As we did before, we set $\rho J = 0$ for simplicity. Following the arguments of Section 2.2.3 we conclude that α must again solve (2.24). In addition, this time, we must also require the boundary condition (2.36) to be satisfied. Notice that none of the spontaneous curvatures we obtained in the channel case fulfils (2.36), but we show in the following how to modify any α solving (2.24) so that also (2.36) is satisfied.

We focus below on $\alpha_{\rm act}$ given by (2.26) since, as already remarked, it is the one that more closely resembles the typical muscular activity patterns observed in undulating snakes. If we consider a function

$$\alpha(s,t) = \alpha_{\rm act}(s,t) + \widetilde{\alpha}(s,t) \tag{2.39}$$

with $\widetilde{\alpha}$ such that

$$\begin{gathered}\widetilde{\alpha}(L,t) = \zeta\sin\left(\frac{L+Vt}{\lambda}\right) - \alpha_{\rm act}(L,t) \quad \text{and} \\ \int_0^L \widetilde{\alpha}(s,t)\cos\left(\frac{s+Vt}{\lambda}\right)ds = 0\,,\end{gathered} \tag{2.40}$$

then α satisfies both (2.24) and (2.36). With α having these properties, $s_0(t) = Vt$ becomes a solution for the equations of motion, and the expression for N, H and f can be deduced following the procedure of Section 2.2.1.

The extra term $\widetilde{\alpha}$ in (2.39) satisfying (2.40) can be taken of the form

$$\widetilde{\alpha}(s,t) = \begin{cases} 0 \text{ if } s \in [0, L-\delta] \\ \sum_{i=3}^{Q} p_i(t)(s-L+\delta)^i \text{ if } s \in [L-\delta, L] \end{cases} \tag{2.41}$$

where δ is an arbitrary constant, which can be taken as small as we want, and $p_i(t)$ with $i = 3, \dots, Q$ are coefficients explicitly depending on t and implicitly depending also on δ and all of the other parameters. These coefficients can be uniquely determined imposing (2.40) and any other $Q-5$ linearly independent relations between them (for example, in the numerical experiment we are about to propose, we imposed $\widetilde{\alpha}_{ss}(L,t) = 0$, which led to a smooth generated force field f concentrated near the head). Notice that the function $\widetilde{\alpha}$ so defined is twice continuously differentiable.

If we take δ small enough then α differs from α_{act} only in a small neighbourhood of the leading edge where the steering term $\widetilde{\alpha}$ is non zero. The reactive shear force and tension are now

$$H(s,t) = H_{\text{act}}(s,t) + EJ\widetilde{\alpha}_s(s,t)\,,$$
$$N(s,t) = N_{\text{act}}(s,t) + EJ\zeta \int_0^s \sin\left(\frac{\xi + Vt}{\lambda}\right)\widetilde{\alpha}_s(\xi,t)\,d\xi$$

and the force exerted on the ground is, in this case,

$$f(s,t) = f_{\text{act}}(s,t) + EJ\zeta^2 \int_0^s \sin\left(\frac{\xi + Vt}{\lambda}\right)\widetilde{\alpha}_s(\xi,t)\,d\xi \sin\left(\frac{s + Vt}{\lambda}\right) + EJ\widetilde{\alpha}_{ss}(s,t)\,.$$

From the last equalities it follows that, if δ is small, also the forces (external and internal) have the same values of the corresponding ones obtained in the channel case with the exception of a small region near the leading edge.

We set $\delta/L = 0.25$ and we give here two graphical comparisons of the same solution fitted with different parameters (Fig.2.5 and Fig.2.6).

In Fig.2.5A and Fig.2.6A we take the same values we considered in Section 2.2.3 for all the parameters. When compared with that of Fig.2.3B, this solution clearly shows the asymmetry that the steering term $\widetilde{\alpha}$ generates in the activation and force pattens in the proximity of the head (leading edge). In Fig.2.5B we take the smaller value for the bending stiffness, $EJ = 10^{-4}\text{Nm}^2$. Notice that this solution, besides the tail-head asymmetry associated with steering, displays a similar force pattern to that of Fig.2.3A (as expected from the formulas we derived in Section 2.2.3), which is generated by a different pattern of spontaneous curvature. Finally, in Fig.2.6B, we consider a rod with the same bending stiffness but moving with a less tortuous gait (smaller ζ). Observe that, also in this case, we obtain an almost stationary force pattern, which is qualitatively similar to that of Fig.2.5B.

Summarizing, we see that a pattern consistent with the picture of snake undulatory locomotion hypothesized in [42] (muscular activity and lateral forces both concentrated near the inflection points of the trajectory, where the propulsive effect of the lateral forces is largest because their component along the direction of motion is largest) emerges either automatically, for specific choices of material parameters (Fig.2.5B), or through adjustment of the gait (Fig.2.6B). Lateral forces near points of maximal and minimal convexity may also be ruled out by eliminating ground contact (by lifting portions of the body near those points), as it is done in [40, 41] and sometimes observed in undulating snakes.

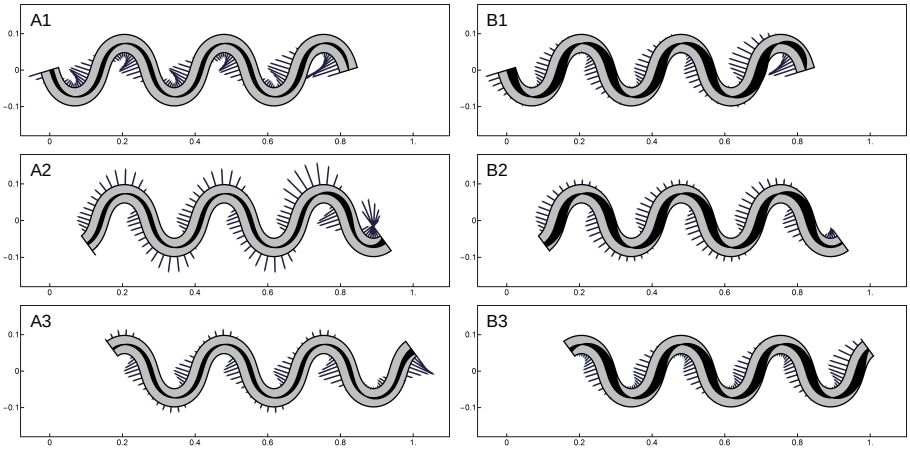

Figure 2.5: Solutions with different bending stiffness, A) $EJ = 10^{-3}\mathrm{Nm}^2$ and B) $EJ = 10^{-4}\mathrm{Nm}^2$, at three times: 1) $Vt/\lambda = 0$, 2) $Vt/\lambda = 2\pi/3$ and 3) $Vt/\lambda = 4\pi/3$. To help visualization, the spontaneous curvatures are here not on scale: the maximal width of the dark shades in B) should be ten times greater than A).

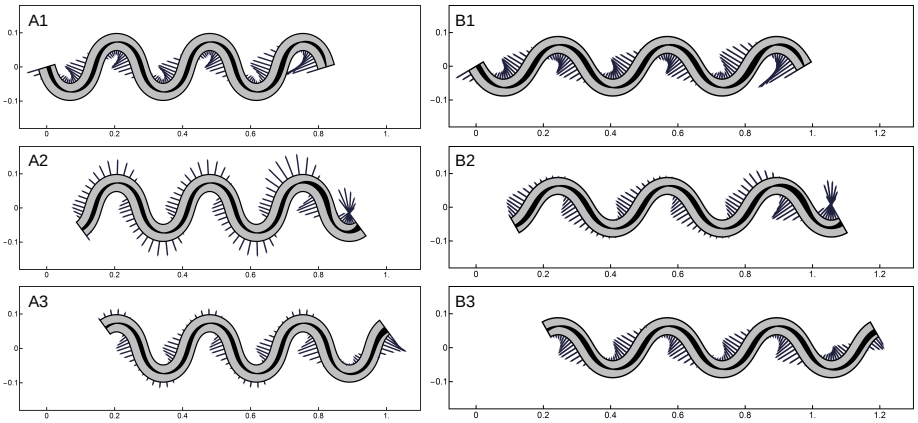

Figure 2.6: Solutions with the same bending stiffness and different path geometries, A) $\zeta = 18.5\mathrm{m}^{-1}$ and B) $\zeta = 15\mathrm{m}^{-1}$, at three times: 1) $Vt/\lambda = 0$, 2) $Vt/\lambda = 2\pi/3$ and 3) $Vt/\lambda = 4\pi/3$.

2.4 Discussion

We have studied the motion of an active rod (a planar inextensible elastic rod of finite length with adjustable spontaneous curvature) arising from the interaction between external constraints and internal actuation by spontaneous curvature. Using Cosserat theory, we have formulated and solved both direct and inverse locomotion problems for two cases: one in which the system is forced to move along a prescribed path, and the other in which the path is not fixed a-priori and the system slides along its tangential direction while subjected to lateral forces preventing lateral slipping. We have obtained a procedure to generate free-path solutions from solutions with prescribed-path, by recognising the dual role

(pushing and steering) played by spontaneous curvature in powering undulatory locomotion of the rod. Finally, we have obtained explicit analytic solutions and formulas that can be used to study the connections between observed motion, internal actuation, and forces transmitted to the environment, and to explore how these connections are affected by the mechanical properties of the system (its bending stiffness).

Although our results hold for a (very specific) model system, it may be interesting to compare some of them with observations made in the context of undulatory locomotion of snakes. For this exercise to make sense, we are formulating the implicit assumption that our mechanism of internal actuation by spontaneous curvature can provide a reasonable proxy for muscular actuation, and that the free-path motion of the organism we are considering does not cause lateral slipping, but only involves longitudinal sliding (as it is sometimes observed).

The first example is formula (2.19), which provides a compact summary of some classical observations on snake locomotion by Gray [1, 2]. Undulatory locomotion in closely fitting channels is possible only if the channel presents a variation of curvature along its track. The formula explains the mechanism by which spontaneous curvature can provide the driving force for locomotion inside a tightly fitting channel, and our analysis delivers formulas to calculate the lateral forces exerted on the channel walls. It would be interesting to compare these with experimental measurements.

A second example is the observation that, among various possible actuation strategies producing the same prescribed motion, the one minimising actuation effort (as measured by the integral norm of spontaneous curvature) is proportional to the arc-length derivative of the curvature of the trajectory. This means that local actuation is maximal at the inflexion points of the trajectory, and zero at points of maximal and minimal curvature. This is closely reminiscent of the typical pattern of muscular actuation emerging from experimental measurements on snakes [36, 37], and it would be interesting to explore further the reasons behind this analogy.

Finally, our analysis suggests that the connection between observed motions, internal actuation, and transmitted forces may be strongly affected by the passive mechanical properties of the system, such as its bending stiffness. The conceptual picture of snake undulatory locomotion in which both muscular activity and lateral forces are concentrated near the inflection points of the trajectory, previously theorised in [42], emerges either automatically, for specific choices of material parameters, or through the adjustment of the gait.

Understanding the mechanisms that control gait selection and, in particular, whether there are optimality criteria explaining gait selection in the biological organisms, and whether some of them may be useful for the engineering of artificial devices represent interesting challenges. Adding some important ingredients, currently not present in our model, may prove necessary. One example is some form of active local control of the frictional interactions between body and ground, as is done in [40, 41]. Moreover, when considering real snakes behaviour it is natural to speculate that muscular activity may be, at least to some extent, a reaction to external stimuli (the forces exerted by the ground on the snake), thereby creating an interplay between the two dynamical variables. It would be interesting to study how our model could be extended to account for such feedback mechanisms. All these questions will require further study.

2.5 Appendix. Existence and uniqueness of free-path locomotion solutions

For the sake of simplicity we take $\rho J = 0$. The following arguments can be easily adjusted for the general case.

Suppose we have a solution of the free-path locomotion problem (2.31)-(2.32)-(2.33) satisfying the boundary conditions (2.34) and the extra requirements (2.30) and (2.35) where $K(s) = k(s_0(t_0) + s)$ for $s \in [0, L]$. Again, there is no loss of generality taking $t_0 = 0$ and $s_0(t_0) = 0$. Let us first suppose, by restricting its domain of definition if necessary, that s_0 is defined on a time interval $[0, t^*)$ such that $s_0(t) \leq L$ for every $t \in [0, t^*)$. The arguments used in Section 2.3.1 show that, within this time interval, the equation for s_0 in terms of the data of the problem reads

$$\begin{aligned} m\ddot{s}_0(t) &= \frac{EJ}{2}\left(K^2(s_0(t)) - \alpha^2(L,t)\right) - \gamma'' L + EJ\int_{s_0(t)}^{L} \alpha(\xi - s_0(t), t)\, K_s(\xi)\, d\xi \\ &+ EJ\int_0^t \alpha(s_0(\tau) - s_0(t) + L, t)\, \dot{\alpha}(L,\tau)\, d\tau\,. \end{aligned} \tag{2.42}$$

The general case in which $s_0(t) > L$ may also occur (i.e., the trailing edge is no longer contained in the image of the initial configuration, see Fig.2.3B) can be handled by applying the following simple, yet technical, argument. As we will show, a local solution s_0 for (2.42) exists and is unique once a positive initial velocity $\dot{s}_0(t_0)$ is given, by requiring that $s_0(t) \leq L$. If a local solution s_0 of (2.42) exists and is unique then, for every given initial conditions, there exists only one solution with a maximal interval of definition. For such maximal solutions we can have either of two cases. In the first, the maximal interval of existence of s_0 with $\dot{s}_0 > 0$ is of the type $[0, t^*)$ and, for every t in the interval, $s_0(t) \leq L$ holds. If that occurs, the only solution of the free-path problem is defined in the time interval $[0, t^*)$, the curvature k can be derived through (2.37) while all the other unknowns can be deduced by the the same procedure we employed in the channel case in Section 2.2.1. In the second case, a solution s_0 of (2.42) satisfying $\dot{s}_0 > 0$ and $s_0(t) \leq L$ can be only defined in a maximal domain of the type $[0, t^*]$. For a solution of this kind we must have $s_0(t^*) = L$, by maximality. In this last case we can still define k through (2.37) as we did before. Then we can reapply all the arguments of Section 2.3.1 finding an equation of the type (2.42) for a new variable s_0^* with new initial conditions for the free-path locomotion problem, namely $s_0^*(t^*) = s_0(t^*)$, $\dot{s}_0^*(t^*) = \dot{s}_0(t^*)$ and the new initial curvature $K^*(s) = k(L + s)$ with $s \in [0, L]$. After that we are able to solve the new integro-differential problem uniquely for s_0^*, recover the value for all the unknowns, and then glue the solutions together. We repeat this procedure until we reach eventually a maximal domain of existence for the general solution.

The existence and uniqueness of free-path locomotion solutions then follows from the local existence and uniqueness of solutions of (2.42) with the extra requirements $\dot{s}_0(t) > 0$ and $s_0(t) \leq L$. This can be proved using standard contraction mapping arguments. The result holds under the very reasonable assumption of α and K being differentiable and uniformly bounded together with their derivatives.

Observe that we can recast (2.42) into a set of integro-differential equations of the form

$$\dot{\mathbf{x}}(t) = \mathbf{G}(\mathbf{x}(t), t) + \int_0^t \mathbf{H}(\mathbf{x}(\tau) - \mathbf{x}(t), \tau, t)\, d\tau\,, \tag{2.43}$$

with

$$\mathbf{x}(t) = (x(t), y(t))\ ,\ \mathbf{H}(\mathbf{x}, \tau, t) = \Big(\, 0\,,\ EJ\alpha(x + L, t)\, \dot{\alpha}(L, \tau)\,\Big) \quad \text{and}$$

$$\mathbf{G}(\mathbf{x}, t) = \left(\frac{y}{m}\,,\ \frac{EJ}{2}\left(K^2(x) - \alpha^2(L, t)\right) - \gamma'' L + EJ \int_x^L \alpha(\xi - x, t)\, K_s(\xi)\, d\xi \right).$$

It is clear that $\mathbf{x}$ solves (2.43) if and only if $s_0(t) \coloneqq x(t)$ solves (2.42). We first extend K and α outside $[0, L] \times [0, \infty)$ while keeping their regularity properties. Then we consider the Cauchy problem for (2.43) with initial conditions $\mathbf{x}(0) = \mathbf{x}_0$ and no extra assumption on the solutions besides differentiability. The problem can be easily proved to be equivalent to that of the existence of a fixed-point for the operator C defined as

$$C\,[\mathbf{x}]\,(t) = \mathbf{x}_0 + \int_0^t \left[\mathbf{G}(\mathbf{x}(\lambda), \lambda) + \int_0^\lambda \mathbf{H}(\mathbf{x}(\tau) - \mathbf{x}(\lambda), \tau, \lambda)\, d\tau \right] d\lambda\,.$$

We restrict the operator C to the space $B^{M,T}_{\mathbf{x}_0}$ of continuous vector valued functions $t \mapsto \mathbf{x}(t)$ defined on the interval $t \in [0, T]$ and such that

$$\|\mathbf{x} - \mathbf{x}_0\| = \max_{t \in [0,T]} |\mathbf{x}(t) - \mathbf{x}_0| \le M\,.$$

There is no loss of generality in assuming that the extensions we considered for K and α lead to the existence of two constants $M_{\mathbf{G}}$ and $M_{\mathbf{H}}$ such that

$$|\mathbf{G}(\mathbf{x}(t), t)| \le M_{\mathbf{G}} \quad \text{and} \quad |\mathbf{H}(\mathbf{x}(\tau) - \mathbf{x}(t), \tau, t)| \le M_{\mathbf{H}} \quad \text{for every } \tau \text{ and } t$$

and for every $\mathbf{x} \in B^{M,T}_{\mathbf{x}_0}$. We can also assume that there are other two constants $L_{\mathbf{G}}$ and $L_{\mathbf{H}}$ such that

$$|\mathbf{G}(\mathbf{x}, t) - \mathbf{G}(\mathbf{y}, t)| \le L_{\mathbf{G}} |\mathbf{x} - \mathbf{y}| \quad \text{and} \quad |\mathbf{H}(\mathbf{x}, \tau, t) - \mathbf{H}(\mathbf{y}, \tau, t)| \le L_{\mathbf{H}} |\mathbf{x} - \mathbf{y}|$$

for every τ and t and for every $\mathbf{x}, \mathbf{y} \in B^{M,T}_{\mathbf{x}_0}$. We have then

$$|\,C\,[\mathbf{x}]\,(t) - \mathbf{x}_0| \le T M_{\mathbf{G}} + T^2 M_{\mathbf{H}}$$

and also

$$\begin{aligned}
|\,C\,[\mathbf{x}]\,(t) - C\,[\mathbf{y}]\,(t)| \ &\le\ \left| \int_0^t \mathbf{G}(\mathbf{x}(\lambda), \lambda) - \mathbf{G}(\mathbf{y}(\lambda), \lambda)\, d\lambda \right| \\
&+\ \left| \int_0^t \int_0^\lambda \mathbf{H}(\mathbf{x}(\tau) - \mathbf{x}(\lambda), \tau, \lambda) - \mathbf{H}(\mathbf{y}(\tau) - \mathbf{y}(\lambda), \tau, \lambda)\, d\tau\, d\lambda \right| \\
&\le\ T L_{\mathbf{G}} \|\mathbf{x} - \mathbf{y}\| + L_{\mathbf{H}} \int_0^t \int_0^\lambda \left| \mathbf{x}(\tau) - \mathbf{x}(\lambda) - \big(\mathbf{y}(\tau) - \mathbf{y}(\lambda)\big) \right| d\tau\, d\lambda \\
&\le\ (T L_{\mathbf{G}} + 2T^2 L_{\mathbf{H}}) \|\mathbf{x} - \mathbf{y}\|\,.
\end{aligned}$$

For small enough T the operator C is a contraction from $B^{M,T}_{\mathbf{x}_0}$ into itself, therefore it has only one fixed point. This proves local existence and uniqueness for the extended version of (2.43). If we take $\mathbf{x}_0 = (0, y_0)$ with $y_0 > 0$ then, restricting the domain of existence to an interval $[0, T^*)$ if necessary, we have by continuity $x(t) \le L$ and $\dot{x}(t) = y(t) > 0$ for every $t \in [0, T^*)$, hence obtaining the unique solution to the original (non-extended) problem.

Chapter 3

Flagellar Swimming

Flagella constitute the mean of propulsion for a large variety of swimming microorganisms, and they are at the base of bio-inspired designs of swimming robots targeted to medical applications [8, 9]. In eukaryotes these long and flexible appendages are typically actuated by distributed internal forces. Mammalian sperms, for example, propagate bending torques along their tails to achieve propulsion [63, 64, 82]. Others, like the bi-flagellate *Chlamydomonas*, perform a rhythmical breaststroke-like routine leading to a rocketing forward motion [83, 84].

On the other hand, passive elastic flagella, when actuated only at the extremity, can also constitute an effective and simpler swimming device. A biological example for that comes from bacteria like *E.Coli*, whose passive helical tail is actuated at one end by a rotary motor inducing a cork-skew like propulsion [84]. Locomotion at very small scales is subject to the so called "Scallop Theorem" [72], which states that the body of a swimmer must undergo time-irreversible shape changes to produce net advancements. How the hydroelastic coupling between a flagellum and the surrounding fluid constitute, by itself, a source of time-irreversibility and propulsion stands as a fundamental problem to address.

Much has been done. Besides the pioneering work by Machin [71], the problem has been explored extensively in more recent years [58, 59, 60]. In [58, 59] Wiggins *et al.* demonstrated that, apart from axial rotations, also the planar beating of an elastic filament with one oscillating end can produce axial propulsive force. These findings have been put in the swimming context by Lauga in [66], who analysed the locomotion capabilities of an internally actuated swimmer model as the one in Fig.3.1B. Numerical experiments also focused on externally actuated swimming of microrobot models, inspired by the geometry of sperm cells, consisting of a cargo with a clamped passive elastica [69, 65] like the one depicted in Fig.3.1A. Both externally and internally actuated elastic swimmers were also analysed through discrete models by Or *et al.* in [73, 74] to grasp the essentials of their motility mechanism. However, in all the aforementioned studies flagellar beating is always restricted to sinusoidal actuations; the swimmers move "head-first" and, on average, on a straight line.

Many questions remain unanswered. For instance, what is the direction of motion for a generic (non-sinusoidal) periodic actuation? Does swimming always take place head-first, or can the sign of swimming velocity be controlled? In this Chapter we provide an answer to these questions. Our analysis is based on

a small-compliance assumption to obtain rigorous approximation of the general continuum equations. Within this limit we provide explicit formulas whose results are expressed through motility maps [78, 79, 80, 81], a visual approach that allows deduction on equations outcome without the need to actually solve them.

We find a sign reversal in direction for the externally actuated swimmer for large enough actuation amplitudes. Moreover, we find that modulation in the velocity of actuation can provide a mechanism to select different direction of motion. Indeed, a flagellar oscillation composed by a fast turn in in one direction and slow turn in the other produces generally a deviation from the symmetry axis around which beating takes place. With these oscillatory inputs the externally actuated swimmer in Fig.3.1A can translate laterally with respect to this symmetry axis, while the internally actuated one in Fig.3.1B is able to move along curved trajectories.

Dependency on the velocity of actuation is not surprising since previous investigations on this kind of model swimmers [66, 73, 74] reported that different displacements arise after different frequencies of oscillation. With our analysis we can look deeper in to the relations between a) given (generic) actuation, b) shape changes of the swimmers c) resulting displacements after every actuation cycle, and we demonstrate how the actuation velocity can be considered as a motion control parameter.

Take first the externally actuated swimmer. As mentioned earlier, in order to obtain a net displacement, the swimmer must undergo non-reciprocal shape changes to overcome the Scallop Theorem. Here the shape of the swimmer is determined by the angle α between the head and the tail at the point of attachment (see Fig.3.1B) and by the geometry of the tail itself. The latter is a result of the dynamics. Because of our small-compliance assumption we do not have propagating bending waves, instead tail geometry during motion is "simple". More precisely, we deduce an explicit formula for the tail deformation at a given time depending only on two parameters: the internal angle α and its velocity $\dot{\alpha}$. This last two quantities can be interpreted then as the shape parameters of the swimmer. Modulations of the actuation velocity lead to different loops in the shape space, resulting in different displacements. Motion control is possible as, given the loop geometry in the shape space $(\dot{\alpha}, \alpha)$, the resulting displacement can be inferred with the aid of the motility maps provided in Section 3.3.2.

A similar analysis is carried out in Section 3.2 for the swimmer in Fig.3.1A. It must be noted that, because of the presence of an external torque, in this case the Scallop Theorem does not apply, see [74, 85]. Indeed, for example, a two-link swimmer ("Purcell Scallop") can display net motions if an oscillating external moment is acting on it. Non-reciprocity is, on the other hand, still crucial. For the two-link swimmer we have net displacements if, as a result of external activation, the angle of one link with respect to an external frame and the internal angle between the two links undergo a non-reciprocal cycle. Motions arise, for our externally activated swimmer, in a similar way. We can assimilate the link angle of the Purcell Scallop with the angle ϕ (see Fig.3.1A), and the internal angle between the links with the geometry of the tail. Also in this case, in fact, the tail geometry is "simple" and it is completely determined by only one parameter: the velocity $\dot{\phi}$. Modulating loops in the space $(\dot{\phi}, \phi)$ leads to different resulting displacements that can be inferred from the motility

maps of Section 3.2.2.

The Chapter is organized as follows. In Section 3.1 we set up the governing equations for both models, following closely the derivation in [66], and we formalize the assumptions on the dynamical parameters. In Section 3.2 we derive an explicit solution for the externally actuated swimmer in Fig.3.1A, we derive and comment the motility maps and also address some optimization problems related to efficiency and velocity of swimming. The same kind of analysis and results are carried out in Section 3.3 for the internally actuated swimmer in Fig.3.1B.

3.1 Governing equations

As mentioned in the introduction, the model microswimmers subject to our study are those illustrated in Fig.3.1A and Fig.3.1B. We restrict ourselves to planar motions of such model swimmers (although the analysis we present here can be carried out also in three dimensions) and we consider the plane of locomotion as the one spanned by the couple of orthonormal vectors $\{\mathbf{e}_1, \mathbf{e}_2\}$. Both of the models consist of a spherical cargo of radius a attached to a passive elastic filament of length L, which we shall refer to as the "flagellum". Both swimmers are surrounded by a Newtonian fluid and moving at a low Reynolds number regime.

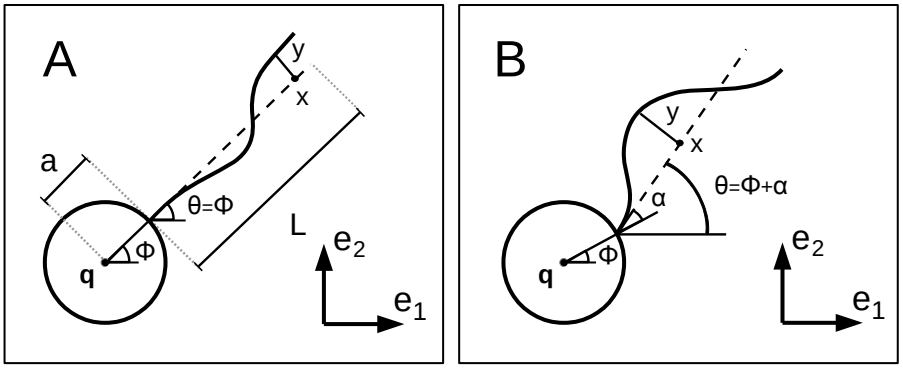

Figure 3.1: Schematic description of A) the externally actuated and B) the internally actuated swimmer model.

In the case of Fig.3.1A, the swimmer's flagellum is clamped orthogonally to the cargo, and the swimming propulsion is achieved thanks to an external torque acting on the sphere. We suppose that such a torque modulates the angle ϕ formed by the horizontal line and the line joining the centre of the cargo $\mathbf{q}$ and the point of attachment. We define the angle ϕ for the swimmer in Fig.3.1B in the same way. Here, however, we suppose that the flagellum is connected to the sphere by a joint, and that the angle θ of the flagellum at the point of attachment can vary. The action of an internal torque modulates the angle difference $\alpha = \theta - \phi$.

In both cases the elastic flagellum is supposed to be inextensible and slender,

that is, denoting r_f the radius of its cross-section, we assume

$$\frac{r_f}{L} \ll 1\,. \tag{3.1}$$

As proven experimentally in [67] the dynamics of interaction between the fluid and such a slender filament can be well described by "resistive force theory", which is the lower order approximation in the parameter r_f/L of the more general "slender body theory" [70, 5], which is derived directly from the Stokes equations. In the limit of small ratio r_f/L long range interactions are neglected, and hydrodynamic forces are assumed to be acting locally. We also neglect hydrodynamic interactions between the flagellum and the cargo. The two key dynamical parameters are the viscous drag coefficients $\xi_{//}$ and $\xi_\perp$ which are the force exerted by the fluid per unit length of the flagellum for motion parallel and perpendicular to its length. The mass of the swimmers is neglected as viscous and elastic forces dominate the dynamics.

Our analysis relies on yet another hypothesis, previously stated in the introduction: we assume that the flagellum, in both cases, has a large bending resistance compared with the viscous forces it is subjected to. More precisely, if we denote B as the bending stiffness of the flagellum and ω as the frequency of actuation (either internal or external), then we assume that the ratio between the typical normal viscous force $\xi_\perp L^2\omega$ and the typical elastic force $L^{-2}B$ acting on the flagellum

$$\epsilon = \frac{\xi_\perp L^2\omega}{L^{-2}B} \tag{3.2}$$

is small. As a consequence, the flagellum does not deviate largely from a straight line. This last assumption is consistent with the use of resistive force theory, as the theory is proven more accurate for slender bodies for which any two point of the system are kept "as far away as possible" [67, 66]. Moreover, the small-slope regime leads to a substantial simplification of the governing equations of the system, allowing the theoretical treatment we propose here.

3.1.1 The small-slope approximation

In setting the equations of motion we follow closely Lauga's derivation in [66]. The arguments leading to the equations do not differ greatly from those presented in [66], and the equations themselves present little discrepancy. In order to elucidate on the few differences we propose here the main passages of the derivation. First we consider the flagellum dynamics, for which the same "bulk" equations hold both for the externally and the internally actuated case.

We denote by $\mathbf{r}$ the curve on the plane describing the position of the middle line of the flagellum. As mentioned in the previous section, we restrict our analysis to the case in which the flagellum is varying mildly around a moving axis of reference. We assume that the direction of the reference axis is given at time t by the normal vector

$$\mathbf{e}_\theta = \cos\theta(t)\,\mathbf{e}_1 + \sin\theta(t)\mathbf{e}_2$$

and that the curve $\mathbf{r}$ has the following expression

$$\mathbf{r} = \mathbf{r}(0,t) + x\mathbf{e}_\theta + y(x,t)\mathbf{e}_\theta^\perp \tag{3.3}$$

where $\mathbf{e}_\theta^\perp = -\sin\theta(t)\,\mathbf{e}_1 + \cos\theta(t)\mathbf{e}_2$ is the normal vector orthogonal to the reference axis and $\mathbf{r}(0,t)$ determines the position of the point of attachment between the cargo and the flagellum. We suppose

$$y(0,t) = 0 \quad \text{and} \quad \frac{\partial y}{\partial x}(0,t) = 0 \tag{3.4}$$

so that, in particular, the orientation of the flagellum at the point of attachment is determined by θ. Notice that, with this assumption, for the externally driven swimmer the angle θ and the orientation of the cargo ϕ coincide. The small-slope approximation consists in the hypothesis

$$\left|\frac{\partial y}{\partial x}\right| \ll 1\,. \tag{3.5}$$

In this regime the variable x can be considered as the arc-length coordinate of the curve $\mathbf{r}$, and it is taken to vary in the interval $[0, L]$. We denote with v_x and v_y the longitudinal and the transversal velocity (respectively) of the flagellum with respect to the reference axis direction. The two quantities are defined by the formula

$$\frac{\partial \mathbf{r}}{\partial t} = v_x \mathbf{e}_\theta + v_y \mathbf{e}_\theta^\perp\,. \tag{3.6}$$

Following [66], in the small-slope approximation the projections on $\mathbf{e}_\theta$ and $\mathbf{e}_\theta^\perp$ of the force balance equation on the flagellum read

$$\begin{cases} \xi_{//} v_x + (\xi_{//} - \xi_\perp) v_y \dfrac{\partial y}{\partial x} = \dfrac{\partial \sigma}{\partial x} \\ \xi_\perp v_y + (\xi_{//} - \xi_\perp) v_x \dfrac{\partial y}{\partial x} = -B\dfrac{\partial^4 y}{\partial x^4} + \dfrac{\partial}{\partial x}\left(\sigma \dfrac{\partial y}{\partial x}\right) \end{cases} \tag{3.7}$$

The left hand sides of the equations account for the viscous forces, while the right hand sides for the elastic ones. The function σ is the Lagrange multiplier enforcing the inextensibility constraint, and it is determined (see again [66]) by the equation

$$\frac{\partial^2 \sigma}{\partial x^2} + B\left(\frac{\xi_{//}}{\xi_\perp} - 1\right)\frac{\partial^2 y}{\partial x^2}\frac{\partial^4 y}{\partial x^4} = B\frac{\partial y}{\partial x}\frac{\partial^5 y}{\partial x^5}\,. \tag{3.8}$$

The boundary conditions at the free edge $x = L$ are given by the vanishing of the applied elastic force $\sigma\mathbf{e}_\theta + (-B\partial^3 y/\partial x^3 + \sigma \partial y/\partial x)\mathbf{e}_\theta^\perp$ and elastic moment $B\partial^2 y/\partial x^2$, which give

$$\sigma(L,t) = 0\ , \quad \frac{\partial^2 y}{\partial x^2}(L,t) = 0 \quad \text{and} \quad \frac{\partial^3 y}{\partial x^3}(L,t) = 0\,. \tag{3.9}$$

Force and moment at the point of attachment $x = 0$ are determined by the interaction with the cargo.

As we stated in the previous section, the cargo does not interact with the flagellum through hydrodynamics. Therefore the viscous force on the sphere is given by $-\nu\dot{\mathbf{q}}$ where ν is the viscous drag coefficient and where we denoted with a 'dot' the derivative with respect to time. For both the externally and the internally actuated swimmers the forces acting on the cargo are the viscous one and the contact force $\sigma\mathbf{e}_\theta + (-B\partial^3 y/\partial x^3 + \sigma\partial y/\partial x)\mathbf{e}_\theta^\perp$ exerted by the flagellum on the sphere. If we apply (3.4) the force balance on the cargo reads

$$-\nu\dot{\mathbf{q}}(t) + \sigma(0,t)\mathbf{e}_\theta - B\frac{\partial^3 y}{\partial x^3}(0,t)\mathbf{e}_\theta^\perp = \mathbf{0}\,. \tag{3.10}$$

The difference between the systems of equations of the two model swimmers lies in the moment balance between the cargo and the flagellum. For the externally actuated swimmer the moments acting on the cargo are: the viscous one, given by $-\nu_{\rm rot}\dot{\phi}$ where $\nu_{\rm rot}$ is the rotational drag coefficient for the sphere; the contact one $a(-B\partial^3 y/\partial x^3+\sigma\partial y/\partial x)+B\partial^2 y/\partial x^2$ coming from the flagellum; and the one given by the external torque $\tau_{\rm ext}$. Using (3.4) and (3.10), the moment balance equation on the cargo reads

$$-\nu_{\rm rot}\dot{\phi}(t)+\nu a\,\mathbf{e}_\phi^\perp\cdot\dot{\mathbf{q}}(t)+B\frac{\partial^2 y}{\partial x^2}(0,t)+\tau_{\rm ext}(t)=0 \tag{3.11}$$

where $\mathbf{e}_\varphi^\perp=-\sin\phi(t)\,\mathbf{e}_1+\cos\phi(t)\mathbf{e}_2$. As for the internally activated swimmer there are only viscus and contact moments acting on the cargo, when, on the other end, we assume that there is internal couple $\tau_{\rm int}$ acting on the flagellum to enforce the angle difference $\alpha=\theta-\phi$. We have

$$-\nu_{\rm rot}\dot{\phi}(t)+\nu a\,\mathbf{e}_\phi^\perp\cdot\dot{\mathbf{q}}(t)+B\frac{\partial^2 y}{\partial x^2}(0,t)=0\quad\text{and}\quad\tau_{\rm int}=-B\frac{\partial^2 y}{\partial x^2}(0,t)\,. \tag{3.12}$$

In the next section we non-dimentionalize all the above equations of motion.

3.1.2 Non-dimensional equations

To avoid notational excess we use the same variables we adopted in the derivation of the dimensional equations to denote their respective normalized quantities. We scale by L the space variables x, y, $\mathbf{r}$, $\mathbf{q}$, and by ω^{-1} the time variable t. The Lagrange multiplier σ is scaled by the elastic force $L^{-2}B$ while $\tau_{\rm ext}$ and $\tau_{\rm int}$ by the viscous torque $\xi_\perp\omega L^3$. We keep the angle variables ϕ and θ (themselves in non-dimensional units) unscaled.

The normalized equations for the flagellum are

$$\begin{cases}\epsilon\left(\gamma v_x+(\gamma-1)v_y\dfrac{\partial y}{\partial x}\right)=\dfrac{\partial\sigma}{\partial x} & (3.13)\\[2ex] \epsilon\left(v_y+(\gamma-1)v_x\dfrac{\partial y}{\partial x}\right)=-\dfrac{\partial^4 y}{\partial x^4}+\dfrac{\partial}{\partial x}\left(\sigma\dfrac{\partial y}{\partial x}\right) & (3.14)\end{cases}$$

where $\gamma=\xi_{//}/\xi_\perp$ is the drag anisotropy factor and ϵ is given by (3.2). The non-dimensional equation for σ becomes

$$\frac{\partial^2\sigma}{\partial x^2}+(\gamma-1)\,\frac{\partial^2 y}{\partial x^2}\frac{\partial^4 y}{\partial x^4}=\frac{\partial y}{\partial x}\frac{\partial^5 y}{\partial x^5}\,. \tag{3.15}$$

while the non-dimensional force balance on the cargo reads

$$-\epsilon\eta\dot{\mathbf{q}}(t)+\sigma(0,t)\mathbf{e}_\theta-\frac{\partial^3 y}{\partial x^3}(0,t)\mathbf{e}_\theta^\perp=\mathbf{0} \tag{3.16}$$

where we set $\eta=\nu/\xi_\perp L$ to be the total viscous drag ratio between the sphere and the flagellum. The moment balance on the cargo for the externally actuated swimmer in non-dimensional units is

$$-\epsilon\eta_{\rm rot}\dot{\phi}(t)+\epsilon\eta\rho\,\mathbf{e}_\phi^\perp\cdot\dot{\mathbf{q}}(t)+\frac{\partial^2 y}{\partial x^2}(0,t)+\epsilon\tau_{\rm ext}(t)=0 \tag{3.17}$$

while for the internally actuated swimmer we have

$$-\epsilon\eta_{\rm rot}\dot{\phi}(t)+\epsilon\eta\rho\,\mathbf{e}_\phi^\perp\cdot\dot{\mathbf{q}}(t)-\epsilon\tau_{\rm int}(t)=0\quad\text{with}\quad\epsilon\tau_{\rm int}(t)=-\frac{\partial^2 y}{\partial x^2}(0,t)\qquad(3.18)$$

where $\eta_{\rm rot}=\nu_{\rm rot}/\xi_\perp L^3$ is the total rotational viscous drag ratio and $\rho=a/L$. Finally, the following boundary conditions must hold

$$y(0,t)=\frac{\partial y}{\partial x}(0,t)=\frac{\partial^2 y}{\partial x^2}(1,t)=\frac{\partial^3 y}{\partial x^3}(1,t)=\sigma(1,t)=0\,.\qquad(3.19)$$

We conclude this section with a few comments on the relevant quantities that arise from the non-dimensionalization of the equation of motion.

In the slender limit (3.1) the two viscosity coefficients on the flagellum have the following expressions

$$\xi_{//}=\frac{2\pi\mu}{\log(L/r_f)-1/2}\quad\text{and}\quad\xi_\perp=\frac{4\pi\mu}{\log(L/r_f)+1/2}\,,\qquad(3.20)$$

where μ is the dynamic viscosity of the fluid [70, 5]. In the same slender limit then the drag anisotropy ratio γ is approximately ~ 0.5. As for the spherical cargo we have $\nu=6\pi\mu a$ and $\nu_{\rm rot}=8\pi\mu a^3$ [77], therefore from (3.20) and the definitions of η and $\eta_{\rm rot}$ we have

$$\eta=\frac{3}{2}\rho\big(\log(L/r_f)+1/2\big)\quad\text{and}\quad\eta_{\rm rot}=2\rho^3\big(\log(L/r_f)+1/2\big)\,.\qquad(3.21)$$

Once the slenderness L/r_f of the flagellum is set, the two parameters η and $\eta_{\rm rot}$ depend solely on $\rho=a/L$.

Finally, let us consider ϵ given by (3.2). As mentioned in the first section, this parameter measures the compliance of the flagellum while subject to a viscous force of order $\xi_\perp\omega L^2$. In the following, we shall refer to ϵ as the "Machin number" and always assume

$$\epsilon\ll 1\,.\qquad(3.22)$$

We point out that this assumption is not always satisfied for material parameters of known manufactured or biological flagellar swimmers; for sperm cells $\epsilon\sim 10^2-10^5$ [64], while for the artificial swimmer in [62] $\epsilon\sim 10^0-10^3$. However, considering a flagellum with $L/r_f\simeq 10^2-10^3$ and Young modulus $E\simeq 10^{11}\mathrm{Nm}^{-2}$, the value for permalloy as in [85], beating in water $\mu=8.90\times 10^4\mathrm{Nm}^{-2}\mathrm{s}$ then (3.22) is satisfied for a reasonable range of frequencies. Indeed, using (3.20) and the formula $B=\pi E r_f^4/4$, we have

$$\epsilon=\frac{\xi_\perp\omega}{B}L^4=\frac{8\mu\omega(L/r_f)^4}{\big(\log(L/r_f)+1/2\big)E}\lesssim\omega\times 10^{-6}\mathrm{s}-\omega\times 10^{-2}\mathrm{s}\,.$$

Besides, the hypothesis (3.22) will enable us to develop an asymptotic approximation scheme for explicit analysis. Moreover, it justifies the adoption of the small-slope equations, as it is explained in the next section. This is the major difference between our analysis and the one presented in [66] where small deviations of the flagellum comes as a consequence of small actuation.

3.1.3 Further simplifications

Following again [66], we further simplify the governing equations by estimating the scaling in ϵ of the various quantities and retaining only on the leading order terms.

If the data driving the motion $\tau_{\text{int}}, \tau_{\text{ext}}$ are of order ~ 1 then, from the physics of the problem and the hypothesis of quasi-rigidity (3.22), we have that the quantities $\dot{\mathbf{q}}$, $\dot{\phi}$, $\dot{\theta}$, v_x, v_y, y are at most of the same order, as it is verified a-posteriori. From (3.17) and (3.18) we have that $\partial^2 y/\partial^2 x \sim \epsilon$ at $x = 0$ in both the externally and the internally driven case. If we project (3.16) on $\mathbf{e}_\theta$ and $\mathbf{e}_\theta^\perp$ then, with the same argument, we obtain $\sigma \sim \epsilon$ and $\partial^3 y/\partial^3 x \sim \epsilon$ at $x = 0$. Given that the other boundary conditions for y and σ are null (3.19), we can conclude from (3.13) and (3.14) that $\sigma, y \sim \epsilon$. Notice that (3.5) is therefore verified.

It will turn out that in the externally driven case σ is in fact of order ϵ^2, but in the internally driven one it is actually of order ϵ. Anyhow, we can drop higher order terms in ϵ from equation (3.14), obtaining

$$\epsilon v_y = -\frac{\partial^4 y}{\partial x^4}(x,t) \tag{3.23}$$

Because of this simplification we can rule out σ from the equation of motion. Indeed, observe that from (3.3) and (3.6) we have

$$v_x = u^x - \dot{\theta} y \quad \text{and} \quad v_y = u^y + \dot{\theta} x + \frac{\partial y}{\partial t} \tag{3.24}$$

where we defined u^x and u^y as the longitudinal and transversal velocity of the attachment point respectively

$$u^x = \frac{\partial \mathbf{r}}{\partial t}(0,t) \cdot \mathbf{e}_\theta \ , \quad u^y = \frac{\partial \mathbf{r}}{\partial t}(0,t) \cdot \mathbf{e}_\theta^\perp \, . \tag{3.25}$$

Therefore, using (3.19) (3.23) and (3.24), if we integrate (3.13) we obtain

$$\begin{aligned}
\sigma(0,t) = \ & -\int_0^1 \frac{\partial \sigma}{\partial x} = -\int_0^1 \epsilon \left(\gamma v_x + (\gamma - 1) v_y \frac{\partial y}{\partial x} \right) \\
&= -\epsilon \gamma u^x + \epsilon \int_0^1 \gamma \dot{\theta} y + \int_0^1 (\gamma - 1) \frac{\partial^4 y}{\partial x^4} \frac{\partial y}{\partial x} \\
&= -\epsilon \gamma u^x + \epsilon \int_0^1 \gamma \dot{\theta} y + (\gamma - 1) \left[\frac{\partial y}{\partial x} \frac{\partial^3 y}{\partial x^3} - \frac{1}{2} \left(\frac{\partial^2 y}{\partial x^2} \right)^2 \right]_0^1 \\
&= -\epsilon \gamma u^x + \epsilon \int_0^1 \gamma \dot{\theta} y + \frac{\gamma - 1}{2} \left(\frac{\partial^2 y}{\partial x^2} \right)^2 (0,t) \, .
\end{aligned}$$

Substituting the above expression for $\sigma(0,t)$ in the projection along $\mathbf{e}_\theta$ of (3.16) we have

$$\epsilon(\eta + \gamma) u^x(t) - \epsilon \eta \rho \sin\alpha \, \dot{\phi}(t) = \epsilon \gamma \dot{\theta}(t) \int_0^1 y(x,t) \, dx + \frac{\gamma - 1}{2} \left(\frac{\partial^2 y}{\partial x^2} \right)^2 (0,t) \tag{3.26}$$

where $\alpha = 0$ in the externally actuated case.

3.2 Externally actuated swimmer

The natural problem for the case of the externally actuated swimmer is that of finding the motion given the external actuation τ_{ext}. We study here first the problem in which ϕ is given, for two reasons: first, it simplifies the asymptotic calculations; second, and more important, the geometry behind the propulsion capabilities of the swimmer is better understood when treated in terms of the configurational parameter ϕ.

Observe that, in this case, the moment balance equation on the cargo (3.17) can be ruled out. More precisely, (3.17) stands to define the external torque τ_{ext} needed to impose the oscillation of ϕ we prescribe. The system of equations for the swimmer therefore consists in: the (simplified) balance of transversal forces on the flagellum (3.23), the projection on $\mathbf{e}_\theta^\perp$ of (3.16), and (3.26). Since $\phi = \theta$ then, using (3.24), the system reads

$$\begin{cases} \epsilon\left(u^y(t) + \dot\phi(t)x + \dfrac{\partial y}{\partial t}(x,t)\right) = -\dfrac{\partial^4 y}{\partial x^4}(x,t) & (3.27)\\ \epsilon\eta\rho\dot\phi(t) - \epsilon\eta u^y(t) = \dfrac{\partial^3 y}{\partial x^3}(0,t) & (3.28)\\ \epsilon(\eta+\gamma)u^x(t) = \epsilon\gamma\dot\phi(t)\displaystyle\int_0^1 y(x,t)\,dx + \frac{\gamma-1}{2}\left(\frac{\partial^2 y}{\partial x^2}\right)^2(0,t) & (3.29)\end{cases}$$

In order to solve for the unknowns u^x, u^y and y, the previous equations must be accompanied to the boundary conditions (3.19).

As we show in the Appendix, given a periodic actuation $\phi(t)$, the system (3.27)-(3.29) admits only one periodic solution. All the analysis and results we present in the following regard this solution alone. In the next section we propose a perturbation scheme to obtain a formal asymptotic solution, which approximates the unperturbed periodic one in a sense defined rigorously in Appendix I.

3.2.1 Asymptotics

We now proceed formally in finding an asymptotic solution of our problem, applying standard perturbation techniques [75]. We look for solutions in the form of a power series in the Machin number

$$y = y_0+\epsilon y_1+\epsilon^2 y_2+\dots, \quad u^x = u_0^x+\epsilon u_1^x+\epsilon^2 u_2^x+\dots, \quad u^y = u_0^y+\epsilon u_1^y+\epsilon^2 u_2^y+\dots \quad (3.30)$$

We can also think the given periodic angle ϕ as coming in power series form $\phi = \phi_0 + \epsilon\phi_1 + \epsilon^2\phi_2\dots$, taking $\phi_0 = \phi$ and $\phi_k = 0$ for $k \geq 1$. Substituting these expression in the equations of motion, and expand all members of the equations in power series in ϵ, we then make coefficient of equal power equal. We obtain a series of problems to be solved successively: equation (3.27) becomes

$$0 = -\frac{\partial^4 y_0}{\partial x^4}(x,t) \quad \text{and} \quad u_{k-1}^y(t) + \dot\phi_{k-1}(t)x + \frac{\partial y_{k-1}}{\partial t}(x,t) = -\frac{\partial^4 y_k}{\partial x^4}(x,t) \quad (3.31)$$

for every $k \geq 1$, while (3.28) gives

$$0 = -\frac{\partial^3 y_0}{\partial x^3}(0,t) \quad \text{and} \quad \eta\rho\dot\phi_{k-1}(t) - \eta u_{k-1}^y(t) = \frac{\partial^3 y_k}{\partial x^3}(0,t) \quad (3.32)$$

for $k \geq 1$. These series of equations come with the following boundary conditions

$$y_k(0,t) = \frac{\partial y_k}{\partial x}(0,t) = \frac{\partial^2 y_k}{\partial x^2}(1,t) = \frac{\partial^3 y_k}{\partial x^3}(1,t) = 0 \quad \text{for } k \geq 0\,. \tag{3.33}$$

Notice that u^x is completely decoupled from u^y and y, as it appears only in (3.29). We can then solve (formally) for u^y and y from (3.31) and (3.32), and subsequently recover the asymptotic expression for u^x though the equality (3.29).

In the following we calculate explicitly the asymptotic solution up to order $k = 1$. Clearly, at the zero order we must have

$$y_0(x,t) = 0\,.$$

Equation (3.31) for $k = 1$ then reads

$$u_0^y(t) + \dot{\phi}(t)x = -\frac{\partial^4 y_1}{\partial x^4}(x,t)\,.$$

The unique solution for y_1 satisfying the previous equation and the boundary conditions (3.33) can be written as

$$y_1(x,t) = -\int_0^x \int_0^{x_1} \int_{x_2}^1 \int_{x_3}^1 \left(u_0^y(t) + \dot{\phi}(t)x_4\right) dx_4 dx_3 dx_2 dx_1\,. \tag{3.34}$$

Substituting (3.34) in (3.32) we have

$$\eta\rho\dot{\phi}(t) - \eta u_0^y(t) = \int_0^1 \left(u_0^y(t) + \dot{\phi}(t)x\right) dx$$

which gives

$$u_0^y(t) = \frac{\eta\rho - \frac{1}{2}}{\eta + 1}\,\dot{\phi}(t)\,. \tag{3.35}$$

Plugging the above expression for u_0^y back in (3.34) we obtain

$$\begin{aligned} y_1(x,t) &= -p_1(x)\dot{\phi}(t) \quad \text{where} \\ p_1(x) &= \int_0^x \int_0^{x_1} \int_{x_2}^1 \int_{x_3}^1 \left(\frac{\eta\rho - \frac{1}{2}}{\eta + 1} + x_4\right) dx_4 dx_3 dx_2 dx_1\,. \end{aligned} \tag{3.36}$$

Notice that the solution we have just found for y_1 states that, at first approximation, the shape of the flagellum during motion is completely determined by the actuation *velocity* $\dot{\phi}(t)$. This is not entirely surprising, since the bending of the flagellum must be proportional to the total moment applied to it, which itself depends on the velocity of the swimmer. We will return on this observation in the next section.

We find now an explicit solution for u_1^y, by considering the $k = 2$ order problem in (3.31), which now reads

$$u_1^y(t) - p_1(x)\ddot{\phi}(t) = -\frac{\partial^4 y_2}{\partial x^4}(x,t)\,.$$

Following the same arguments as in the case of y_1 we obtain the integral formula

$$y_2(x,t) = -\int_0^x \int_0^{x_1} \int_{x_2}^1 \int_{x_3}^1 \left(u_1^y(t) - p_1(x_4)\ddot{\phi}(t)\right) dx_4 dx_3 dx_2 dx_1$$

which, substituted in (3.32) for $k = 2$, gives

$$-\eta u_1^y(t) = \int_0^1 \left(u_1^y(t) - p_1(x)\ddot{\phi}(t) \right) dx \,.$$

From the previous equation we have

$$u_1^y(t) = \frac{\ddot{\phi}(t)}{\eta + 1} \int_0^1 p_1 \,. \tag{3.37}$$

We can know find the solution for the first orders of u^x. If we replace the asymptotic expansion of y in (3.29) we get

$$\epsilon(\eta + \gamma)u^x = \epsilon^2 \gamma \int_0^1 \dot{\phi} y_1 + \epsilon^2 \frac{\gamma - 1}{2} \left(\frac{\partial^2 y_1}{\partial x^2} \right)^2 (0,t) + \mathcal{O}(\epsilon^3) \,,$$

from which we obtain the expressions for the orders $k = 0$ and $k = 1$ of the u^x asymptotic expansion

$$u_0^x = 0 \quad \text{and} \quad u_1^x = -\left(\frac{\gamma}{\eta + \gamma} \int_0^1 p_1 \; + \frac{1 - \gamma}{2(\eta + \gamma)} p_1''(0)^2 \right) \dot{\phi}^2 \,, \tag{3.38}$$

where we denoted with a 'prime' the derivative of p_1 with respect to x.

3.2.2 Motility maps

Having found the first order of approximation for u^x and u^y we turn now on the analysis of motion of the swimmer. Specifically, we study here the resulting approximated solution for the coordinate $\mathbf{q}$ of the cargo, and we show how a given (periodic) actuation ϕ can lead to propulsion. The quantity we shall consider is

$$\Delta\mathbf{q} := \mathbf{q}(1) - \mathbf{q}(0) = \int_0^1 \dot{\mathbf{q}}(t)\, dt$$

namely the net displacement of the cargo after one period.

Before entering in the explicit calculations we make here two important remarks on the definition of $\Delta\mathbf{q}$. Firstly, since from (3.25) we have

$$\dot{\mathbf{q}} = \frac{d}{dt}\Big(\mathbf{r}(0,t) - \rho \mathbf{e}_\phi \Big) = u^x \mathbf{e}_\phi + u^y \mathbf{e}_\phi^\perp - \frac{d}{dt} \rho \mathbf{e}_\phi \,,$$

where $\{u^x, u^y\}$ is the (periodic) solution to the unperturbed problem, then if we consider $\Delta_n \mathbf{q}$, namely the net displacement of the cargo after the n^{th} period, we obtain

$$\Delta_n \mathbf{q} := \int_n^{n+1} \dot{\mathbf{q}} = \int_n^{n+1} \left(u^x \mathbf{e}_\phi + u^y \mathbf{e}^\perp - \frac{d}{dt} \rho \mathbf{e}_\phi \right) = \int_0^1 u^x \mathbf{e}_\phi + u^y \mathbf{e}_\phi^\perp = \Delta\mathbf{q}$$

because of the periodicity of u^x, u^y and ϕ. The definition of $\Delta\mathbf{q}$ is well defined, as it gives the net displacement of the cargo after *any* period of the actuation. Secondly, we observe that we can restrict our analysis to the case in which the activated angle ϕ oscillates around 0 (i.e. the flagellum is beating around the horizontal axis) without loss of generality. Indeed, for a general periodic function ϕ we can always find $\tilde{\phi}$ oscillating around zero such that $\phi(t) = \phi^* + \tilde{\phi}(t)$ for

some constant ϕ^*. Since the equations (3.27)-(3.29) only depend on the time derivative of the prescribed angle, the two inputs ϕ and $\tilde{\phi}$ generates the same velocities u^x and u^y. Therefore, if we denote $\mathbf{q}$ the coordinate of the cargo when the controlled angle is ϕ and $\tilde{\mathbf{q}}$ when the angle evolution is given by $\tilde{\phi}$, we have

$$\Delta\mathbf{q} = \int_0^1 u^x \mathbf{e}_{\phi^*+\tilde{\phi}} + u^y \mathbf{e}^{\perp}_{\phi^*+\tilde{\phi}} = \mathbf{R}(\phi^*) \int_0^1 u^x \mathbf{e}_{\tilde{\phi}} + u^y \mathbf{e}^{\perp}_{\tilde{\phi}} = \mathbf{R}(\phi^*)\Delta\tilde{\mathbf{q}}$$

where $\mathbf{R}(\phi^*)$ is the rotation on the plane by the angle $\phi*$, which reads

$$\mathbf{R}(\phi^*) = \begin{pmatrix} \cos\phi^* & -\sin\phi^* \\ \sin\phi^* & \cos\phi^* \end{pmatrix} \tag{3.39}$$

in matrix form for the basis $\{\mathbf{e}_1, \mathbf{e}_2\}$. As it is intuitive, an oscillation about a given angle produces the same kinematics of swimming, up to a rotation, as when the same oscillation is performed about the horizontal.

We now turn into the calculations involving the asymptotic solution we found in the previous section. As a first thing we expand $\dot{\mathbf{q}}$ into a power series in the Machin number up to the order $k = 1$, that is $\dot{\mathbf{q}} = \dot{\mathbf{q}}_0 + \epsilon\dot{\mathbf{q}}_1 + \mathcal{O}(\epsilon^2)$. From (3.35) and (3.38) we have

$$\dot{\mathbf{q}}_0 = u_0^x \mathbf{e}_\phi + u_0^y \mathbf{e}^{\perp}_\phi - \frac{d}{dt}\rho\mathbf{e}_\phi = \frac{\eta\rho - \frac{1}{2}}{\eta+1}\dot{\phi}\mathbf{e}^{\perp}_\phi - \frac{d}{dt}\rho\mathbf{e}_\phi = \left(\frac{\eta\rho - \frac{1}{2}}{\eta+1} - \rho\right)\frac{d}{dt}\mathbf{e}_\phi \tag{3.40}$$

while from (3.37) and (3.38) we obtain

$$\dot{\mathbf{q}}_1 = u_1^x \mathbf{e}_\phi + u_1^y \mathbf{e}^{\perp}_\phi = U_1^x \dot{\phi}^2 \mathbf{e}_\phi + U_1^y \ddot{\phi}\mathbf{e}^{\perp}_\phi \tag{3.41}$$

where

$$U_1^x = -\frac{\gamma}{\eta+\gamma}\int_0^1 p_1 \; - \left(\frac{1-\gamma}{\eta+\gamma}\right)\frac{p_1''(0)^2}{2} \quad \text{and} \quad U_1^y = \frac{1}{\eta+1}\int_0^1 p_1 \tag{3.42}$$

are constants. From this expansion we can deduce an approximated formula for the displacement, that is $\Delta\mathbf{q} = \Delta\mathbf{q}_0 + \epsilon\Delta\mathbf{q}_1 + \mathcal{O}(\epsilon^2)$. We have

$$\Delta\mathbf{q}_0 = \int_0^1 \left(\frac{\eta\rho - \frac{1}{2}}{\eta+1} - \rho\right)\frac{d}{dt}\mathbf{e}_\phi = \mathbf{0}\,. \tag{3.43}$$

Notice that $\mathbf{q}_0$ can be seen as the trajectory of the cargo of a swimmer with a rigid straight flagellum, since for $\epsilon = 0$ equations (3.27)-(3.29) describe precisely this system. The result in (3.43) then says that a rigid swimmer, whose orientation is controlled externally, always undergoes reciprocal motions.

Now, the expression (3.41) for $\dot{\mathbf{q}}_1$ has the following form

$$\mathbf{A}(\phi)\dot{\phi}^2 + \mathbf{B}(\phi)\ddot{\phi}\,. \tag{3.44}$$

We can draw a simple, yet general, argument about whether (3.44) gives a non-zero result when integrated over one period. Observe that

$$\mathbf{A}(\phi)\dot{\phi}^2 + \mathbf{B}(\phi)\ddot{\phi} = \frac{d}{dt}\Big(\mathbf{B}(\phi)\dot{\phi}\Big) + \Big(\mathbf{A}(\phi) - \frac{d\mathbf{B}}{d\phi}(\phi)\Big)\dot{\phi}^2\,.$$

So, if $\mathbf{A} - d\mathbf{B}/d\phi = 0$ then the integral of (3.44) over a period of ϕ gives always a null result. On the other hand, whenever $\mathbf{A} - d\mathbf{B}/d\phi \neq 0$ we can always find

a periodic ϕ such that the integral is non-zero. Indeed, suppose that the curve given by $t \to (\dot{\phi}(t), \phi(t)) \subset \mathbb{R}^2$ parametrizes the boundary $\partial\Omega$ of a domain Ω in $\mathbb{R}^2$ (which it is not to be confused with the plane of locomotion). Then, with the position $\psi = \dot{\phi}$, from the Stokes theorem we have

$$\begin{aligned} \int_0^1 \mathbf{A}(\phi)\dot{\phi}^2 + \mathbf{B}(\phi)\ddot{\phi} &= \int_0^1 \mathbf{A}(\phi)\psi\dot{\phi} + \mathbf{B}(\phi)\dot{\psi} \\ &= \int_{\partial\Omega} \mathbf{A}(\phi)\psi d\phi + \mathbf{B}(\phi)\, d\psi = \int_\Omega \mathbf{A}(\phi) - \frac{d\mathbf{B}}{d\phi}(\phi)\, d\psi d\phi\,. \end{aligned} \tag{3.45}$$

It is easy to see that, using for instance a function ϕ of the form $\phi(t) = \phi^* + A\sin(2\pi t)$, we can always find a set Ω that gives a non-zero result in (3.45) whenever $\mathbf{A} - d\mathbf{B}/d\phi \neq 0$.

Taking $\mathbf{A}(\phi) = U_1^x \mathbf{e}_\phi$ and $\mathbf{B}(\phi) = U_1^y \mathbf{e}_\phi^\perp$ we have $\mathbf{A} - d\mathbf{B}/d\phi = C\mathbf{e}_\phi$ where $C = U_1^x + U_1^y$. Applying the definitions (3.36) and (3.42) we have, after some calculations,

$$C = -(1-\gamma)\left(\frac{5 + 12\eta(2+5\rho) + 4\eta^2(7+42\rho+45\rho^2)}{1440(1+\eta)^2(\gamma+\eta)}\right). \tag{3.46}$$

From (3.45) then we obtain

$$\Delta\mathbf{q}_1 = \int_\Omega \mathbf{V}(\phi)\, d\psi d\phi \quad \text{where} \quad \mathbf{V}(\phi) = C\,(\cos\phi\mathbf{e}_1 + \sin\phi\mathbf{e}_2) \tag{3.47}$$

is a vector field that has to be interpreted as a map from $\mathbb{R}^2$ in the variables ψ and ϕ (although being independent from ψ) with values in the locomotion plane, while Ω is the planar domain in $\mathbb{R}^2$ whose boundary is given by

$$\partial\Omega = \left\{(\dot{\phi}(t), \phi(t))\,;\, t \in [0,1]\right\} \subset \mathbb{R}^2\,. \tag{3.48}$$

Observe that since $\gamma \neq 1$ then C is non-zero: as in [66, 61] drag anisotropy is essential to achieve locomotion. We can write the approximated expression for $\Delta\mathbf{q}$ through the following formula

$$\Delta\mathbf{q} = \epsilon \int_\Omega \mathbf{V}(\phi)\, d\psi d\phi + \mathcal{O}(\epsilon^2) \tag{3.49}$$

which is the most important result of our analysis for the externally actuated swimmer model.

Observe that the vector field $\mathbf{V}$ defined in (3.47) is independent from the given actuation ϕ. The integral in (3.49), and therefore the direction and magnitude of the displacement $\Delta\mathbf{q}$, can be estimated with the visual aid of the vector field plot and by guessing the geometry of Ω. In the following we show some examples of that, illustrating the "motility maps" for various angle actuations.

This formulation [78, 79, 80, 81] embrace the spirit of robotic locomotion analysis, with one important difference. The typical robotic locomotion problem is to find the time evolution of a body coordinate as a result to a given cycle of shape or body parameters, where such parameters are assumed to be completely controllable. It is not the case here, since the shape of the swimmer flagellum is rather a result of the dynamics. However, we somehow *can* control the shape of the flagellum, although indirectly. Indeed, as we mentioned in the previous section, at first approximation the deviation of the flagellum from its reference

axis $y = -\epsilon p_1 \dot{\phi} + \mathcal{O}(\epsilon^2)$ is fully described by the angle velocity; this because of the elasticity of the flagellum and the viscous nature of the forces applied to it. We can then refer to $\dot{\phi}$ as the flagellum "shape" parameter. By modulating the orientation ϕ and the shape $\dot{\phi}$ we can vary Ω, and in turn determine $\Delta\mathbf{q}$ in magnitude and direction, at least at the first the order in the Machin number.

Notice that we have a finite displacement only if the measure of the set Ω is non-zero. In other words: locomotion is enabled if the orientation ϕ and the shape $\dot{\phi}$ undergo a non-reciprocal cycle. As mentioned in the introduction, this have been pointed out in the case of a two-link model swimmer in [74]. What we gain with our analysis in this matter is that shape and orientation are one the time derivative of the other, and non-reciprocity happens naturally exactly because of this fact, indeed

$$\int_\Omega d\psi d\phi = \int_{\partial\Omega} \psi \, d\phi = \int_0^1 \dot{\phi}^2 dt > 0\,. \tag{3.50}$$

Notice that this result implies that, whenever the curve $t \to (\dot{\phi}(t), \phi(t))$ parametrizes the boundary of a domain in the plane, then it is always circuiting it in the counter-clockwise direction.

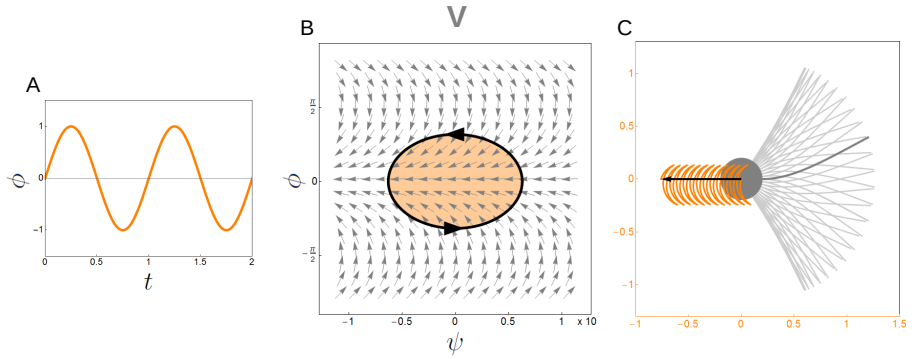

Figure 3.2: A) Sinusoidal actuation. B) Resulting domain Ω (orange) on the space (ψ, ϕ) and normalized vector field $\mathbf{V}$ (grey arrows). C) Various snapshots of the swimmer as seen in the frame $\{\mathbf{e}_1, \mathbf{e}_2\}$ moving with the centre of the cargo. In orange, the trajectory of the cargo (as seen in a fixed frame) given by the truncation at first order $\mathbf{q}_0 + \epsilon\mathbf{q}_1$.

Let us consider first the most simple example, namely that of a sinusoidal actuation $\phi(t) = \sin 2\pi t$ as in Fig.3.2A. Here Ω is the set contained in the ellipse $\partial\Omega$ centred in the origin (see Fig.3.2B). From (3.46) we have that $C < 0$, therefore the horizontal component $\mathbf{V} \cdot \mathbf{e}_1$ of the vector field is always negative for every point in Ω in this case. On the other end, the projection $\mathbf{V} \cdot \mathbf{e}_2$ is an odd function with respect of the variable ϕ. Because of the symmetry of Ω the integral in (3.49) has a null component in the $\mathbf{e}_2$ direction. The motion is then horizontal and the swimmer moves head-first, from right to left, as shown in Fig.3.2C. We recovered here the known result from previous numerical investigations [65, 69].

Observe now what happens if we take the non-sinusoidal actuation shown in Fig.3.3AI. The amplitude of the oscillation is the same as the previous example, however, now when $\phi > 0$ the oscillation runs slower, while when $\phi < 0$ it goes

faster. We have an asymmetric set of integration Ω that gathers more points in which $\mathbf{V}\cdot\mathbf{e}_2 > 0$ rather than points where $\mathbf{V}\cdot\mathbf{e}_2 < 0$, as Fig.3.3BI illustrates. As a result the swimmer moves sideways with respect to the axis of symmetry of the oscillation, with a positive displacement in the vertical direction at every period (see Fig.3.3CI). In order to obtain a negative displacement in the vertical direction we can consider the "negative" of the previous angle evolution, such as the one shown in Fig.3.3AII. This time the oscillation is faster for $\phi > 0$ and slower for $\phi < 0$, and the resulting set Ω is the reflection about the ψ axis of the previous one. The motion of the swimmer is depicted in Fig.3.3CII. In all numerical calculations in the Chapter we set $L/r_f = 10^3$ and $\gamma = 0.5$. For the simulation in this Section we took $\epsilon = 0.7$ and $\rho = 0.2$.

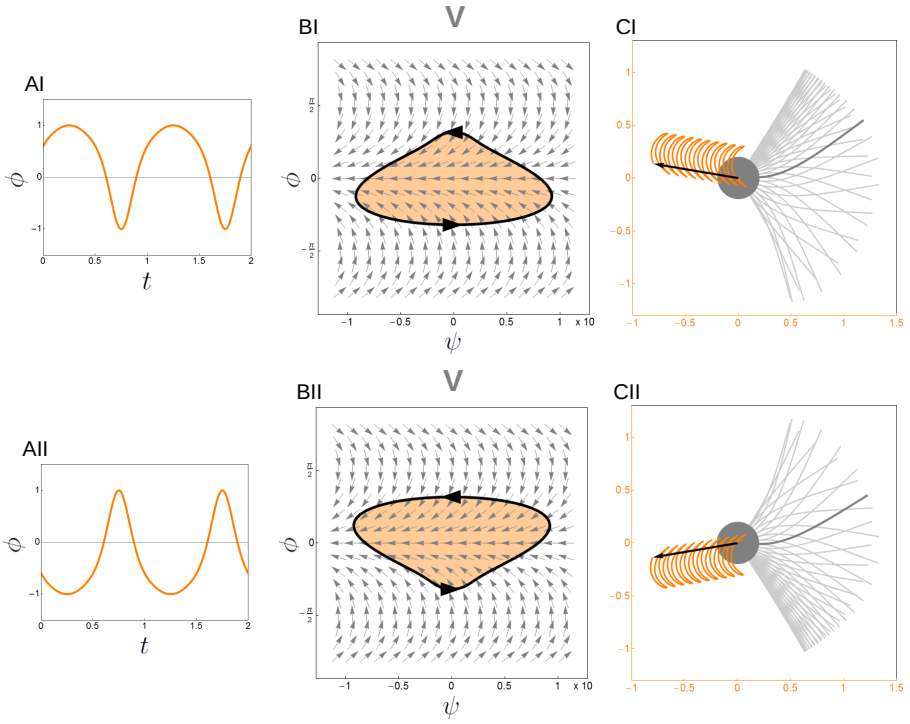

Figure 3.3: A) Non-sinusoidal actuations. B) Resulting domains Ω and normalized vector field $\mathbf{V}$. C) Swimmer kinematics.

In all the examples we have seen so far we had the swimmer moving in the negative horizontal direction, head-first. Equation (3.49) tells that this is in fact the case for *every* actuation such that $|\phi| < \pi/2$. Indeed, since $\mathbf{V}\cdot\mathbf{e}_1 < 0$ for every point in the domain Ω generated by such an oscillation, and since the signed area of Ω is always positive (3.50), the projection on $\mathbf{e}_1$ of the integral in (3.49) is negative.

We conclude this section showing that, in addition to be able to control the vertical displacement of the swimmer, we can also control the sign of the horizontal motion, making the swimmer going from left to right or from right to left. We exploit here the fact that $\mathbf{V}\cdot\mathbf{e}_1 = C\cos\phi$ changes sign for $|\phi| > \pi/2$. Indeed, if we consider the sinusoidal actuations $\phi(t) = A\sin(2\pi t)$ and we denote

$\Omega(A)$ their generated domains, we have

$$\Delta\mathbf{q}_1 \cdot \mathbf{e}_1 = \int_{\Omega(A)} \mathbf{V}(\phi) \cdot \mathbf{e}_1 \, d\psi d\phi = C \int_{\Omega(A)} \cos(\phi) \, d\psi d\phi = C(2\pi)^2 A J_1(A) \quad (3.51)$$

where J_1 is the first Bessel function of the first kind. So, at first order approximation, the horizontal displacement $\Delta\mathbf{q}\cdot\mathbf{e}_1 = \epsilon\Delta\mathbf{q}_1\cdot\mathbf{e}_1 + \mathcal{O}(\epsilon^2)$ do change sign, as $\Delta\mathbf{q}_1 \cdot \mathbf{e}_1$ has the graph illustrated in Fig.3.4A. In fact, as A grows, the horizontal displacement goes from being negative to being positive and then negative again, passing from local maxima to local minima that grow in modulus. In Fig.3.4B we show what happens with the integral in (3.51) as we vary A. While the domains $\Omega(A)$ grow larger and larger, they end up to gather, alternatively, more points in which $\mathbf{V} \cdot \mathbf{e}_1 < 0$ or more points where $\mathbf{V} \cdot \mathbf{e}_1 > 0$.

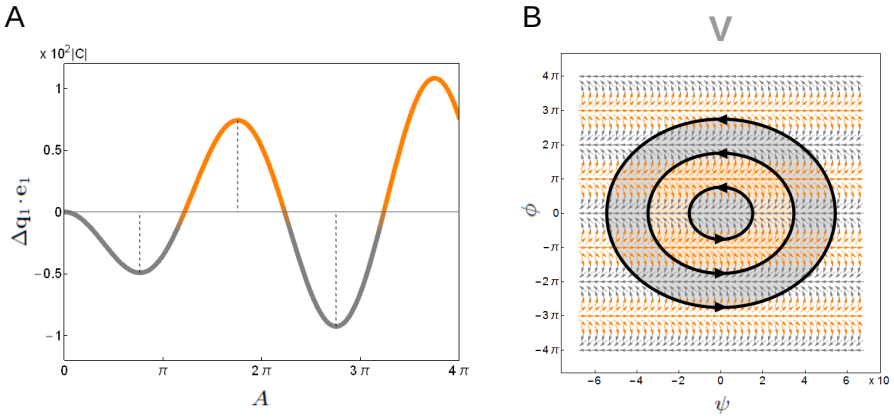

Figure 3.4: A) $\Delta\mathbf{q}_1 \cdot \mathbf{e}_1$ as a function of the amplitude A of oscillation. The first order horizontal displacement attains both positive (orange) and negative (grey) values, passing from local maxima to local minima (dotted lines). B) Domains generated by the actuations relative to local maxima and minima of $\Delta\mathbf{q}_1 \cdot \mathbf{e}_1$. Vectors for which $\mathbf{V} \cdot \mathbf{e}_1 < 0$ ($\mathbf{V} \cdot \mathbf{e}_1 > 0$) are plotted in grey (orange).

3.2.3 Optimality

Since our analysis provides some novel explicit formulas for the dynamics of the microswimmer, it is worth considering whether they can deliver some results regarding the optimization of the locomotion process.

First we recall that, if we fix the slenderness parameter L/r_f for the flagellum, then η can be written solely in terms of ρ as in (3.21). In turn, substituting (3.21) in (3.46), we have that also the parameter $C = C(\rho)$ can be seen as a function of the ratio $\rho = a/L$. By restricting ourselves to sinusoidal actuations of the type $\phi(t) = A\sin(2\pi t)$, we can endure to optimize some dynamical quantities in the parameters A and ρ.

From the last example in the previous section we see (3.51) there is no amplitude A that maximizes the displacement $\Delta\mathbf{q}$, which displays local maxima growing larger and larger as $A \to \infty$. This is not entirely surprising because, since we work with fixed frequencies, as A becomes larger the velocity $\dot{\phi}$ in

which the oscillation is driven tends to infinity. In view of this observation we then consider here $\mathcal{V}$, namely the ratio between the average velocity in body-length of the swimmer units $\omega L|\Delta\mathbf{q}|/(2a+L)$ and the velocity ωA related to the oscillation

$$\mathcal{V} := \frac{\omega L|\Delta\mathbf{q}|}{(2a+L)\omega A} = \epsilon\frac{|C(\rho)|}{2\rho+1}(2\pi)^2|J_1(A)| + \mathcal{O}(\epsilon^2)\,. \tag{3.52}$$

At the first order in the Machin number velocity ratio $\mathcal{V}$ can be written as a product $C_{\mathcal{V}}(\rho)J_{\mathcal{V}}(A)$ where

$$C_{\mathcal{V}}(\rho) = \frac{|C(\rho)|}{2\rho+1} \quad \text{and} \quad J_{\mathcal{V}}(A) = (2\pi)^2|J_1(A)| \tag{3.53}$$

are two coefficients that can be maximized independently in ρ and A respectively. Their graphs and their maximum points are displayed in Fig.3.5.

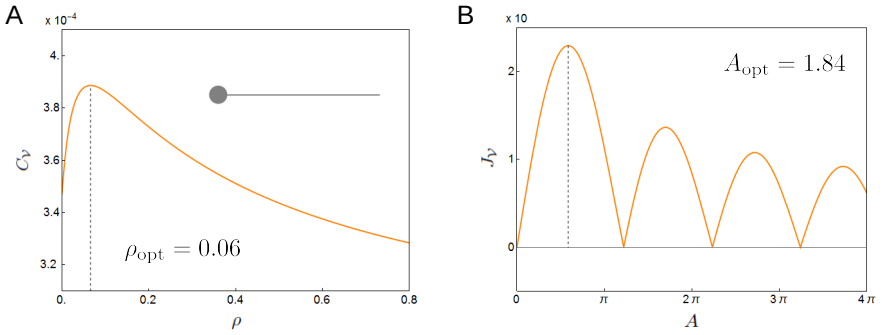

Figure 3.5: A) Ratio ρ_{opt} maximizing coefficient $C_{\mathcal{V}}$ and relative swimmer. B) Amplitude A_{opt} maximizing coefficient $J_{\mathcal{V}}$. Dotted lines indicate maximum values.

The other quantity that we can optimize is the locomotion efficiency $\mathcal{E}$. We define $\mathcal{E}$ as the ratio between: the total power expended by the external (dimensional) torque $\omega\xi_\perp L^3\tau_{\rm ext}$ during one period, and the power needed to move an inactive swimmer along its reference axis by a distance $L|\Delta\mathbf{q}|$ with average velocity $L\omega|\Delta\mathbf{q}|$; the distance and average velocity, respectively, that the external actuation produces. We have

$$\mathcal{E} := \frac{(\omega L|\Delta\mathbf{q}|)^2(\nu+\xi_{//}L)}{\int(\omega\xi_\perp L^3\tau_{\rm ext})(\omega\dot{\phi})}\,.$$

Here we consider $\tau_{\rm ext}$ as the external torque needed to generate the sinusoidal oscillation $\phi(t) = A\sin(2\pi t)$. By expanding the first three terms in equation

(3.17) we obtain the following approximated expression

$$\begin{aligned}\tau_{\text{ext}} &= (\eta_{\text{rot}} + \eta\rho^2)\dot{\phi} - \eta\rho u_0^y - \frac{\partial^2 y_1}{\partial x^2}(0,t) + \mathcal{O}(\epsilon)\\ &= \left(\eta_{\text{rot}} + \eta\rho^2 - \eta\rho\left(\frac{\eta\rho - \frac{1}{2}}{\eta+1}\right) + p_1''(0)\right)\dot{\phi} + \mathcal{O}(\epsilon)\\ &= \left(\eta_{\text{rot}} + \frac{4\eta\left(1+3\rho+3\rho^2\right)+1}{12\,(\eta+1)}\right)\dot{\phi} + \mathcal{O}(\epsilon)\\ &= T_0\dot{\phi} + \mathcal{O}(\epsilon) \quad \text{where} \quad T_0 = \eta_{\text{rot}} + \frac{4\eta\left(1+3\rho+3\rho^2\right)+1}{12\,(\eta+1)}\,. \end{aligned} \tag{3.54}$$

Using again (3.21), we have $T_0 = T_0(\rho)$. With $\tau_{\text{ext}} = \dot{\phi}\,T_0 + \mathcal{O}(\epsilon)$, the formula for the efficiency gives

$$\begin{aligned}\mathcal{E} &= \epsilon^2\frac{(\eta+\gamma)}{T_0}\left(\frac{\left|\int_\Omega \mathbf{V}\,d\psi d\phi\right|^2}{\int_0^1 \dot{\phi}^2 dt}\right) + \mathcal{O}(\epsilon^3)\\ &= \epsilon^2\frac{(\eta+\gamma)}{T_0}\left(\frac{\left|C(2\pi)^2 A J_1(A)\right|^2}{2(\pi A)^2}\right) + \mathcal{O}(\epsilon^3)\\ &= \epsilon^2\frac{(\eta+\gamma)}{T_0}C^2 8\pi^2 J_1(A)^2 + \mathcal{O}(\epsilon^3)\,.\end{aligned}$$

As it was for the previous case, also the efficiency can be written, at first approximation, as a product $C_{\mathcal{E}}(\rho)J_{\mathcal{E}}(A)$ of two functions

$$C_{\mathcal{E}}(\rho) = \frac{C^2(\rho)(\eta(\rho)+\gamma)}{T_0(\rho)} \quad \text{and} \quad J_{\mathcal{E}}(A) = 8\pi^2 J_1(A)^2$$

that can be maximized autonomously, one for the actuation amplitude A and the other for ρ. Graphs of the two coefficients and optimal values for A and ρ are given in Fig.3.6. Notice that $\mathcal{V}$ and $\mathcal{E}$ are optimized by the same angle amplitude.

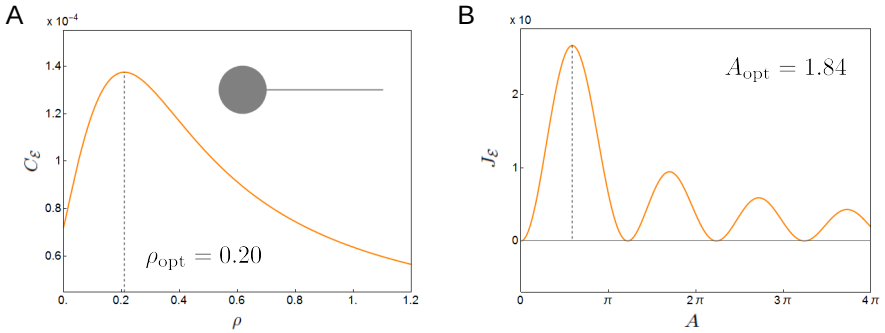

Figure 3.6: A) Coefficient $C_{\mathcal{E}}$ and the optimal swimmer. B) Coefficient $J_{\mathcal{E}}$.

3.2.4 Prescribed torque

We consider here the analysis of the problem for the externally actuated swimmer in the case where τ_{ext} is given. The system of equations in this case consists in (3.27)-(3.29) and the equation for the moment balance on the cargo (3.17). As we prove in Appendix I, this problem admits only one periodic solution in the unknowns u^x, u^y, y and $\dot{\phi}$, if the prescribed torque τ_{ext} is periodic. Such a solution can be approximated using the asymptotic approach we adopted in the case of prescribed angle actuation. We obtain a formal series expression for u^x, u^y and y of the type (3.30) and ϕ can also be computed in the power series form

$$\phi = \phi_0 + \epsilon\phi_1 + \epsilon^2\phi_2 \dots \tag{3.55}$$

We provide the explicit calculations of the asymptotic coefficients in Appendix II, while we discuss here the main results.

An important formula we derive is the zero-order expression for the resulting angle evolution $\phi(t)$, that reads

$$\phi_0(t) = \phi_{\text{in}} + T_0^{-1} \int_0^t \tau_{\text{ext}} \tag{3.56}$$

where T_0 is given by (3.54) and ϕ_{in} is the angle at time $t = 0$. Not surprisingly we recover the same zero-order relation we have in the case in which ϕ is given and τ_{ext} is the torque needed to produce it. Interpreting formula (3.56) we can say that we can bring ourselves back to the case of prescribed angle as the angle can, in a sense, be prescribed, at least up to a multiplicative constant and an integration in the time variable.

We can combine (3.56) with another result of the asymptotic calculations, that is the expression for the displacement $\Delta\mathbf{q}$. If τ_{ext} has zero average during one period, the formula we obtain for $\Delta\mathbf{q}$ is in fact the same as in (3.49) with ϕ replaced by ϕ_0, namely

$$\Delta\mathbf{q} = \epsilon \int_\Omega \mathbf{V}(\phi_0)\, d\psi d\phi_0 + \mathcal{O}(\epsilon^2)$$

where $\mathbf{V}$ is given by (3.47) and Ω is the domain contained in the closed curve

$$\partial\Omega = \left\{ (\dot{\phi}_0(t), \phi_0(t)) \,;\, t \in [0,1] \right\} \subset \mathbb{R}^2 \,. \tag{3.57}$$

Clearly, then, all the motility results deduced in Section 3.2.2 applies here with with ϕ replaced by ϕ_0.

As for the optimality, we can consider sinusoidal actuations of the kind $\tau_{\text{ext}} = \Lambda\cos(2\pi t)$ then, since we have

$$\phi_0 = \frac{\Lambda T_0^{-1}}{2\pi} \sin(2\pi t)\,,$$

the two quantities considered in the previous section now read

$$\mathcal{V} = \epsilon \frac{|C(\rho)|}{2\rho+1} (2\pi)^2 \left| J_1\left(\frac{\Lambda T_0^{-1}}{2\pi}\right)\right| + \mathcal{O}(\epsilon^2) \quad \text{and}$$

$$\mathcal{E} = \epsilon^2 \frac{(\eta+\gamma)}{T_0} C^2 8\pi^2 J_1^2\left(\frac{\Lambda T_0^{-1}}{2\pi}\right) + \mathcal{O}(\epsilon^3)\,.$$

We can optimize the least order approximation of $\mathcal{V}$ and $\mathcal{E}$ in terms of the actuation amplitude Λ and the parameter ρ, although not independently as it is for the prescribed angle case. In particular, given ρ, in both cases the optimal torque amplitude is $\Lambda_{\text{opt}} = 2\pi T_0(\rho) A_{\text{opt}}$, where A_{opt} is the optimal angle amplitude for $\mathcal{V}$ and $\mathcal{E}$.

3.3 Internally actuated swimmer

For the swimmer in Fig.3.1B we do not treat the case of prescribed (internal) torque, and we consider only the problem in which the angle difference $\alpha = \theta - \phi$ is given. We restrict our analysis to the physically significant case $|\alpha| < \pi/2$.

The governing equations reduce to (3.23), the projection on $\mathbf{e}_\theta^\perp$ of (3.16), (3.26) and the first equation in (3.18), together with boundary conditions (3.19). Setting $\theta := \phi + \alpha$, we obtain the following system

$$\begin{cases} \epsilon\left(u^y(t) + \dot\theta x + \dfrac{\partial y}{\partial t}(x,t)\right) = -\dfrac{\partial^4 y}{\partial x^4}(x,t) & (3.58) \\ \epsilon M(\alpha)\begin{pmatrix} u^x \\ u^y \\ \dot\phi \end{pmatrix} = \begin{pmatrix} \epsilon\gamma\dot\theta \int_0^1 y + \frac{\gamma-1}{2}\left(\frac{\partial^2 y}{\partial x^2}\right)^2(0,t) \\ -\frac{\partial^3 y}{\partial x^3}(0,t) \\ \frac{\partial^2 y}{\partial x^2}(0,t) \end{pmatrix} & (3.59) \end{cases}$$

where

$$M(\alpha) = \begin{pmatrix} \eta+\gamma & 0 & -\eta\rho\sin\alpha \\ 0 & \eta & -\eta\rho\cos\alpha \\ -\eta\rho\sin\alpha & -\eta\rho\cos\alpha & (\eta_{\text{rot}} + \eta\rho^2) \end{pmatrix}$$

System (3.58)-(3.59) defines a set of equations in the unknowns u^x, u^y, $\dot\phi$ and y that, given a periodic α, has only one periodic solution. As for the externally driven case, the periodic solution can be approximated using standard series expansion methods. All these technical results are proven in Appendix I.

3.3.1 Asymptotics

We look again for formal solutions where u^x, u^y and y are given by (3.30). While writing also ϕ and θ as a power series of ϵ, we assume that their coefficients satisfy $\theta_0 = \phi_0 + \alpha$ and $\theta_k = \phi_k$ for $k \geq 1$. We provide here the main passages of the calculation of the expansions up to the order $k = 1$, providing the mean to obtain explicit solutions. We do not report the final formulas because of their excessive complexity.

The equation for the coefficients y_k is given by (3.31) with $\dot\theta_k$ instead of $\dot\phi_k$, together with the boundary conditions (3.33). As in the externally actuated case we have $y_0 = 0$, while y_1 can be written as in (3.34) with $\dot\phi_0 + \dot\alpha$ instead of $\dot\phi$. In turn

$$\frac{\partial^3 y_1}{\partial x^3}(0,t) = u_0^y(t) + \frac{1}{2}(\dot\phi_0(t) + \alpha(t)) \quad \text{and} \quad \frac{\partial^2 y_1}{\partial x^2}(0,t) = -\frac{u_0^y(t)}{2} - \frac{1}{3}(\dot\phi_0(t) + \alpha(t))$$

Notice that the first order term in the expansion of the first component in the

right hand side of (3.59) is zero. Therefore, the first order in ϵ of (3.59) reads

$$M_0(\alpha)\begin{pmatrix} u_0^x \\ u_0^y \\ \dot\phi_0 \end{pmatrix} = \dot\alpha \begin{pmatrix} 0 \\ -\frac{1}{2} \\ -\frac{1}{3} \end{pmatrix}$$

where M_0 is given by (3.80). We can invert the matrix M_0 obtaining that u_0^x, u_0^y, $\dot\phi_0$ and $\dot\theta_0$ can be written in the following form

$$u_0^x = U_0^x(\alpha)\dot\alpha\,,\ u_0^y = U_0^y(\alpha)\dot\alpha\,,\ \dot\phi_0 = \varphi_0(\alpha)\dot\alpha \quad \text{and} \quad \dot\theta_0 = \vartheta_0(\alpha)\dot\alpha \tag{3.60}$$

where U_0^x, U_0^y and φ_0 are functions that can be calculated explicitly, while $\vartheta 0 = \varphi_0 + 1$. Taking two primitives Φ_0 and $\Theta_0$respectively for φ_0 and ϑ_0 that are compatible with the initial conditions we can write

$$\phi_0 = \Phi_0(\alpha) \quad \text{and} \quad \theta_0 = \Theta_0(\alpha)\,. \tag{3.61}$$

In turn, we have that

$$\begin{aligned} y_1(x,t) &= -p_1(x,\alpha)\dot\alpha \quad \text{where} \\ p_1(x,\alpha) &= \int_0^x \int_0^{x_1} \int_{x_2}^1 \int_{x_3}^1 \Big(U_0^y(\alpha) + \Theta_0'(\alpha)x_4\Big)\, dx_4 dx_3 dx_2 dx_1 \end{aligned} \tag{3.62}$$

Notice that the bending of the flagellum, at first approximation, depend both on the internal angle α and its velocity $\dot\alpha$.

Proceeding with the calculations, we can write y_2 as

$$y_2(x,t) = -\int_0^x \int_0^{x_1} \int_{x_2}^1 \int_{x_3}^1 \Big(u_1^y(t) + \frac{\partial y_1}{\partial t}(x_4,t) + \dot\phi_1(t)x_4\Big)\, dx_4 dx_3 dx_2 dx_1\,. \tag{3.63}$$

which gives

$$\frac{\partial^3 y_2}{\partial x^3}(0,t) = u_1^y(t) + \frac{\dot\phi_1(t)}{2} - \dot\alpha^2 \int_0^1 \frac{\partial p_1}{\partial \alpha}(\alpha,x)\,dx - \ddot\alpha \int_0^1 p_1(\alpha,x)\,dx \quad \text{and}$$

$$\frac{\partial^2 y_2}{\partial x^2}(0,t) = -\frac{u_1^y(t)}{2} - \frac{\dot\phi_1(t)}{3} + \dot\alpha^2 \int_0^1\int_z^1 \frac{\partial p_1}{\partial \alpha}(\alpha,x)\,dxdz + \ddot\alpha \int_0^1\int_z^1 p_1(\alpha,x)\,dxdz\,.$$

The second order term in the expansion of the first component in the right hand side of (3.59) is

$$\gamma\dot\theta_0 \int_0^1 y_1 + \frac{\gamma-1}{2}\left(\frac{\partial^2 y_1}{\partial x^2}\right)^2(0,t) = \left(-\gamma\Theta_0(\alpha)\int_0^1 p_1(\cdot,\alpha) + \frac{\gamma-1}{2}\left(\frac{\partial^2 p_1}{\partial x^2}\right)^2(0,\alpha)\right)\dot\alpha^2$$

therefore

$$M_0(\alpha)\begin{pmatrix} u_1^x \\ u_1^y \\ \dot\phi_1 \end{pmatrix} = \begin{pmatrix} -\gamma\Theta_0(\alpha)\int_0^1 p_1(\cdot,\alpha) + \frac{\gamma-1}{2}\frac{\partial^2 p_1^2}{\partial x^2}(0,\alpha) \\ \int_0^1 \frac{\partial p_1}{\partial\alpha}(\alpha,x)\,dx \\ \int_0^1\int_z^1 \frac{\partial p_1}{\partial\alpha}(\alpha,x)\,dxdz \end{pmatrix}\dot\alpha^2 + \begin{pmatrix} 0 \\ \int_0^1 p_1(\alpha,\cdot) \\ \int_0^1\int_z^1 p_1(\alpha,\cdot) \end{pmatrix}\ddot\alpha$$

We can invert again the matrix M_0 obtaining the solution for u_1^x, u_1^y and $\dot\phi_1 = \dot\theta_1$. It is easy to conclude that these expressions have a common form, that is

$$u_1^x = A_1^x(\alpha)\dot\alpha^2 + B_1^x(\alpha)\ddot\alpha \tag{3.64}$$

$$u_1^y = A_1^y(\alpha)\dot\alpha^2 + B_1^y(\alpha)\ddot\alpha \tag{3.65}$$

$$\dot\phi_1 = A_1^\phi(\alpha)\dot\alpha^2 + B_1^\phi(\alpha)\ddot\alpha \tag{3.66}$$

where all the functions of α in the right hand sides can be calculated explicitly.

3.3.2 Motility maps

A first consequence of the asymptotic analysis of the previous section is that the internal angle α and its velocity $\dot{\alpha}$, at first approximation, completely determine the shape of the swimmer in motion. The angle α gives the relative orientation of the reference axis of the flagellum with respect to the cargo. The bending deformation is given by (3.62) as the product of the input velocity $\dot{\alpha}$ times a shape function p_1, depending also on α.

In the following we show how the geometry in the shape space $(\dot{\alpha}, \alpha)$ of the actuation plays a crucial role in the resulting swimming behaviour.

We start by considering the orientation ϕ of the cargo. Since we know that the unperturbed problem has a periodic solution $\dot{\phi}$, we can consider the net variation of the angle ϕ over one (and indeed *any*) period of the actuation

$$\Delta\phi := \int_0^1 \dot{\phi}\,.$$

Expanding the solution $\Delta\phi = \Delta\phi_0 + \epsilon\Delta\phi_1 + \mathcal{O}(\epsilon^2)$ we have that, using (3.60) and (3.61),

$$\Delta\phi_0 = \int_0^1 \varphi_0(\alpha)\dot{\alpha} = \left[\Phi_0(\alpha)\right]_0^1 = 0\,.$$

Next, we notice that formula (3.66) for $\dot{\phi}_1$ has the form (3.44). Using (3.45), with the position $\dot{\alpha} = \psi$, we obtain

$$\Delta\phi_1 = \int_\Omega W(\alpha)\, d\psi d\alpha \quad \text{where} \quad W = A_1^\phi - \frac{dB_1^\phi}{d\alpha} \tag{3.67}$$

and Ω is a domain in $\mathbb{R}^2$ such that

$$\partial\Omega = \{(\dot{\alpha}(t), \alpha(t))\,;\, t \in [0,1]\} \subset \mathbb{R}^2\,. \tag{3.68}$$

Numerical calculations show that W is non-zero for every $\rho > 0$, it is odd with respect to α and negative for $\alpha > 0$. As a result, the net variation of the angle

$$\Delta\phi = \epsilon \int_\Omega W(\alpha)\, d\psi d\alpha + \mathcal{O}(\epsilon^2)\,. \tag{3.69}$$

is in general non-zero, and the swimmer can change its orientation. Observe that in this case, while $\dot{\phi}$ is periodic,

$$\phi(t+n) = \phi(t) + n\Delta\phi \tag{3.70}$$

is not periodic since $\Delta\phi$ is non-zero.

Let us consider now the $\mathbf{q}$ coordinate of the cargo given by the solution of the unperturbed problem (3.58)-(3.59). Using (3.70), the displacement $\Delta_n\mathbf{q}$ at the n^{th} actuation cycle is

$$\begin{aligned}
\Delta_n\mathbf{q} &= \int_n^{n+1} \dot{\mathbf{q}} \;=\; \int_n^{n+1} \left(u^x \mathbf{e}_\theta + u^y \mathbf{e}_\theta^\perp - \frac{d}{dt}\rho\mathbf{e}_\phi\right) \\
&= \int_0^1 \left(u^x \mathbf{e}_{\theta+n\Delta\phi} + u^y \mathbf{e}_{\theta+n\Delta\phi}^\perp - \rho\dot{\phi}\mathbf{e}_{\phi+n\Delta\phi}^\perp\right) \\
&= \mathbf{R}(n\Delta\phi) \int_0^1 \left(u^x \mathbf{e}_\theta + u^y \mathbf{e}_\theta^\perp - \rho\dot{\phi}\mathbf{e}_\phi^\perp\right) \;=\; \mathbf{R}(n\Delta\phi)\Delta_0\mathbf{q}
\end{aligned}$$

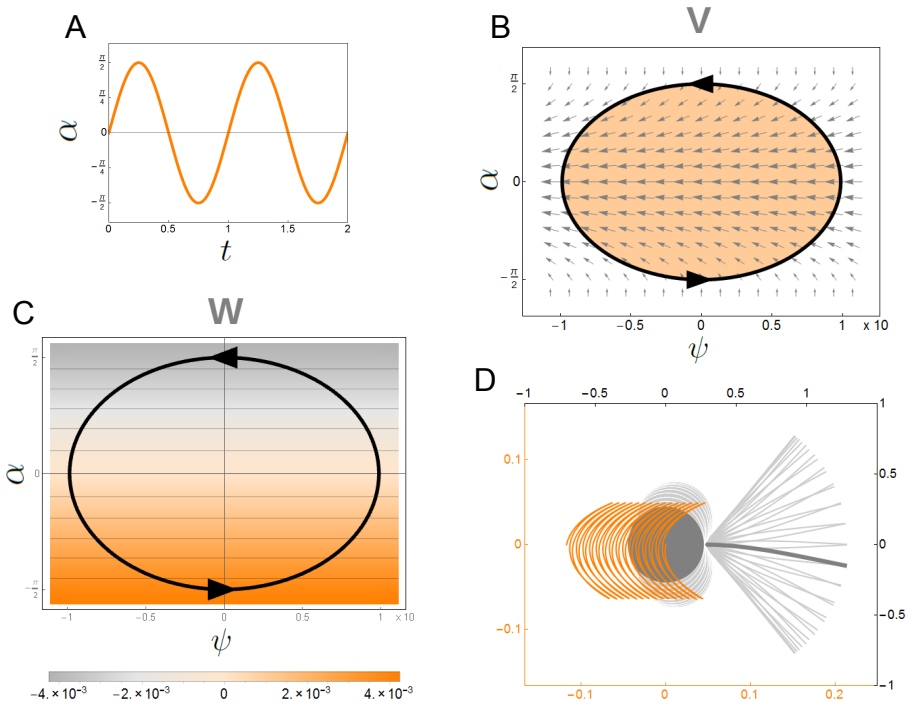

Figure 3.7: A) Sinusoidal actuation. B) Resulting domain Ω (orange) on the shape space (ψ, α) and normalized vector field $\mathbf{V}$ (grey arrows). C) Resulting loop in shape space and W (shaded colours). D) Various snap-shots of the swimmer as seen in the frame $\{\mathbf{e}_1, \mathbf{e}_2\}$ moving with the attachment point $\mathbf{r}(0,t)$. In orange, the trajectory of the cargo (as seen in a fixed frame) given by the truncation at first order $\mathbf{q}_0 + \epsilon\mathbf{q}_1$.

where $\mathbf{R}$ is the rotation matrix (3.39). If $\Delta\phi \neq 0$ and $\Delta_0\mathbf{q} \neq \mathbf{0}$ the swimmer moves along a curve passing through the points $\sum_i^n \Delta_i\mathbf{q}$ with $n \geq 0$. In the following we deduce the first order approximation formula for $\Delta_0\mathbf{q} = \Delta_0\mathbf{q}_0 + \epsilon\Delta_0\mathbf{q}_1 + \mathcal{O}(\epsilon^2)$. It must be noted that the formula holds only for actuations α such that $\alpha(0) = 0$. However, for actuations such that $\alpha \neq 0$, the following construction can be modified accordingly.

Expanding $\dot{\mathbf{q}} = \dot{\mathbf{q}}_0 + \epsilon\dot{\mathbf{q}}_1 + \mathcal{O}(\epsilon^2)$, from (3.60) and (3.61) we have that

$$\dot{\mathbf{q}}_0 = (u_0^x \mathbf{e}_{\theta_0} + u_0^y \mathbf{e}_{\theta_0}^\perp) - \rho\dot{\phi}_0 \mathbf{e}_{\phi_0}^\perp$$

has an expression of the form $\mathbf{P}(\alpha)\dot{\alpha}$, which gives always a null result when integrated over a period. Therefore $\Delta_0\mathbf{q}_0 = 0$. The first order coefficient in the expansion for $\dot{\mathbf{q}}$ reads

$$\dot{\mathbf{q}}_1 = \underbrace{(u_1^x \mathbf{e}_{\theta_0} + u_1^y \mathbf{e}_{\theta_0}^\perp)}_{I} + \underbrace{\phi_1 (u_0^x \mathbf{e}_{\theta_0}^\perp - u_0^y \mathbf{e}_{\theta_0})}_{II} - \underbrace{\rho\dot{\phi}_1 \mathbf{e}_{\phi_0}^\perp}_{III} + \underbrace{\phi_1\rho\dot{\phi}_0 \mathbf{e}_{\phi_0}}_{IV} .$$

Now, from (3.61) and (3.64)-(3.66) we see that terms I and III have again the form (3.44). Using (3.45) they can be written, respectively, as integrals of two

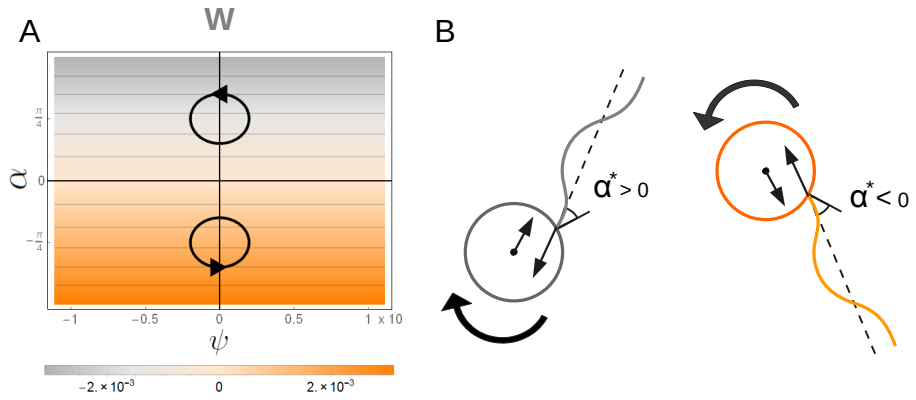

Figure 3.8: A) Loops in shape space generated by two sinusoidal beating around a non-zero internal angle α^*. When $\alpha^* > 0$ ($\alpha^* < 0$) the generated loop circles an area in which W assumes negative (positive) values. B) Sign of resulting rotations is consistent with sign of torque generated by miss-alignment of viscous and propulsive forces.

vector fields $\mathbf{V}_I$ and $\mathbf{V}_{III}$ over Ω, where the boundary $\partial\Omega$ is given by (3.68). On the other hand, terms II and IV are products of ϕ_1 times an expression of the type $\mathbf{P}(\alpha)\dot{\alpha}$. If we choose a function $\mathbf{\Pi}_0(\alpha)$ with $d\mathbf{\Pi}_0/d\alpha = P$ such that $\mathbf{\Pi}_0(0) = \mathbf{0}$, then we have

$$\int_0^1 \phi_1 \mathbf{\Pi}_0'(\alpha)\dot{\alpha} = [\phi_1 \mathbf{\Pi}_0(\alpha)]_0^1 - \int_0^1 \dot{\phi}_1 \mathbf{\Pi}_0(\alpha) = -\int_0^1 \dot{\phi}_1 \mathbf{\Pi}_0(\alpha)\,.$$

Since $\dot{\phi}_1 \mathbf{\Pi}_0(\alpha)$ has now the form (3.44), then II and IV can be written, respectively, as integrals of two vector fields $\mathbf{V}_{II}$ and $\mathbf{V}_{IV}$ over Ω. Taking $\mathbf{V} = \mathbf{V}_I + \mathbf{V}_{II} + \mathbf{V}_{III} + \mathbf{V}_{IV}$ we have

$$\Delta\mathbf{q}_1 = \int_\Omega \mathbf{V}(\alpha)\, d\psi d\alpha\,. \tag{3.71}$$

Combining (3.71) with the expansion $\mathbf{R}(n\Delta\phi) = \mathrm{Id} + \epsilon n \Delta\phi_1 \mathbf{R}(\pi/2) + \mathcal{O}(n\epsilon^2)$ for the rotation we obtain

$$\Delta_n \mathbf{q} = \epsilon\Big(\mathbf{Id} + n\epsilon\Delta\phi_1 \mathbf{R}(\pi/2)\Big) \int_\Omega \mathbf{V}(\alpha)\, d\psi d\alpha + \mathcal{O}(\epsilon^2, n\epsilon^3)\,. \tag{3.72}$$

Together with (3.67), formula (3.72) allows for a motility analysis solely based on the geometry of Ω.

As a first result from (3.69) we have that for domains Ω that are symmetric with respect to the ψ axis there are, at first approximation, no net rotations of the swimmer after any cycle. This happens, for example, with a sinusoidal actuation around 0. In Fig.3.7 we show the case where $\alpha(t) = \pi/2\sin(2\pi t)$, $\epsilon = 0.5$ and $\rho = 0.27$. Since $\mathbf{V}\cdot\mathbf{e}_1 < 0$ for every $|\alpha| < \pi/2$ while $\mathbf{V}\cdot\mathbf{e}_2$ is odd with respect to α, the swimmer moves head-first and, on average, on the horizontal axis. We recover here the same swimming behaviour described by previous studies [66, 67].

A second result we deduce from (3.69) is that the swimmer rotates when it performs sinusoidal beating of the flagellum $\alpha(t) = \alpha^* + A\sin(2\pi t)$ around a

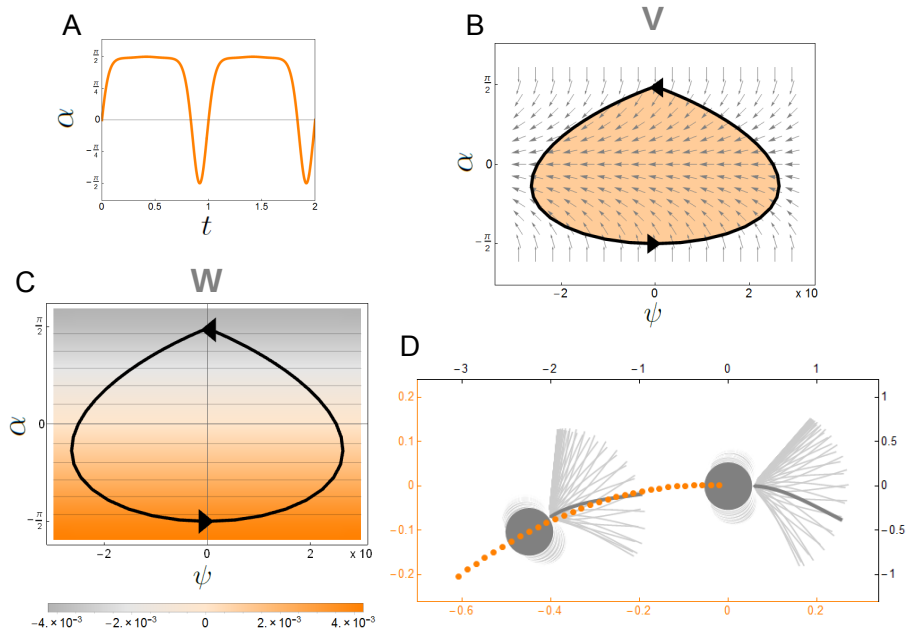

Figure 3.9: A) Non-sinusoidal actuation. B) Resulting domain Ω on the shape space and normalized vector field $\mathbf{V}$. C) Resulting loop in shape space with respect to W. D) Various snap-shots of the swimmer during two different cycles of actuation, as seen on the frame $\{\mathbf{e}_1, \mathbf{e}_2\}$ moving with the point of attachment. The $\mathbf{q}$ coordinate after every cycle (orange dots) is obtained summing the leading order values of the displacements (3.72).

non-zero internal angle α^*. The sign of W leads to a counter-clockwise rotation of the swimmer for $\alpha^* < 0$ and a clockwise rotation for $\alpha^* > 0$. This can be interpreted with the following heuristic argument, sketched in Fig.3.8B. Suppose that a sinusoidal beating always pushes the cargo with a force that is, on average, directed along the mean direction of the flagellum, as in the case when α oscillates around 0. Such a force must always oppose an equal and opposite one given by the viscous resistance on the cargo. If the flagellum is not perpendicular to the cargo on average, the two forces are not aligned and a moment is created. The sign of such a moment is consistent with the rotation directions dictated by (3.69). While this effect has never been discussed before (to our knowledge), it does not rely on large actuation amplitudes and, we remark, it can also be deduced within the small-actuation regime presented in [66].

The novel physical insight that (3.69) and (3.72) give is related to non-sinusoidal actuations, when Ω is non-symmetric with respect to its horizontal axis. Taking again $\epsilon = 0.5$ and $\rho = 0.27$, let us consider the actuation in Fig.3.9A, for which $\dot{\alpha}$ is much larger when $\alpha < 0$. The part of the resulting domain Ω where W is positive is larger then the part of Ω where W is negative. As a result the swimmer rotates counter-clockwise at every actuation cycle. The displacement $\Delta_0\mathbf{q}$ is, at first approximation, directed in the negative direction in the plane of locomotion since $\mathbf{V} \cdot \mathbf{e}_1 < 0$ for every point in the space (ψ, α). Moreover, since

$\mathbf{V} \cdot \mathbf{e}_2 > 0$ for $\alpha < 0$, $\Delta_0\mathbf{q}$ displays in this case also a positive component in the vertical direction. The composition of rotations and translations at every cycle generates the curved path illustrated in Fig.3.9D.

3.3.3 Optimality

An interesting feature of the internally actuated swimmer is its ability to move along curved paths. It is natural to consider whether there exists a design for the swimmer (the parameter ρ) that maximizes this effect (the angle $\Delta\phi_1$).

As shown in the previous section, there are two distinct strategies by which the swimmer can rotate: one is through actuations around a non-zero internal angle (Fig.3.7A), and the other is through non-symmetric actuations around $\alpha = 0$ (Fig.3.9C). To optimize the first turning strategy the actuation α has to produce a set Ω that is located around the maximum of $|W|$. A good choice for ρ is then the one that maximizes $\max_\alpha |W|$. For the second strategy we can argue that the best ρ is the one for which W displays the steepest gradient in values around $\alpha = 0$. The good choice in this case is that of ρ that maximizes $|dW/d\alpha(0)|$. Fig.3.10 illustrates the graphs of $\max_\alpha |W|$ and $|dW/d\alpha(0)|$ as functions of ρ, showing the existence of optimal values for both.

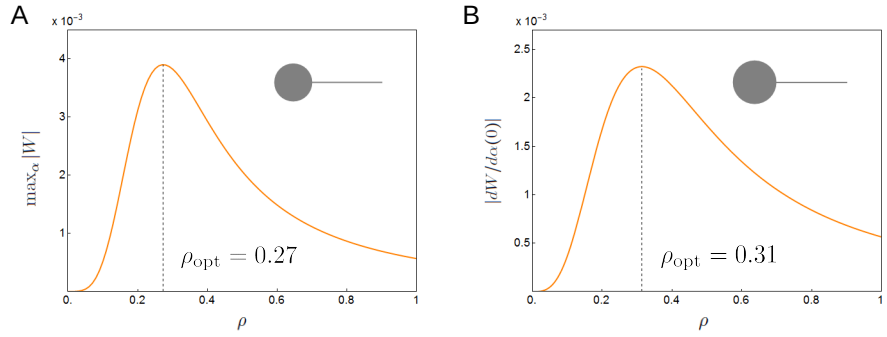

Figure 3.10: Variations of A) $\max_\alpha |W|$ and B) $|dW/d\alpha(0)|$ as functions of ρ and resulting optimal swimmers.

Finally, we consider sinusoidal actuations of the form $\alpha(t) = A\sin(2\pi t)$, leading to no net rotation. We test the values for different A and ρ of the following quantities: velocity ratio $\mathcal{V}$ given by (3.52), displacement after one cycle $\mathcal{D}^L = |\Delta\mathbf{q}|$ (measured in flagellum length units), displacement $\mathcal{D}^a = L|\Delta\mathbf{q}|/a$ (in units of cargo radii), and the efficiency

$$\mathcal{E} = \frac{(\omega L|\Delta\mathbf{q}|)^2(\nu + \xi_{//}L)}{\int(\omega\xi_\perp L^3\tau_{\text{int}})(\omega\dot{\alpha})}$$

defined in an analogous way as in the case of the externally actuated swimmer. Taking the lowest order terms in ϵ of

$$\mathcal{V} = \epsilon\frac{|\Delta_0\mathbf{q}_1|}{(2\rho+1)A} + \mathcal{O}(\epsilon^2)\ , \quad \mathcal{D}^L = \epsilon|\Delta_0\mathbf{q}_1| + \mathcal{O}(\epsilon^2)$$

$$\mathcal{D}^a = \epsilon\frac{|\Delta_0\mathbf{q}_1|}{\rho} + \mathcal{O}(\epsilon^2)\ , \quad \mathcal{E} = \epsilon^2\frac{(\eta+\gamma)|\Delta_0\mathbf{q}_1|^2}{\int_0^1 \frac{\partial^2 p_1}{\partial x^2}(0,\alpha)\dot{\alpha}^2 dt} + \mathcal{O}(\epsilon^3)\,,$$

and denoting them $\mathcal{V}_1$, $\mathcal{D}_1^L$, $\mathcal{D}_1^a$ and $\mathcal{E}_2$ respectively, we plot their graphs as functions of ρ for different values of A, from 0 to $\pi/2$. The results are shown in Fig.3.11. For every fixed ρ each quantity grows as A gets larger, so the optimal amplitude is $A = \pi/2$ for all cases. For any given amplitude A, we can detect optimal values for ρ for all the quantities. Such optimal values vary as A varies, but mildly. The swimmer designs resulting from the average of the optimal ρ's are displayed in Fig.3.11E.

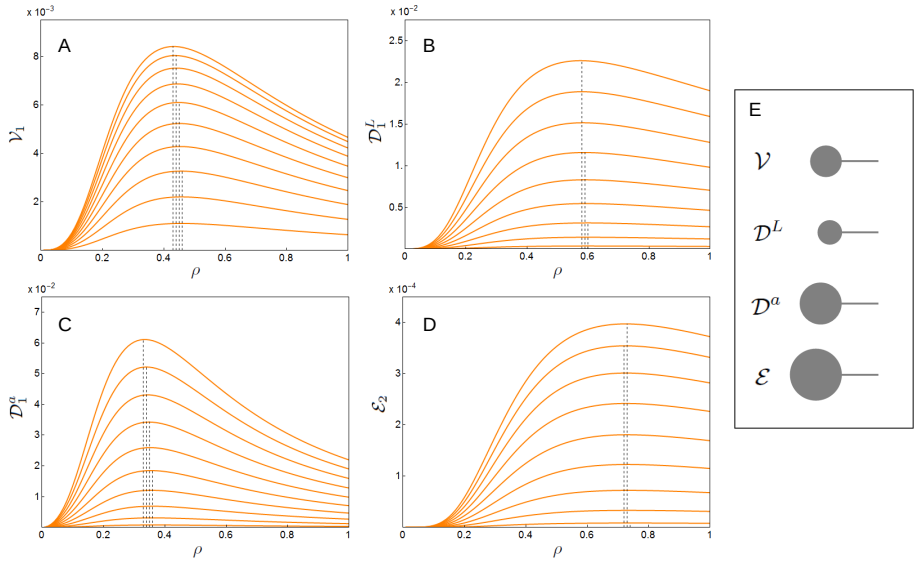

Figure 3.11: Variations as functions of ρ for different amplitudes A of: A) velocity $\mathcal{V}_1$, B) displacement $\mathcal{D}_1^L$, C) displacement $\mathcal{D}_1^a$ and D) efficiency $\mathcal{E}_2$. For every fixed ρ each quantity grows monotonically as A ranges from 0 to $\pi/2$ (linear steps), however, optimal values for ρ vary mildly as A varies. E) Swimmer geometries resulting from the average of such optimal values.

3.4 Appendix I. Rigorous approximation results

We propose here a scheme for the proof of existence and uniqueness of a periodic solution for the problems treated in Section 3.2, 3.2.4 and 3.3. After that, we show how the formal asymptotic solutions we proposed for each case approximate the unperturbed periodic ones. We provide the detailed proof for the case of the internally actuated swimmer (3.58)-(3.59). The other two cases can be treated following the same passages with minor changes.

Let us start by setting some notations. We denote $\mathcal{W}_j$, with $j \geq 0$, the normalized eigenfunction of the operator $-\partial^4$ with boundary conditions (3.19), relative to the eigenvalue λ_j^4. For an exhaustive discussion on the operator $-\partial^4$ and its eigenfunctions we refer the reader to [58]. In our case we have

$$\mathcal{W}_j(x) = (\cos\lambda_j x - \cosh\lambda_j x) - (\sin\lambda_j x - \sinh\lambda_j x)\frac{\cos\lambda_j + \cosh\lambda_j}{\sin\lambda_j + \sinh\lambda_j} \tag{3.73}$$

where the λ_j's are given implicitly by the following formula

$$\cos\lambda_j \cosh\lambda_j = -1 \quad (\text{observe that } \lambda_j \neq 0 \text{ and } \lambda_j \simeq (2j+1)\frac{\pi}{2} \text{ as } j \to \infty).$$

The $\mathcal{W}_j$'s are mutually orthogonal and together form a base of the square integrable functions space $\mathcal{L}^2([0,1])$. Finally, we denote with $\mathcal{C}^0_{\text{per}}$ and $\mathcal{C}^1_{\text{per}}$, respectively, the space of continuous and continuously differentiable periodic functions on $[0,1]$.

Consider now equation (3.58). We first proceed formally, substituting in (3.58) the expression

$$y(x,t) = \sum_j \hat{y}_j(t)\mathcal{W}_j(x) \tag{3.74}$$

and supposing that we can interchange the order of differentiation and summation, thereby deriving (3.74) term by term. Then, we substitute u^y and $\dot{\theta}x = (\dot{\phi} + \dot{\alpha})x$ in the left end side of (3.58) with

$$\sum_j u^y(t)\hat{1}_j\mathcal{W}_j(x) \quad \text{and} \quad \sum_j(\dot{\phi}(t) + \dot{\alpha}(t))\hat{x}_j\mathcal{W}_j(x)\,,$$

where $\{\hat{1}_j\}$ and $\{\hat{x}_j\}$ are the Fourier coefficients relative to the orthonormal base $\{\mathcal{W}_j\}$ of the functions 1 and x respectively. By matching coefficients relative to same eigenfunctions, we obtain the following sequences of ODEs

$$\epsilon\frac{d\hat{y}_j}{dt}(t) = -\lambda_j^4\hat{y}_j(t) - \epsilon\left(u^y(t)\hat{1}_j + (\dot{\phi}(t) + \dot{\alpha}(t))\hat{x}_j\right), \text{ for every } j \geq 0. \tag{3.75}$$

Given the initial conditions $\hat{y}_j(0)$, coefficients $\hat{y}_j$ can be written as

$$\hat{y}_j(t) = e^{-\lambda_j^4 t/\epsilon}\hat{y}_j(0) - e^{-\lambda_j^4 t/\epsilon}\int_0^t e^{\lambda_j^4 s/\epsilon}\left[u^y(s)\hat{1}_j + (\dot{\phi}(s) + \dot{\alpha}(s))\hat{x}_j\right]ds\,. \tag{3.76}$$

Suppose now that u^y and $\dot{\phi}$, along with the given function α, are periodic. Then, there exist only one periodic solution for (3.75), namely the one that corresponds to the initial condition

$$\hat{y}_j(0) = -\frac{e^{-\lambda_j^4/\epsilon}}{1 - e^{-\lambda_j^4/\epsilon}}\int_0^1 e^{\lambda_j^4 s/\epsilon}\left[u^y(s)\hat{1}_j + (\dot{\phi}(s) + \dot{\alpha}(s))\hat{x}_j\right]ds$$

as one can check by substituting the expression above in (3.76). If we also suppose that $u^y, \dot{\phi} \in \mathcal{C}^0_{\rm per}$ and $\alpha \in \mathcal{C}^1_{\rm per}$ then, a simple analysis gives

$$\|\hat{y}_j\|_\infty \le \frac{\epsilon}{\lambda_j^4}\left(\|u^y\|_\infty \hat{1}_j + \left\|\dot{\phi}+\dot{\alpha}\right\|_\infty \hat{x}_j\right)$$

where we denoted with $\|\cdot\|_\infty$ the uniform norm on $[0,1]$. The previous inequality shows that, given $u^y, \dot{\phi} \in \mathcal{C}^0_{\rm per}$ and $\alpha \in \mathcal{C}^1_{\rm per}$, and considering periodic solutions $\hat{y}_j$ of (3.76), then series (3.74) converges absolutely and uniformly with respect to t and x. The same holds the derivatives in x of (3.74) up to the third order. Moreover, equation (3.58) is solved by (3.74) in the weak sense. By construction, the periodic solution given by (3.74) is unique.

A crucial result for the remaining of our proof is summarized in the following

Lemma. Consider the one parameter family of operators T_ϵ defined for every $u \in \mathcal{C}^0_{\rm per}$ as the only periodic solution $v = T_\epsilon(u)$ of the equation

$$\epsilon \frac{dv}{dt}(t) = -\lambda v(t) + u(t)$$

where $\lambda > 0$ and $\epsilon \ge 0$. Then, we have that a) $T_\epsilon : \mathcal{C}^0_{\rm per} \to \mathcal{C}^0_{\rm per}$ are bounded operators with $\|T_\epsilon\| \le 1/\lambda$ for every $\epsilon \ge 0$, and b) the function $\epsilon \mapsto \|T_\epsilon\|$ is continuous for $\epsilon \to 0$.

Proof. Let us observe that, following the same arguments we adopted earlier, we can write

$$T_\epsilon(u)(t) = e^{-\lambda t/\epsilon}u_0 + \epsilon^{-1}e^{-\lambda t/\epsilon}\int_0^t e^{\lambda s/\epsilon}u(s)\,ds \qquad (3.77)$$
$$\text{where} \quad u_0 = \epsilon^{-1}\frac{e^{-\lambda/\epsilon}}{1-e^{-\lambda/\epsilon}}\int_0^1 e^{\lambda s/\epsilon}u(s)\,ds\,.$$

Moreover, we have $\|T_\epsilon\| \le 1/\lambda$, which proves a). In order to prove b) we have to show that, for every $u \in \mathcal{C}^0_{\rm per}$,

$$T_\epsilon(u) \underset{\epsilon\to 0}{\longrightarrow} T_0(u) \quad \text{in the uniform norm, where} \quad T_0(u) = \frac{u}{\lambda}\,. \qquad (3.78)$$

We first check the limit above for $u \in \mathcal{C}^1_{\rm per}$. Let us observe that, after an integration by parts,

$$\epsilon^{-1}e^{-\lambda t/\epsilon}\int_0^t e^{\lambda s/\epsilon}u(s)\,ds = \frac{u(t)}{\lambda} - u_0\frac{e^{-\lambda t/\epsilon}}{\lambda} - \frac{e^{-\lambda t/\epsilon}}{\lambda}\int_0^t e^{\lambda s/\epsilon}u'(s)\,ds\,.$$

Now, since $T_\epsilon(u) - T_0(u)$ is a continuous periodic function, we can evaluate its uniform norm in any of the intervals $[k, k+1]$ with $k \ge 0$. We have

$$\begin{aligned}\|T_\epsilon(u) - T_0(u)\|_\infty &= \sup_{t\in[k,k+1]}\left|u_0 e^{-\lambda t/\epsilon}\left(1-\frac{1}{\lambda}\right) - \frac{e^{-\lambda t/\epsilon}}{\lambda}\int_0^t e^{\lambda s/\epsilon}u'(s)\,ds\right| \\ &\le e^{-\lambda k/\epsilon}\,|u_0|\left(1-\frac{1}{\lambda}\right) + \sup_{t\in[k,k+1]}\left|\frac{e^{-\lambda t/\epsilon}}{\lambda}\int_0^t e^{\lambda s/\epsilon}\,ds\right|\,\|u'\|_\infty \\ &= e^{-\lambda k/\epsilon}\,|u_0|\left(1-\frac{1}{\lambda}\right) + \frac{\epsilon}{\lambda^2}(1-e^{-\lambda k/\epsilon})\,\|u'\|_\infty\,.\end{aligned}$$

The previous inequality must hold for every $k \geq 0$, therefore

$$\|T_\epsilon(u) - T_0(u)\|_\infty \leq \frac{\epsilon}{\lambda^2} \|u'\|_\infty ,$$

which proves (3.78) for every continuously differentiable u. To generalize the same result for every $u \in \mathcal{C}^0_{\text{per}}$ we can approximate u with a function in $\mathcal{C}^1_{\text{per}}$ and apply a classical "$\frac{\varepsilon}{3}$ argument" thanks to the uniform bound for the operator norms $\|T_\epsilon\| \leq 1/\lambda$.

Finally, let us observe that from (3.78) we have

$$\|T_0(u)\|_\infty = \lim_{\epsilon\to 0} \|T_\epsilon(u)\|_\infty \leq \liminf_{\epsilon\to 0} \|T_\epsilon\| \, \|u\|_\infty .$$

But then, since $\|T_0\| = 1/\lambda$ we obtain

$$\frac{1}{\lambda} = \|T_0\| \leq \liminf_{\epsilon\to 0} \|T_\epsilon\| \leq \limsup_{\epsilon\to 0} \|T_\epsilon\| \leq \frac{1}{\lambda}$$

which proves b). □

We put here in evidence the dependence of the periodic solution y of (3.58) on the parameter ϵ, and also the (functional) dependence on u^y, $\dot\phi$, and α by writing

$$y(x,t) = y_\epsilon \left[u^y, \dot\phi; \alpha\right](x,t).$$

After that, we define the following

$$y^*_\epsilon \left[u^y, \dot\phi; \alpha\right](x,t) := \epsilon^{-1} y_\epsilon \left[u^y, \dot\phi; \alpha\right](x,t) \quad \text{and}$$

$$\sigma^*_\epsilon \left[u^y, \dot\phi; \alpha\right](t) := \gamma\dot\phi(t) \int_0^1 y^*_\epsilon \left[u^y, \dot\phi; \alpha\right](x,t)\, dx + \frac{\gamma - 1}{2} \left(\frac{\partial^2 y^*_\epsilon}{\partial x^2} \left[u^y, \dot\phi; \alpha\right] \right)^2 (0,t) .$$

Notice that, for every fixed x, y^* is a uniformly convergent sum of operators of the kind discussed in the lemma. The same is true for each of its derivatives in x up to the third order, and also for the integral term (multiplying $\gamma\dot\phi$) in the expression of σ^*.

Now, with y given by (3.74), system (3.59) reads

$$M(\alpha(t)) \begin{pmatrix} u^x(t) \\ u^y(t) \\ \dot\phi(t) \end{pmatrix} - \begin{pmatrix} \epsilon\sigma^*_\epsilon \left[u^y, \dot\phi; \alpha\right](t) \\ -\frac{\partial^3 y^*_\epsilon}{\partial x^3} \left[u^y, \dot\phi; \alpha\right](0,t) \\ \frac{\partial^2 y^*_\epsilon}{\partial x^2} \left[u^y, \dot\phi; \alpha\right](0,t) \end{pmatrix} = \begin{pmatrix} 0 \\ 0 \\ 0 \end{pmatrix} .$$

Denoting $U = (u^x, u^y, \dot\phi)$ we write the left hand side of the above set of equations as $G_\epsilon[U; \alpha]$, so that

$$G_\epsilon[U; \alpha] = \mathbf{0} . \tag{3.79}$$

From the lemma we can prove that G_ϵ is a family of (non-linear) operators in the parameter ϵ defined in $X \times Y$ with values in X, where $X := \left(\mathcal{C}^0_{\text{per}}\right)^{\times 3}$ and $Y := \mathcal{C}^1_{\text{per}}$. The operators G_ϵ are continuous and continuously differentiable with respect to U. Moreover, the map $\epsilon \mapsto \partial G_\epsilon / \partial U$ is continuous for $\epsilon \to 0$. Now, the existence and uniqueness of a periodic solution for the system (3.58)-(3.59) follows if, for every fixed $\alpha \in Y$, there exist only one $U = U_\epsilon[\alpha] \in X$ that solves

(3.79). We prove this last statement by applying the implicit function theorem for Banach spaces (see for instance [76] Th,7.13-1). For the theorem to apply, we recall,

$$\frac{\partial G_\epsilon}{\partial U}\left[U;\alpha\right]$$

must be continuous as a function of U and α, and invertible as a linear operator from X to itself at a given point (U,α). We show that the invertibility condition holds for the case $\epsilon = 0$ which, by continuity, proves the hypotheses of the theorem for every small enough values of ϵ. Observe first that $y_\epsilon^*\left[u^y,\dot\phi;\alpha\right](x,t)$ is the only periodic solution of

$$u^y(t) + (\dot\phi(t) + \dot\alpha(t))x + \epsilon\frac{\partial y_\epsilon^*}{\partial t} = -\frac{\partial^4 y_\epsilon^*}{\partial x^4}$$

satisfying the boundary condition (3.19). For $\epsilon = 0$ the solution can be written explicitly as

$$\begin{aligned} y_0^*\left[u^y,\dot\phi;\alpha\right](x,t) &= -\int_0^x\int_0^{x_1}\int_{x_2}^1\int_{x_3}^1 u^y(t) + (\dot\phi(t)+\dot\alpha(t))x_4\,dx_4dx_3dx_2dx_1 \\ &= -\frac{x^2}{120}\Big(u^y(t)(30-20x+5x^2) + (\dot\phi(t)+\dot\alpha(t))(20-10x+x^3)\Big) \end{aligned}$$

therefore, in particular, we have

$$\begin{aligned} \frac{\partial^2 y_0^*}{\partial x^2}\left[u^y,\dot\phi;\alpha\right](0,t) &= -\frac{u^y(t)}{2} - \frac{\dot\phi(t)+\dot\alpha(t)}{3} \quad \text{and} \\ -\frac{\partial^3 y_0^*}{\partial x^3}\left[u^y,\dot\phi;\alpha\right](0,t) &= -u^y(t) - \frac{\dot\phi(t)+\dot\alpha(t)}{2}\,. \end{aligned}$$

At $\epsilon = 0$ the operator G_ϵ then becomes

$$G_0\left[U;\alpha\right] = M_0(\alpha)U + \begin{pmatrix} 0 \\ \dot\alpha/2 \\ \dot\alpha/3 \end{pmatrix}$$

where $M_0(\alpha)$ is the following matrix

$$\begin{pmatrix} \eta+\gamma & 0 & -\eta\rho\sin\alpha \\ 0 & \eta+1 & 1/2-\eta\rho\cos\alpha \\ -\eta\rho\sin\alpha & 1/2-\eta\rho\cos\alpha & (\eta_{\rm rot}+\eta\rho^2+1/3) \end{pmatrix}. \tag{3.80}$$

We have $\partial G_0/\partial U = M_0$, which shows that the derivative of G_ϵ is invertible for $\epsilon = 0$ and, indeed, for every small enough values of ϵ. The hypotheses of the implicit function theorem are fulfilled, and the uniqueness and existence of a periodic solution U_ϵ is verified.

Let us now prove that the truncated asymptotic solution U_1 we have calculated in Section 3.3.1, where

$$U_1 = \begin{pmatrix} u_0^x + \epsilon u_1^x \\ u_0^y + \epsilon u_1^y \\ \dot\phi_0 + \epsilon\dot\phi_1 \end{pmatrix},$$

approximates the periodic unperturbed solution U_ϵ. We assume here, for simplicity, that α is periodic and smooth. Notice that every results we stated above still apply. Moreover, from the calculations in Section 3.3.1, we have that U_1 is itself also smooth and periodic.

As a first step we show that there is a triplet R_ϵ, bounded in the norm of X uniformly for every ϵ small enough, such that

$$G_\epsilon[U_1] = \epsilon^2 R_\epsilon(t). \tag{3.81}$$

The equality (3.81) follows by asymptotic construction, however, we check the details here in the following. It is easy to verify that the periodic solution y of (3.58) can be written as

$$y_\epsilon\left[u^y, \dot\phi; \alpha\right](x,t) = -\epsilon \sum_{n,j} \frac{\tilde u_n^y \hat 1_j + (\tilde{\dot\phi}_n + \tilde{\dot\alpha}_n)\hat x_j}{\epsilon i 2\pi n + \lambda_j^4} e^{in2\pi t} \mathcal{W}_j^{(0)}(x)$$

where $\tilde{\dot\phi}_n$, $\tilde u_n^y$ and $\tilde{\dot\alpha}_n$ are the Fourier coefficients of $\dot\phi$, u^y and $\dot\alpha$ respectively. Observe now that

$$\frac{1}{\epsilon i 2\pi n + \lambda_j^4} = \frac{1}{\lambda_j^4} - \frac{\epsilon i 2\pi n}{(\epsilon i 2\pi n + \lambda_j^4)\lambda_j^4} = \frac{1}{\lambda_j^4} - \frac{\epsilon i 2\pi n}{\lambda_j^8} + \frac{\epsilon^2 (i 2\pi n)^2}{(\epsilon i 2\pi n + \lambda_j^4)\lambda_j^8}$$

therefore, denoting $u_1 = (u_0^y + \epsilon u_1^y, \dot\phi_0 + \epsilon\dot\phi_1)$, we have

$$\begin{aligned}
y_\epsilon[u_1;\alpha](x,t) &= -\epsilon \sum_{n,j} \frac{\tilde u_{0,n}^y \hat 1_j + (\tilde{\dot\phi}_{0,n} + \tilde{\dot\alpha}_n)\hat x_j}{\lambda_j^4} e^{in2\pi t} \mathcal{W}_j^{(0)}(x) \\
&+\epsilon^2 \sum_{n,j} \left(i2\pi n \frac{\tilde u_{0,n}^y \hat 1_j + (\tilde{\dot\phi}_{0,n} + \tilde{\dot\alpha}_n)\hat x_j}{\lambda_j^8} - \frac{\tilde u_{1,n}^y \hat 1_j + \tilde{\dot\phi}_{1,n}\hat x_j}{\lambda_j^4} \right) e^{in2\pi t} \mathcal{W}_j^{(0)}(x) \\
&+\epsilon^3 \sum_{n,j} \left(i2\pi n \frac{\tilde u_{1,n}^y \hat 1_j + \tilde{\dot\phi}_{1,n}\hat x_j}{(\epsilon i 2\pi n + \lambda_j^4)\lambda_j^4} - (i2\pi n)^2 \frac{\tilde u_{0,n}^y \hat 1_j + (\tilde{\dot\phi}_{0,n} + \tilde{\dot\alpha}_n)\hat x_j}{(\epsilon i 2\pi n + \lambda_j^4)\lambda_j^8} \right) e^{in2\pi t} \mathcal{W}_j^{(0)}(x),
\end{aligned}$$

where $\tilde{\dot\phi}_{0,n}$, $\tilde{\dot\phi}_{1,n}$, $\tilde u_{0,n}^y$ and $\tilde u_{1,n}^y$ are the Fourier coefficients of $\dot\phi_0$, $\dot\phi_1$, u_0^y and u_1^y respectively. It is straightforward to verify that can rewrite the previous equality as

$$y_\epsilon[u_1;\alpha](x,t) = \epsilon y_1(x,t) + \epsilon^2 y_2(x,t) + \epsilon^3 y_\epsilon^R[u_1;\alpha]$$

where y_1 and y_2 are the asymptotic coefficient for y that we have calculated in Section 3.3.1. Replacing $y_\epsilon^*[u_1;\alpha] = \epsilon^{-1} y_\epsilon[u_1;\alpha]$ into the expression for $G_\epsilon[U_1;\alpha]$, we can verify that we have (3.81) where R_ϵ can be calculated explicitly. The resulting R_ϵ is bounded in the norm of X uniformly for every ϵ small enough.

Finally observe that, from previous augments, the operator G_ϵ is locally invertible in U for every fixed α. So, from (3.79) and (3.81), by eventually restrict our set of choice for ϵ, we have

$$U_1 - U_\epsilon = G_\epsilon^{-1}[\epsilon^2 R_\epsilon;\alpha] - G_\epsilon^{-1}[0;\alpha] = \epsilon^2 \int_0^1 \frac{\partial G_\epsilon^{-1}}{\partial U}\left[\tau\epsilon^2 R_\epsilon;\alpha\right] d\tau \cdot R_\epsilon.$$

The integral term in the right hand side of the equality can be shown to be bounded in the norm of X by a constant $\mathcal{C}$

$$\left\| \int_0^1 \frac{\partial G_\epsilon^{-1}}{\partial U} \left[\tau \epsilon^2 R_\epsilon; \alpha \right] d\tau \cdot R_\epsilon \right\|_X \leq \mathcal{C}$$

which can be taken independent from ϵ for a small enough set of values of the parameter. For such set of values of ϵ then we have the following inequality

$$\|U_1 - U_\epsilon\|_X \leq \epsilon^2 \mathcal{C}\,,$$

which state rigorously that the asymptotic solution actually furnish an approximation for the only periodic solution of the unperturbed problem. An analogous result can be deduced for the difference between the truncated asymptotic solution for y and its unperturbed counterpart.

3.5 Appendix II. Prescribed external torque: formal asymptotic solution.

The unperturbed equation of the system in the case of the external given torque are those listed in the beginning of Section 3.2.4. As it was for the prescribed angle case u^x is decoupled from the other unknowns of the problem. If we take u^x, u^y, y as in (3.30) and ϕ as in (3.55), the coefficients of u^y, y and ϕ must solve

$$-\eta_{\rm rot}\dot{\phi}_k + \eta\rho(u_k^y - \rho\dot{\phi}_k) + \frac{\partial^2 y_{k+1}}{\partial x^2}(0,t) + \tau_k = 0 \quad \text{for } k \geq 0\,, \tag{3.82}$$

where we assumed $\tau_0 = \tau_{\rm ext}$ and $\tau_k = 0$ for $k \geq 1$, together with (3.31), (3.32) and the boundary conditions (3.33). Then, each coefficient of u^x can be directly calculated expanding (3.29). If the initial value $\phi_{\rm in}$ for the angle at $t = 0$ is prescribed, we impose $\phi_0(0) = \phi_{\rm in}$ and $\phi_k(0) = 0$ for $k \geq 0$.

At the zero-order we have $y_0(x,t) = 0$, therefore y_1 can be written as (3.34) with $\dot{\phi}_0$ instead of $\dot{\phi}$. Substituting this expression for y_1 in (3.32) and (3.82) we obtain the following linear system

$$\begin{cases} \eta\rho\dot{\phi}_0 - \eta u_0^y = u_0^y + \dfrac{1}{2}\dot{\phi}_0 \\ -\eta_{\rm rot}\dot{\phi}_0 + \eta\rho(u_0^y - \rho\dot{\phi}_0) - \dfrac{1}{3}\dot{\phi}_0 - \dfrac{1}{2}u_0^y + \tau_{\rm ext} = 0 \end{cases}$$

which allow us to solve for u_0^y and $\dot{\phi}_0$ in terms of $\tau_{\rm ext}$. If we consider the constants $U_0^y = (\eta\rho + 1/2)/(\eta + 1)$ and T_0 given by (3.54), then we have

$$u_0^y(t) = U_0^y\,\dot{\phi}_0(t) \quad \text{and} \quad \dot{\phi}_0(t) = T_0^{-1}\tau_{\rm ext}(t)$$

which gives (3.56). In turn $y_1(x,t) = -p_1(x)\dot{\phi}_0(t)$ with p_1 given by (3.36), thus the $k = 2$ order problem in (3.31) is solved by

$$y_2(x,t) = -\int_0^x \int_0^{x_1} \int_{x_2}^1 \int_{x_3}^1 \left(u_1^y(t) + \dot{\phi}_1(t)x_4 - p_1(x_4)\ddot{\phi}_0(t) \right) dx_4 dx_3 dx_2 dx_1\,.$$

Substituting the previous in (3.32) and (3.82) we obtain

$$\begin{cases} \eta\rho\dot{\phi}_1 - \eta u_1^y = u_1^y + \dfrac{1}{2}\dot{\phi}_1 - \left(\displaystyle\int_0^1 p_1\right)\ddot{\phi}_0 \\ -\eta_{\mathrm{rot}}\dot{\phi}_1 + \eta\rho(u_1^y - \rho\dot{\phi}_1) - \dfrac{1}{3}\dot{\phi}_1 - \dfrac{1}{2}u_1^y + \left(\displaystyle\int_0^1\int_x^1 p_1\right)\ddot{\phi}_0 = 0 \end{cases}$$

Defining the following constants

$$\varphi_1 = T_0^{-1}\left(\int_0^1\int_x^1 p_1 + \frac{\eta\rho - \frac{1}{2}}{\eta+1}\int_0^1 p_1\right) \quad \text{and} \quad \widetilde{U}_1^y = U_0^y\varphi_1 + U_1^y\,,$$

where U_1^y is given by (3.42), we can write the solutions of the previous system as

$$u_1^y(t) = \widetilde{U}_1^y\,\ddot{\phi}_0 \quad \text{and} \quad \dot{\phi}_1(t) = \varphi_1\ddot{\phi}_0(t)\,.$$

If we now expand the right hand side of (3.29) we get

$$\epsilon(\eta+\gamma)u^x = \epsilon^2\gamma\int_0^1 \dot{\phi}_0 y_1 + \epsilon^2\frac{\gamma-1}{2}\left(\frac{\partial^2 y_1}{\partial x^2}\right)^2(0,t) + \mathcal{O}(\epsilon^3)$$

therefore obtaining

$$u_0^x = 0 \quad \text{and} \quad u_1^x = U_1^x\,\dot{\phi}_0^2$$

where U_1^x is given by (3.42). In the following we suppose that τ_{ext} has zero average, thus ϕ_0 is periodic. For simplicity we also assume $\tau_{\mathrm{ext}}(0) = 0$ so that $\phi_1(t) = \varphi_1\dot{\phi}_0(t)$, but the result we propose here holds for any initial value of the external torque.

Let us consider the expansion $\dot{\mathbf{q}} = \dot{\mathbf{q}}_0 + \epsilon\dot{\mathbf{q}}_1 + \mathcal{O}(\epsilon^2)$. At the zero-order we have

$$\dot{\mathbf{q}}_0 = u_0^x\,\mathbf{e}_{\phi_0} + u_0^y\,\mathbf{e}_{\phi_0}^\perp - \rho\dot{\phi}_0\,\mathbf{e}_{\phi_0}^\perp = (U_0^y - \rho)\,\dot{\phi}_0\,\mathbf{e}_{\phi_0}^\perp$$

while at the first order

$$\begin{aligned}\dot{\mathbf{q}}_1 &= \left(u_1^x\,\mathbf{e}_{\phi_0} + u_1^y\,\mathbf{e}_{\phi_0}^\perp + u_0^x\phi_1\,\mathbf{e}_{\phi_0}^\perp - u_0^y\phi_1\,\mathbf{e}_{\phi_0} - \rho\dot{\phi}_1\,\mathbf{e}_{\phi_0}^\perp + \rho\dot{\phi}_0\phi_1\,\mathbf{e}_{\phi_0}\right) \\ &= (U_1^x - U_0^y\varphi_1 + \rho\varphi_1)\,\dot{\phi}_0^2\mathbf{e}_{\phi_0} + \left(\widetilde{U}_1^y - \rho\varphi_1\right)\ddot{\phi}_0\mathbf{e}_{\phi_0}^\perp\,.\end{aligned}$$

If we now expand $\Delta\mathbf{q} = \Delta\mathbf{q}_0 + \epsilon\Delta\mathbf{q}_1 + \mathcal{O}(\epsilon^2)$, then

$$\Delta\mathbf{q}_0 = \int_0^1 (U_0^y - \rho)\,\dot{\phi}_0\,\mathbf{e}_{\phi_0}^\perp = (U_0^y - \rho)\,[\mathbf{e}_{\phi_0}]_0^1 = 0$$

because of the periodicity of ϕ_0. On the other hand, since $\dot{\mathbf{q}}_1$ has the form (3.44) with $\mathbf{A}(\phi_0) = (U_1^x - U_0^y\varphi_1 + \rho\varphi_1)\,\mathbf{e}_{\phi_0}$ and $\mathbf{B}(\phi_0) = \left(\widetilde{U}_1^y - \rho\varphi_1\right)\mathbf{e}_{\phi_0}^\perp$, if we apply (3.45) we obtain

$$\Delta\mathbf{q}_1 = \int_\Omega\left(\mathbf{A}(\phi_0) - \frac{d\mathbf{B}}{d\phi_0}(\phi_0)\right)d\psi d\phi_0 = (U_1^x - U_0^y\varphi_1 + \widetilde{U}_1^y)\int_\Omega \mathbf{e}_{\phi_0}d\psi d\phi_0$$

where $\partial\Omega$ is given by (3.57). Since $U_1^x - U_0^y\varphi_1 + \widetilde{U}_1^y = U_1^x + U_1^y = C$ we conclude

$$\Delta\mathbf{q} = \epsilon\int_\Omega \mathbf{V}(\phi_0)d\psi d\phi_0 + \mathcal{O}(\epsilon^2)$$

where $\mathbf{V}$ is given by (3.47).

Bibliography

[1] Gray J (1946). The mechanism of locomotion in snakes. *Journal of Experimental Biology*. **23**, 101.

[2] Gray J, Lissmann H W. (1950). The kinetics of locomotion of the grass-snake. *Journal of Experimental Biology*. **26**, 354.

[3] Alexander R M N (2003). Principles of Animal Locomotion. *Princeton University Press*.

[4] Taylor G. (1951). Analysis of the swimming of microscopic organisms. *Proceedings of the Royal Society of London A*. **209**, 447.

[5] Lighthill J (1976). Flagellar hydrodynamics. *Siam Review*. **18**, 161.

[6] Fletcher D. A., Theriot J. A. (2004). An introduction to cell motility for the physical scientist. *Physical Biology*. **1**, T1.

[7] Murphy R. R., Tadokoro S., Nardi D., Jacoff A., Fiorini P., Choset H., Erkmen A. M. (2008). Search and rescue robotics. In: *Springer Handbook of Robotics*. Springer Berlin Heidelberg.

[8] Roper M, Dreyfus R, Baudry J, Fermigier M, Bibette J, Stone H A (2008). Do magnetic micro-swimmers move like eukaryotic cells?. *Proceedings of the Royal Society of London A: Mathematical, Physical and Engineering Sciences*. **464**, 877.

[9] Pak O S, Gao W, Wang J, Lauga E (2011). High-speed propulsion of flexible nanowire motors: Theory and experiments. *Soft Matter*. **7**, 8169.

[10] Cicconofri G, DeSimone A (2015). Motility of a model bristle-bot: A theoretical analysis. *International Journal of Non-Linear Mechanics*. In press.

[11] Cicconofri G, DeSimone A (2015). A Study of Snake-like Locomotion Through the Analysis of a Flexible Robot Model. *Submitted for publication*.

[12] Cicconofri G, DeSimone A (2015). Motion planning and motility maps for flagellar microswimmers. *In preparation*.

[13] Altshuler E, Pastor J M, Garcimartn A, Zuriguel I, Maza D (2013). Vibrot, a simple device for the conversion of vibration into rotation mediated by friction: preliminary evaluation. *PloS one*. **8**, e67838.

[14] Becker F, Boerner S, Lysenko V, Zeidis I, Zimmermann K (2014). On the Mechanics of Bristle-Bots-Modeling, Simulation and Experiments. In: ISR/Robotik: 41st International Symposium on Robotics: Proceedings of (pp. 1-6), June 2014. *VDE*.

[15] Casey T M (1991). Energetics of caterpillar locomotion: biomechanical constraints of a hydraulic skeleton. *Science*. **252**, 112.

[16] Childress S, Hosoi A, Schultz W W, Wang Z J (2012). Natural Locomotion in Fluids and on Surfaces: Swimming, Flying, and Sliding. The IMA Volumes in Mathematics and its Applications, no. 155. *New York, NY: Springer*.

[17] Childress S (1981). Mechanics of swimming and flying. *Cambridge, UK: Cambridge University Press*.

[18] DeSimone A, Guarnieri F, Noselli G, Tatone A (2013). Crawlers in viscous environments: Linear vs nonlinear rheology. *International Journal of Non-Linear Mechanics*. **56**, 142.

[19] DeSimone A, Tatone A (2012). Crawling motility through the analysis of model locomotors: two case studies. *The European Physical Journal E*. **35**, 85.

[20] Farkas M (1994). Periodic motions. *New York, NY: Springer-Verlag*.

[21] Gidoni P, Noselli G, DeSimone A (2014). Crawling on directional surfaces. *International Journal of Non-Linear Mechanics* **61**, 65.

[22] Giomi L, Hawley-Weld N, Mahadevan L (2013). Swarming, swirling and stasis in sequestered bristle-bots. *Proceedings of The Royal Society A*. **469**, 20120637.

[23] Holmes P, Full R J, Koditschek D, Guckenheimer J (2006). The dynamics of legged locomotion: Models, analyses, and challenges. *SIAM Review*. **48**, 207.

[24] Hosoi A E (2011). Locomotion at low Reynolds numbers. In: Ben Amar M et al., eds. New Trends in the Physics and Mechanics of Biological Systems: Lecture Notes of the Les Houches Summer School: Volume 92, July 2009. *Oxford University Press*.

[25] Klingner J, Kanakia A, Farrow N, Reishus D, Correll N (2014). A stick-slip omnidirectional powertrain for low-cost swarm robotics: Mechanism, calibration, and control. In: Intelligent Robots and Systems (IROS 2014): IEEE/RSJ International Conference on (pp. 846-851), September 2014. *IEEE*.

[26] Lai J H, del Alamo J C, Rodrguez-Rodrguez J, Lasheras J C (2010). The mechanics of the adhesive locomotion of terrestrial gastropods. *The Journal of Experimental Biology*. **213**, 3920.

[27] Lauga E, Hosoi A E (2006). Tuning gastropod locomotion: Modeling the influence of mucus rheology on the cost of crawling. *Physics of Fluids*. **18**, 113102.

[28] Noselli G, DeSimone A (2014). A robotic crawler exploiting directional frictional interactions: experiments, numerics and derivation of a reduced model. *Proceedings of the Royal Society A.* **470**, 20140333.

[29] Mahadevan L, Daniel S, Chaudhury M K (2004). Biomimetic ratcheting motion of a soft, slender, sessile gel. *Proceedings of the National Academy of Sciences.* **101**, 23.

[30] Polderman J W, Willems J C (1998). Introduction to mathematical systems theory: a behavioral approach. *New York, NY: Springer-Verlag.*

[31] Shepherd R F, Ilievski F, Choi W, Morin S A, Stokes A A, Mazzeo A D, Chen X, Wang M, Whitesides G M (2011). Multigait soft robot. *Proceedings of the National Academy of Sciences.* **108**, 20400.

[32] Tanaka Y, Ito K, Nakagaki T, Kobayashi R (2012). Mechanics of peristaltic locomotion and role of anchoring. *Journal of The Royal Society Interface.* **9**, 222.

[33] Trivedi D, Rahn C D, Kier W M, Walker I D (2008). Soft robotics: Biological inspiration, state of the art, and future research. *Applied Bionics and Biomechanics.* **5**, 99.

[34] Kim S, Laschi C, Trimmer B (2013). Soft robotics: a bio-inspired evolution in robotics. *Trends in Biotechnology.* **31**, 287.

[35] Bekker M G (1956). Theory of Land Locomotion. *University of Michigan Press.*

[36] Jayne B C. (1988). Muscular mechanisms of snake locomotion: an electromyographic study of lateral undulation of the Florida banded water snake (Nerodia fasciata) and the yellow rat snake (Elaphe obsoleta). *Journal of Morphology.* **197**, 159.

[37] Moon B R, Gans C (1998). Kinematics, muscular activity and propulsion in gopher snakes. *Journal of Experimental Biology.* **201**, 2669.

[38] Baum M J, Kovalev A E, Michels J, Gorb S N (2014). Anisotropic Friction of the Ventral Scales in the Snake Lampropeltis getula californiae. *Tribology Letters* **54**, 139.

[39] Berth R A, Westhoff G, Bleckmann H, Gorb S N (2009). Surface structure and frictional properties of the skin of the Amazon tree boa Corallus hortulanus (Squamata, Boidae). *Journal of Comparative Physiology A.* **195**, 311.

[40] Hu D L, Nirody J, Scott T, Shelley M J (2009). The mechanics of slithering locomotion. *Proceedings of the National Academy of Sciences.* **106**, 10081.

[41] Hu D L, Shelley M J (2012). Slithering locomotion. In: Natural Locomotion in Fluids and on Surfaces, S.Childress et al. (editors), pp. 117-135, The IMA Volumes in Mathematics and its Applications. Vol **155**. *Springer-Verlag.*

[42] Guo Z V, Mahadevan L (2008). Limbless undulatory propulsion on land. *Proceedings of the National Academy of Sciences*. **105**, 3179.

[43] Alouges F, DeSimone A, Giraldi L, Zoppello M (2013). Self-propulsion of slender microswimmers by curvature control: N-link swimmers. *Int.J. Nonlinear Mechanics*. **56**, 142.

[44] Hirose S (1993). Biologically inspired robots: snake-like locomotors and manipulators. *Oxford University Press*.

[45] Chirikjian G S, Burdick J W (1995). The kinematics of hyper-redundant robot locomotion. *IEEE Transactions on Robotics and Automation* **11**, 781.

[46] Boyer F, Shaukat A, Mathieu P (2012). Macrocontinuous dynamics for hyperredundant robots: Application to kinematic locomotion bioinspired by elongated body animals. *IEEE Transactions on Robotics*. **28**, 303.

[47] Boyer F, Porez M, Khalil W (2006). Macro-continuous computed torque algorithm for a three-dimensional eel-like robot. *IEEE Transactions on Robotics*. 563.

[48] Trivedi D, Lotfi A, Rahn C D (2008). Geometrically exact models for soft robotic manipulators. *IEEE Transactions on Robotics*. **24**, 773.

[49] Renda F, Cianchetti M, Giorelli M, Arienti A, Laschi C (2012). A 3D steady-state model of a tendon-driven continuum soft manipulator inspired by the octopus arm. *Bioinspiration and Biomimetics*. **7**, 025006.

[50] Chrispell JC, Fauci LJ, Shelley M (2013). An actuated elastic sheet interacting with passive and active structures in a viscoelastic fluid. *Physics of Fluids*. **25**, 013103.

[51] Antman S S (2005). Nonlinear problems of elasticity. Vol **107**. *New York: Springer*.

[52] Libai A, Simmonds J G (2005). The nonlinear theory of elastic shells. *Cambridge University Press*.

[53] Bigoni D, Dal Corso F, Bosi F, Misseroni D (2014). Eshelby-like forces acting on elastic structures: theoretical and experimental proof. *Mechanics of Materials* (in press).

[54] Long, J H (1998). Muscles, elastic energy, and the dynamics of body stiffness in swimming eels. *American zoologist*. **38**, 771.

[55] Gay-Balmaz F, Vakhtang P (2012). Dynamics of elastic rods in perfect friction contact. *Physical Review Letters*. **109**, 244303.

[56] Vankerschaver J (2007). A class of nonholonomic kinematic constraints in elasticity. *Journal of Physics A: Mathematical and Theoretical*. **40**, 3889.

[57] Shapere A, Wilczek F (1989). Geometry of self-propulsion at low Reynolds number. *Journal of Fluid Mechanics*. **198**, 557.

[58] Wiggins C H, Riveline D, Ott A, Goldstein R E (1998). Trapping and wiggling: elastohydrodynamics of driven microfilaments. *Biophysical Journal.* **74**, 1043.

[59] Wiggins C H, Goldstein R E (1998). Flexive and propulsive dynamics of elastica at low Reynolds number. *Physical Review Letters.* **80**, 3879.

[60] Wolgemuth C W, Powers T R, Goldstein R E (2000). Twirling and whirling: Viscous dynamics of rotating elastic filaments. *Physical Review Letters.* **84**, 1623.

[61] Becker L E, Koehler S A, Stone H A (2003). On self-propulsion of micromachines at low Reynolds number: Purcell's three-link swimmer. *Journal of fluid mechanics.* **490**, 15.

[62] Dreyfus R, Baudry J, Roper M L, Fermigier M, Stone H A, Bibette J (2005). Microscopic artificial swimmers. *Nature.* **437**, 862-865.

[63] Camalet S, Julicher F (2000). Generic aspects of axonemal beating. *New Journal of Physics.* **2**, 24.1.

[64] Gadelha H, Gaffney E A, Smith D J, Kirkman-Brown, J C (2010). Nonlinear instability in flagellar dynamics: a novel modulation mechanism in sperm migration?. *Journal of The Royal Society Interface.* **7**, 1689.

[65] Gadelha H (2013). On the optimal shape of magnetic swimmers. *Regular and Chaotic Dynamics.* **18**, 75.

[66] Lauga E (2007). Floppy swimming: Viscous locomotion of actuated elastica. *Physical Review E.* **75**, 041916.

[67] Yu T S, Lauga E, Hosoi A E (2006). Experimental investigations of elastic tail propulsion at low Reynolds number. *Physics of Fluids.* **18**, 0917011.

[68] Keaveny E E, Maxey M R (2008). Spiral swimming of an artificial microswimmer. *Journal of Fluid Mechanics.* **598**, 293.

[69] Abbott J J, Peyer K E, Lagomarsino M C, Zhang L, Dong L, Kaliakatsos I K, Nelson B J (2009). How should microrobots swim?. *International Journal of Robotics Research.* **28**, 1434.

[70] Cox R G (1970). The motion of long slender bodies in a viscous fluid Part 1. General theory. *Journal of Fluid mechanics.* **44**, 791.

[71] Machin K E (1958). Wave propagation along flagella. *Journal of Experimental Biology.* **35**, 796.

[72] Purcell E M (1977). Life at low Reynolds number. *American Journal of Physics.* **45**, 3.

[73] Passov E, Or Y (2012). Dynamics of Purcells three-link microswimmer with a passive elastic tail. *The European Physical Journal E.* **35**, 1.

[74] Gutman E, Or Y (2014). Simple model of a planar undulating magnetic microswimmer. *Physical Review E.* **90**, 013012.

[75] Nayfeh A H (2008). Perturbation methods. *John Wiley & Sons*.

[76] Ciarlet P G (2013). Linear and nonlinear functional analysis with applications (Vol. 130). *SIAM*.

[77] Batchelor G K (2000). An introduction to fluid dynamics. *Cambridge university press*.

[78] Desimone A, Heltai L, Alouges F, Lefebvre-Lepot A. (2012). Computing optimal strokes for low Reynolds number swimmers. In: *Natural Locomotion in Fluids and on Surfaces*. Springer New York.

[79] Burton L J, Hatton R L, Choset H, Hosoi A E (2010). Two-link swimming using buoyant orientation. *Physics of Fluids*. **22**, 091703.

[80] Hatton R L, Choset H (2010). Connection vector fields and optimized coordinates for swimming systems at low and high Reynolds numbers. In: *ASME 2010 Dynamic Systems and Control Conference*. American Society of Mechanical Engineers.

[81] Avron J E, Raz O (2008). A geometric theory of swimming: Purcell's swimmer and its symmetrized cousin. *New Journal of Physics*. **10**, 063016.

[82] Gaffney E A, Gadlha H, Smith D J, Blake J R, Kirkman-Brown J C (2011). Mammalian sperm motility: observation and theory. *Annual Review of Fluid Mechanics*. **43**, 501.

[83] Goldstein R E (2015). Green Algae as Model Organisms for Biological Fluid Dynamics. *Annual Review of Fluid Mechanics*. **47**, 343.

[84] Guasto J S, Rusconi R, Stocker R (2012). Fluid mechanics of planktonic microorganisms. *Annual Review of Fluid Mechanics*. **44**, 373.

[85] Alouges F, DeSimone A, Giraldi L, Zoppello M. Can Magnetic Multilayers Propel Artificial Microswimmers Mimicking Sperm Cells? *SoRo*. **2**, to appear.